PhD Dissertation

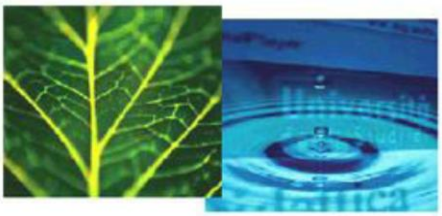

International Doctorate School in Information and Communication Technologies

DISI - University of Trento

ADVANCED PRE-PROCESSING AND CHANGE-DETECTION TECHNIQUES FOR THE ANALYSIS OF MULTITEMPORAL VHR REMOTE SENSING IMAGES

Silvia Marchesi

Advisor:
Prof. Bruzzone Lorenzo
Università degli Studi di Trento

Co-Advisor:
Dott. Bovolo Francesca
Università degli Studi di Trento

April 2011

Alla mia nonna

Abstract

Remote sensing images regularly acquired by satellite over the same geographical areas (multitemporal images) provide very important information on the land cover dynamic. In the last years the ever increasing availability of multitemporal very high geometrical resolution (VHR) remote sensing images (which have sub-metric resolution) resulted in new potentially relevant applications related to environmental monitoring and land cover control and management. The most of these applications are associated with the analysis of dynamic phenomena (both anthropic and non anthropic) that occur at different scales and result in changes on the Earth surface. In this context, in order to adequately exploit the huge amount of data acquired by remote sensing satellites, it is mandatory to develop unsupervised and automatic techniques for an efficient and effective analysis of such kind of multitemporal data.

In the literature several techniques have been developed for the automatic analysis of multitemporal medium/high resolution data. However these techniques do not result effective when dealing with VHR images. The main reasons consist in their inability both to exploit the high geometrical detail content of VHR data and to model the multiscale nature of the scene (and therefore of possible changes). In this framework it is important to develop unsupervised change-detection(CD) methods able to automatically manage the large amount of information of VHR data, without the need of any prior information on the area under investigation. Even if these methods usually identify only the presence/absence of changes without giving information about the kind of change occurred, they are considered the most interesting from an operational perspective, as in the most of the applications no multitemporal ground truth information is available.

Considering the above mentioned limitations, in this thesis we study the main problems related to multitemporal VHR images with particular attention to registration noise (i.e. the noise related to a non-perfect alignment of the multitemporal images under investigation). Then, on the basis of the results of the conducted analysis, we develop robust unsupervised and automatic change-detection methods. In particular, the following specific issues are addressed in this work:

1. Analysis of the effects of registration noise in multitemporal VHR images and definition of a method for the estimation of the distribution of such kind of noise useful for defining:

   a. Change-detection techniques robust to registration noise (RN); the proposed techniques are able to significantly reduce the false alarm rate due to RN that is raised by the standard CD techniques when dealing with VHR images.

   b. *Effective registration methods; the proposed strategies are based on a multiscale analysis of the scene which allows one to extract accurate control points for the registration of VHR images.*

2. Detection and discrimination of multiple changes in multitemporal images; this techniques allow one to overcome the limitation of the existing unsupervised techniques, as they are able to identify and separate different kinds of change without any prior information on the study areas.

3. Pre-processing techniques for optimizing change detection on VHR images; in particular, in this context we evaluate the impact of:

   a. *Image transformation techniques on the results of the CD process;*
   b. *Different strategies of image pansharpening applied to the original multitemporal images on the results of the CD process.*

For each of the above mentioned topic an analysis of the state of the art is carried out, the limitations of existing methods are pointed out and the proposed solutions to the addressed problems are described in details. Finally, experimental results conducted on both simulated and real data are reported in order to show and confirm the validity of all the proposed methods.

Keywords

Multitemporal image analysis, change detection, registration noise, image registration, pansharpening, very high resolution (VHR) images, remote sensing.

Ringraziamenti

Con questa tesi si chiude un importante capitolo della mia vita, iniziato quasi dieci anni fa.
Da studentessa universitaria prima e da *PhD Studen*t poi ho vissuto intensamente questo ambiente universitario. Le giornate trascorse su libri, paper, presentazioni, progetti mi hanno fatta crescere e maturare in maniera profonda.
Per tutto questo devo ringraziare in primo luogo mamma e papà, genitori davvero speciali, che mi hanno sempre spronata, appoggiata, incoraggiata nei momenti di sconforto e, è bello dirlo, anche ammirata quando ho conquistato i miei primi piccoli successi. Con loro non posso non menzionare il mio fratellone Giovi, che ha dato un grosso contributo allo sviluppo del mio spirito critico, alimentando costruttive discussioni davvero difficili da intraprendere con chiunque altro. E con lui nonna e zia, che con orgoglio hanno seguito questi miei anni di crescita.
Ringrazio il mio Matteo,conosciuto all'inizio di questo capitolo e che mi accompagnerà fino alla fine della storia. 'Perchè con lui la mia vita è ancora più meravigliosa'.
Un grazie va al prof, Lorenzo, che mi ha dato l'opportunità di affrontare il dottorato, di conoscere questo mondo, di espormi pubblicamente, di imparare a difendere la mia idea, il mio lavoro. Assieme a lui ringrazio Francesca per i consigli e le discussioni scientifiche.
Infine, senza fare nomi perchè non vorrei dimenticare nessuno, ringrazio tutti i compagni di quest'avventura, quelli che han condiviso situzioni di frustrazione professionale, quelli che han trovato un senso, quelli con i quali mi sono confrontata e quelli che mi hanno fatta sentire una buona amica, perchè in questi anni ho trovato anche grandi amici.

Contents

Chapter 1

1. Introduction

In this chapter we make an introduction to the problem of performing multitemporal analysis on very high geometrical resolution images. In details, we report a brief overview on the last generation of satellite sensors that acquire very high geometrical resolution (VHR) images, and we present the applications related to the analysis of multitemporal VHR data. We also describe the most critical issue related to the analysis of such kind of data, giving motivations of the introduced work. In addition, we describe the specific objectives faced in the thesis and the novel contributions of it. Finally, we describe the structure and organization of this thesis.

1.1. Overview on the last generation of remote sensing systems

Remote Sensing (RS) is the science and art of acquiring information (spectral, spatial, temporal) about material objects, area, or phenomenon, without coming into physical contact with the objects, or area, or phenomenon under investigation [1]. A sensor is used to measure the energy emitted and reflected from the object and transferred as electromagnetic radiation through the space. According to the source of the energy measured by the sensors, RS systems can be divided into two categories: passive and active. The formers detect the reflected or emitted radiation from natural sources, while the latter make use of sensors that measure reflected responses from objects that are irradiated from artificially-generated energy sources, such as radar systems. In addition, with respect to the wavelength regions in which the sensor measures the received quantity of energy, the remote sensing systems can be divided into: visible and reflective infrared systems (from 0.4 to 3 micrometers), thermal systems (from 3 to 14 micrometers) and microwave systems (from 0.1 to 100 centimeters).

In this dissertation, we consider remote sensing systems for Earth observation, focusing on the analysis of the information, in the form of digital images, coming from passive sensors mounted on satellites. Starting from 1972, when the first world's satellite for the Earth observation (Landsat-1) has been launched, several missions for the observation of the Earth have been developed. In the last decade, the remote sensing technology had a significant evolution that resulted in the launch of satellites mounting on-board sensors capable to acquire images with very high resolution (VHR). The pioneering high resolution images acquired by SPOT missions are now integrated with multispectral images having metric or sub-metric resolution acquired by new remote sensing satellites (e.g., Ikonos, Quickbird, GeoEye-1, and WorldView-2) and other new missions characterized by sensors that can acquire

VHR images are planned for the next years. In this thesis, optical very high geometrical resolution multispectral images provided by the last generation of sensors will be considered.

In the following paragraph we briefly recall the characteristics of the most popular VHR imaging systems, in which we are mainly interested in this work.

1.1.1 VHR imaging systems

Geometric resolution refers to the satellite sensor's ability to effectively image a portion of the Earth's surface in a single pixel and is typically expressed in terms of Ground Sample Distance (GSD), which indicates the smallest unit that is mapped to a single pixel within an image. The resolution of satellite images varies depending on the physical properties of the sensors used and the altitude of the satellite's orbit. The latest commercial satellites could acquire images with a GSD lower than 0.5 m (i.e. GeoEye-1), however, due to US Government restrictions on civilian imaging the data are commercialized only after decreasing the resolution till obtaining a GSD of at least 0.5 m. GSD for intelligence and military purposes may have a resolution of less than a centimeter with the potential for real-time (live) imaging.

The term VHR imaging systems usually refers to images with GSD lower than 1 meter, provided by the last generation of sensors. These systems have been developed starting from XXI century (i.e. Ikonos satellite launched in 1999 and Quickbird satellite launched in 2001); and they have been preceded by the SPOT satellites, appeared starting from 1986 and characterized by a high geometrical resolution (10 m for the panchromatic band and 20 m for the multispectral ones). Before them the most popular multispectral sensors were the ones mounted on Landsat satellites (from 1 to 7). Landsat 7, the last satellite of the Landsat program, launched in April 1999, can acquire a panchromatic band with 15 m spatial resolution and seven multispectral bands (in the visible, near and thermal infrared) with 30 m spatial resolution (except for the thermal band which has 60 m of resolution).

In the following a list of the major VHR RS systems with the main characteristics of each is reported.

- **Ikonos**: launched on September 1999, provides multispectral images (spectral channels of acquisition: blue, green, red and near infrared) with a spatial resolution of 3.2 m and panchromatic images with a resolution of 0.82 m. Time of revisit is from 3 to 5 days depending on the latitude [2].
- **Eros A**: launched on December 2000, provides only panchromatic images with a spatial resolution of 1.8 m. Time of revisit is from 2.1 to 9.5 days depending on the latitude [3].
- **QuickBird**: launched on October 2001, provides multispectral images (blue, green, red and near infrared) with a spatial resolution of 2.4 m and panchromatic images with a resolution of 0.6 m. Time of revisit is from 1 to 3.5 days depending on the latitude [2].
- **Spot 5**: launched on May 2002, the last satellite of the SPOT family, provides multispectral images (green, red, near infrared and mid infrared) with a spatial resolution of 10 m and panchromatic images with a resolution that varies from 2.5 to 5 m. Time of revisit is from 2 to 3 days depending on the latitude [2].
- **Eros B**: launched on April 2005, provides only panchromatic images with a spatial resolution of 0.7 m. Time of revisit is from 2.1 to 9.5 days depending on the latitude[3].
- **GeoEye-1**: launched on December 2004 provides multispectral images (blue, green, red and near infrared) with a spatial resolution of 1.65 m and panchromatic images with a resolution of 0.41 m (degraded to 0.5 m for civil applications). Time of revisit is from 2.1 to 8.3 days [4].
- **WorldView-1**: launched in September 2007, provides only panchromatic images with a spatial resolution of 0.5 m. Time of revisit is from 1.7 to 5.9 days depending on the latitude [2].

- **RapidEye**: launched in August 2008, made up of a constellation of 5 satellites containing identical instruments, provides multispectral images (blue, green, red, red edge and near infrared) with a spatial resolution of 5 m. Time of revisit is about 1 day [5].
- **WorldView-2**: launched in October 2009, provides multispectral images (blue, green, red and near infrared, plus red edge, coastal, yellow and near infrared 2) with a spatial resolution of 1.8 m and panchromatic images with a resolution of 0.5 m. Time of revisit is from 1.1 to 3.7 days depending on the latitude [2].
- **Pleiades-1**: will be launched in early 2011 and will reach a spatial resolution of 2 m for multispectral images (blue, green, red and near infrared) and of 0.5 m for panchromatic images. It will have a revisit time of 1 day once the complete constellation (Pleiades-1 and Pleiades-2) will be operating [6].
- **Pleiades-2**: will be launched in 2012 and will complete the Pleiades constellation of satellites (same characteristics of Pleiades-1) [6].
- **GeoEye-2**: will be launched in early 2013 and it will reach a spatial resolution of 0.25 m. However, restrictive licensing by the US government makes it likely that only the US Government and some of its allies will have access to imagery at the full design resolution [4].

Please note that all the described systems are in a polar sun-synchronous orbit and the reported spatial resolution value is referred at nadir.

1.2. Multitemporal VHR images: applications and related problems

Very high geometrical resolution images acquired by modern remote sensing sensors mounted on board of the last generation of satellites are a very important information source for many potential applications related to environmental monitoring and land control and management. In particular, the increased spatial resolution (with respect to previous generation satellites) makes it possible to address many new applications related to the analysis of scenes at a local scale with a very high geometrical detail (e.g., urban areas and infrastructure analysis, precision farming, building detection, etc.). In this scenario, a very important domain is related to applications that require a regular analysis of a given geographical area for the detection of possible alterations or changes occurred on the ground. Possible applications are related to: monitoring of natural resources in order to define risk maps, analysis of changes occurred after natural disasters in order to derive damage maps at high resolution, building abuse discovering, etc [7].

These applications require the use of images acquired on the same geographical area at different times (multitemporal images) and the development of proper automatic change-detection techniques. Although the scientific literature presents many works related to change-detection techniques applied to medium and high resolution images acquired by the previous generation of remote sensing sensors, only few techniques have been developed in the last years for the detection of changes in VHR data. Moreover, the techniques developed for medium resolution images are largely insufficient to exploit in a proper and automatic way the richness of information contained in multitemporal VHR data. This is mainly due to: a) their inability to properly exploit the spatial-context information and the geometrical detail content; b) their intrinsic single-scale nature that does not make it possible to model the multiscale properties of objects in VHR images; c) their unsuitability to deal with the distortions (mainly registration noise and shadows) present in VHR multitemporal images. In addition, given a specific geographical area, the very high geometrical resolution of new generation sensors results in a higher amount of data to analyze than in the case of medium resolution sensors.

Therefore, for a proper exploitation of VHR images in real applications related to extended areas, it is mandatory to develop effective automatic techniques that can properly handle the huge amount of available data and the high geometric content.

In order to give to the reader an idea of the differences between medium and very high geometrical resolution images, Figure 1.1 shows two images acquired over an area of the city of Trento (Italy) by the multispectral sensor mounted on Landsat5 satellite (Figure 1.1 (a)) and by the one mounted on the Quickbird satellite (Figure 1.1 (b)). Observing the two images it is simple to imagine the potentiality of new applications arisen from the high geometrical content of VHR data and the need of developing new and proper techniques for effectively manage such kind of data.

(a) (b)

Figure 1.1. True color composition of the remote sensing images acquired over the city of Trento (Italy) by multispectral sensor mounted on (a) Landsat 5 satellite and (b) Quickbird satellite.

The problems related to the analysis of multitemporal VHR images faced in this thesis are specifically related to the following aspects:

1. Most of the techniques developed for the analysis of multitemporal data require a perfect alignment of the images under investigation. In order to obtain a pair of images where corresponding pixels are associated with the same position on the ground (co-registered images), pre-processing steps are needed, including: geometric correction and image registration. However, in practice it is not possible to obtain a pair of perfect aligned images. The co-registration procedure becomes more complex and critical (and therefore intrinsically less accurate) when very high resolution images are considered. These images can be acquired with different view angles and often show different geometrical distortions that, even after proper geometric corrections, strongly affect the precision of the registration process, thus resulting in a significant residual registration noise (RN) [8]. This noise sharply decreases the accuracy of most of the techniques developed for the analysis of multitemporal data. Observing Figure 1.2 (a) and (b) it is simple to note the differences in the acquisition view angle and in the illumination conditions (shadows). The impact of these differences on a multitemporal analysis is emphasized in Figure 1.2 (c) where the false color composition of the multitemporal images in Figure 1.2 (a) and (b) is reported.

(a) (b) (c)

Figure 1.2. True color composition of the images acquired over the same geographical area of the city of Trento by the Quickbird satellite in: (a) October 2005 and (b) July 2006. (c) False color composition of the multitemporal images.

2. The detection of multiple changes (*i.e.*, different kinds of change) in multitemporal remote sensing images is a complex problem (not only for VHR images). When multispectral images having *B* spectral bands are considered, an effective solution to this problem is to exploit all available spectral channels in the framework of supervised or partially supervised approaches [9]. However, in many real applications it is difficult/impossible to collect ground truth information for either multitemporal or single date images. On the opposite, unsupervised methods available in the literature are not effective in handling the full information present in multispectral and multitemporal images. They usually consider a simplified sub-space of the original feature space having small dimensionality and thus characterized by a possible loss of change information.
3. The last generation of VHR multispectral sensors can acquire a panchromatic (PAN) image characterized by very high geometrical resolution and low spectral resolution (no spectral diversity and low capacity in distinguishing different kind of changes); and a set of multispectral (MS) images with lower spatial resolution, and higher spectral resolution. In order to take advantage of both high geometrical and spectral resolutions in the change detection process, it is common practice to apply a proper pre-processing, namely pansharpening (PS). PS merges the properties of panchromatic and multispectral data for spatial detail injection from PAN to MS, resulting in a set of images with both high spectral resolution and enhanced geometrical resolution. However, pansharpening can introduce in the images spatial artifacts and spectral distortions that can affect the accuracy of change-detection maps. Although several quality indexes have been proposed for evaluating pansharpening methods, they are not specifically conceived for CD applications [10].

1.3. Objectives and novel contributions of the thesis

According to the problems related to the analysis of multitemporal VHR data described in the previous section, in this thesis the attention is focused on the understanding and the modeling of the main properties of multitemporal VHR images and on the use of the results of this analysis for the definition of proper unsupervised change detection methodologies. In particular, at first we focused our attention on the analysis of the properties of registration noise (RN) (i.e. noise that arises from a non perfect alignment of the multitemporal images), then, according to the results of such analysis, we derived both registration and change-detection techniques effective on VHR multitemporal images. Furthermore pre-processing techniques for optimizing the results of change detection were considered. The activity is mainly oriented to address some of the main limitations of the existing techniques, de-

veloped for medium resolution images. In greater details, the following specific topics are considered in this work:

a) Analysis of the effects of registration noise in multitemporal VHR images in order to derive an adaptive estimation of it;
b) Registration techniques effective on VHR multitemporal images, which overcome the limitations of the techniques developed specifically for medium resolution images;
c) Techniques for the detection of changes in multispectral VHR images robust to the problems related to registration noise and that consider the contextual information;
d) Automatic methods for the detection and separation of multiple changes in multitemporal images. Please note that for this specific topic the analysis has been conducted on both medium and VHR images, as no unsupervised techniques developed for medium resolution images exist able to separate different kinds of change, as previously pointed out;
e) Analysis of image transformation techniques for change-detection applications on VHR images;
f) Analysis of the effects of pansharpening in change detection on VHR images.

In order to address the aforementioned issues, we developed novel approaches and techniques for the automatic analysis of VHR multitemporal images. The main goals of these methods are briefly described in the following:

a) Analysis and adaptive estimation of the registration noise distribution in multitemporal VHR images

According to the problem related to the presence of registration noise described in the previous section in this thesis we aim at analyzing the properties of registration noise in multitemporal VHR images in order to formulate an adaptive technique for the explicit estimation of the distribution of residual RN between multitemporal images. This distribution is a starting point for the development of novel registration techniques and change-detection techniques robust to such source of noise, as it will be presented in the following. This study is developed within a polar framework for change vector analysis (CVA) recently introduced in the literature for change detection in medium resolution multispectral images [11]. In this context, the novel contributions of this work consist in: i) the analysis of the effects of registration noise in multitemporal and multispectral VHR images; ii) the definition of the properties of registration noise in VHR images; and iii) the formulation of an adaptive and distribution-free technique for the estimation of the distribution of the registration noise in the polar domain.

b) A registration noise driven technique for the alignment of VHR images

As pointed out in the previous section, image registration is one of the most important steps in the analysis of multitemporal remote sensing images. In this thesis we aim at developing a novel technique for a robust and accurate registration of VHR images, which is especially suitable for change-detection applications. The proposed technique follows the standard scheme of the registration process [12]: (i) feature (i.e. CPs) extraction; (ii) feature matching and transform model estimation; and (iii) image resampling and transformation. In particular, the presented method automatically extracts the CPs, estimates the disparity map that represents the non-parametric spatial transformation to be applied to the image and finally warps the moving image on the reference one. The proposed method takes advantages from the analysis anticipated in the previous subsection on the effects of registration noise; the technique for the estimation of the distribution of registration noise (RN), in fact, is exploited for automatically extracting and matching the CPs. Unlike standard registration methods,

the proposed procedure: (i) is effective in obtaining good registration accuracy on the most critical points of the images where misregistration has a high probability to results in the detection of false changes; and (ii) is not affected by the presence of changes between the two images.

c) A context-sensitive technique robust to registration noise for change detection in VHR multispectral images

One of the most important problems, as pointed out before, in the development of change-detection techniques for VHR data is represented by registration noise arising from a non-prefect alignment of the multitemporal images under investigation [8]. Another important problem in change detection on VHR images concerns the modeling of the spatial context information of the scene [13]. In order to overcome the aforementioned problems, in this thesis we present an adaptive context-sensitive technique, which: i) reduces the impact of registration noise in change detection on VHR multispectral images through a multiscale strategy; ii) considers the spatial dependencies of neighborhood pixels through the definition of multitemporal parcels (i.e. homogeneous regions both in space and time domain). As for the method presented in b), this technique takes advantages from the analysis conducted in a).

d) Automatic and unsupervised detection of multiple changes in multitemporal images

In relation with the problems of detecting and separating different kinds of change in an automatic and unsupervised way, in this thesis we present a framework for the detection of multiple changes in multitemporal and multispectral remote sensing images that allows one to overcome the limits of standard unsupervised methods. Please note that the problem of multiple changes has been faced in this thesis both for medium and very high resolution images, as also for medium resolution it has not been implemented in the literature. The framework is based on: i) a compressed yet efficient 2-dimensional (2D) representation of the change information; and ii) a 2-step automatic decision strategy. First the multidimensional feature space of SCVs is compressed into a 2-dimensional feature space without neglecting any available spectral band (and thus possible information about changes). Second, an automatic 2-step method for separating unchanged from changed patterns and distinguishing different kinds of change is presented.

e) Image transformation for change detection in VHR multispectral images

As stated before, in real change-detection problems pre-processing is often not sufficient to guarantee the ideal condition in which radiometric changes in corresponding pixels on the multitemporal images are associated with true changes on the ground. Usually, residual components of noise (e.g. due to residual radiometric differences, residual misregistration, etc.) result in false alarms in the change-detection maps, which cannot be easily identified in the phase of post-processing [14].

In this thesis, we address the aforementioned problems by exploiting data transformation techniques for separating the different sources of noise from real changes in different components to be selectively exploited in the change-detection phase [1]. In particular, we study the effectiveness of Principal Component Analysis (PCA) and Independent Component Analysis (ICA) and of theirs kernelized version, i.e. KPCA and KICA, respectively, as a preliminary step to change detection. These techniques are integrated in standard change-detection methods and their performances are analyzed on different data sets, thus deriving general conclusions on their effectiveness in change-detection applications.

f) Analysis of the effects of pansharpening in change detection on VHR images

The pansharpening procedure is commonly used on VHR images in order to merge the high geometrical content of the panchromatic channel with the spectral content of the multispectral ones. This procedure may result in artifacts that could be dangerous on the results of a change-detection process applied to the pansharpened images. In this thesis we aim at analyzing the impact of pansharpening on the accuracy of change detection investigating whether the improvement in geometrical resolution of change-detection maps given by pansharpening is significantly affected or not by artefacts introduced by the PS process in an unsupervised way. To this end five different multiresolution approaches are considered. A ranking of pansharpening techniques from the most to the less effective for CD is obtained by defining a novel unsupervised objective strategy based on similarity measures for comparing change-detection maps. In order to avoid the introduction of any bias in the analysis and to better understand the impact of pansharpening on change detection, the CD step is performed according to the standard change vector analysis (CVA) technique [15].

1.4. Structure of the thesis

The thesis is organized into nine chapters. The present chapter gave a brief overview on the remote sensing systems with a particular attention to the last generation of very high geometrical resolution sensors. It presented the problems related to the analysis of multitemporal VHR data and introduced the motivation, the objectives and the main novel contributions of this thesis. The following chapters will describe in details the studies and methodologies developed in order to fulfil the objectives presented in section 1.3.

Chapter 2 presents an exhaustive review of the state of the art related to the analysis of multitemporal VHR images focusing the attention on the change-detection problem.

Then, after these two chapters of introduction and state of the art, the other chapters are divided into three main parts. The first one regards registration noise and registration techniques and it includes chapter 3 and chapter 4. In chapter 3 an analysis of the effects of the registration noise is described and the properties of such kind of noise are derived. This analysis results in the definition of the strategy for the adaptive estimation of the RN distribution which is useful for both registration and change-detection methods. Chapter 4 presents the registration methods for VHR multitemporal images that we developed according to the results of the analysis on RN performed in chapter 3.

The second part is related to change-detection methods and includes chapters 5 and 6. In chapter 5 we present the change-detection method we have developed taking advantage form the analysis conducted in chapter 3. This method is robust to registration noise and considers the contextual information; this aspect is very important when dealing with VHR images. Chapter 6 describes an automatic and unsupervised technique for the detection of changes. The main advantage of this algorithm is its ability of identifying and separating different kinds of change.

The third part involves an analysis of the pre-processing techniques for optimizing change detection and includes chapter 7 and 8. In detail, chapter 7 presents an analysis of the effects of image transformation on the change-detection results; different image transformation techniques are considered and compared. Instead, chapter 8 presents an analysis of the effects of pansharpening methods on the results of the change-detection process. Five different pansharpening methods are considered and compared.

Finally chapter 9 draws the conclusion of this thesis. Furthermore, future developments of the research activities are discussed.

Chapter 2

2. Analysis of multitemporal VHR remote sensing images

This chapter presents a review on the techniques for the analysis of multitemporal VHR remote sensing images with particular attention to the process of detecting changes. In particular, the main characteristic of the very high geometrical resolution multitemporal images are highlighted and the limitations of the existing techniques for the analysis of medium resolution images are pointed out. Then the techniques proposed in the literature effective on VHR data are illustrated, by focusing on the methods for image registration and change-detection. Finally the change-detection techniques that are at the base of the most of the works proposed in this thesis are described in detail.

2.1. Introduction

The rapid development of the remote sensing technology in the last few years resulted in the design of satellite systems characterized by a very high geometrical resolution (e.g., Ikonos, Quickbird, EROS, GeoEye-1, World View-2) and of airborne sensors capable to merge high geometrical resolution with high spectral resolution, as pointed out in the previous chapter. This scenario offers enormous potentialities with respect to new possible applications that require detailed analysis of natural and/or anthropic scenes. In this context, the remote sensing community has promoted the development of novel techniques capable to efficiently process this kind of data by properly exploiting the huge amount of geometrical information contained in each considered scene. The problem of the analysis of VHR images can be faced in different manners depending on the considered kind of images and on the final objective of the data processing. From a general point of view, among the most relevant methodologies that have potentially important and strategic applications, the automatic image classification methods and all the techniques aimed at solving detection problems (in terms of both specific object detection in single-date images and change detection in multi-temporal images) cover important roles. In this thesis we focus the attention on the specific problem of the analysis of multitemporal VHR remote sensing images. In greater details, in this chapter we summarize the state of the art on the existing techniques for the analysis of multitemporal data with particular attention to the problem of change detection. The applications related to such problem require the use of images acquired on the same geographical area at different times (multitemporal images) and the development of proper automatic techniques for the detection of changes occurred on the ground between them.

Several different automatic change-detection techniques have been proposed in the image processing and remote sensing literature[16], [17], [18]. These techniques have been successfully employed in many different application domains, like analysis of growth of urban areas, cadastral map updating, risk analysis, damage assessment, etc. [18]. However, the most of the available methods are oriented to the analysis of images acquired by medium resolution (MR) sensors and result completely ineffective when dealing with images showing metric resolution (see section 1.2). The main limitations of CD techniques originally developed for MR images [18], when applied to VHR images consist in their inability both to exploit the high geometrical detail content of VHR data and to model the multiscale nature of the scene (and therefore of possible changes). In order to better exploit the spatial correlation among neighboring pixels and to get accurate and reliable CD maps (both in regions corresponding to border or geometrical details and in homogeneous areas) it is necessary to integrate the spectral information with the spatial one and to model the multiscale properties of the scene. Furthermore, the acquisition process of VHR images results in significant radiometric and geometric differences between multitemporal images (due to differences in atmospheric conditions, in the acquisition angle, in shadows characteristics, etc.). Such differences are extremely more critical than in MR images. Therefore, image pre-processing like image registration, geometric and radiometric corrections results in a critical task that strongly affect the quality of the CD process.

In the following section an overview on the unsupervised change-detection approaches is given. In particular, in section 2.2.1 a brief overview on the unsupervised CD techniques developed in the literature for VHR images is given. Considering the importance of the pre-processing step in the analysis of multitemporal images in section 2.3 some of the existing techniques for the registration of VHR images are summarized,. Finally in section 2.4 the polar framework based on Change Vector Analysis that is at the base of most of the techniques proposed in this thesis is described.

For a detailed analysis of the state of the art of each specific problem treated in the thesis, please refer to the introduction section of each chapter.

2.2. Unsupervised change-detection techniques

In the literature, two main approaches to change detection can be identified: the unsupervised and the supervised approach. The former requires a priori information on the investigated area and allows one to determine both the presence/absence and the kind of change occurred, while the latter does not assume availability of ground truth data and usually identifies only the presence/absence of changes. Even if the large part of unsupervised change detection does not produce information about the kind of changes, it has a high importance in the remote-sensing community since obtaining *a priori* information about land covers results often difficult or impossible. According to this consideration the unsupervised approach is the most interesting from an operational perspective. Moreover it is usually characterized by a very low computational burden.

Unsupervised change-detection techniques are based on the comparison of the spectral reflectance of the multitemporal images and a subsequent analysis of the comparison output. In the literature, the most widely used unsupervised CD methods are based on a three-step procedure (see Figure 2.1): (a) pre-processing; (b) pixel-based comparison of the images; and (c) image analysis/thresholding. In the first step the two images under consideration are processed in order to make them as more comparable as possible. This procedure includes radiometric and geometric correction and registration[1],[8], [19],[20]. The comparison step aims at producing the difference image, in which the differences between the two considered acquisitions are highlighted. Different mathematical operators can be adopted to perform the comparison, depending on the kind of data under investigation (this choice

gives rise to different techniques [21], [22], [23]). In particular, considering optical multispectral images (as in this thesis) the difference image is retrieved by applying the subtraction operator. After image comparison, a new image is obtained in which changes are empathized. In order to extract such changes a proper unsupervised image analysis technique should be applied. Among the unsupervised methods, the most widely used is based on the selection of a threshold that aims at separating changed from unchanged pixels. This threshold can be retrieved both manually by a trial and error procedure (according to the desired trade-off between false and missed alarms rate) or automatically (e.g. by analyzing the statistical distribution of the image after comparison, by fixing the false alarms probability or following a Bayesian minimum-error procedure [15]).

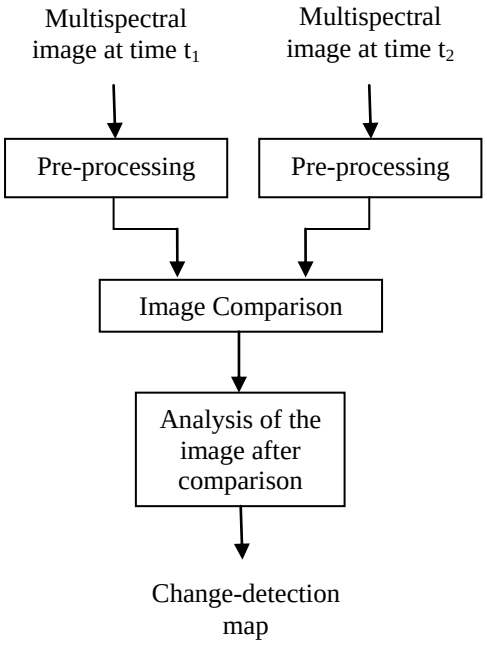

Figure 2.1. Block scheme of a standard unsupervised change-detection approach

2.2.1 Unsupervised change-detection techniques for VHR remote sensing images

From previous discussions it emerges that the techniques developed for medium resolution data are often not effective on VHR images and that, in order to overcome the limitation of these techniques, it is important to develop novel methodologies able to integrate the spectral information with the spatial one and model the multiscale properties of the scene. In the literature some methods exist capable to exploit the above-mentioned concepts [13], [24], [25], [26], [27], [28]. Usually, the change detection problem is faced after applying supervised classification to VHR images [29], [30]. The context information is exploited in the classification process according to segmentation techniques [31], [32] and to the extraction of texture feature, and the change detection map is obtained by comparing the classification maps [33]. However, as previously pointed out, the supervised nature of these techniques [24] is critical from the application point of view, as ground truth information is often not available.

In the last five years some works have been published regarding unsupervised CD techniques for VHR images. These works can be divided into two main groups. Analyzing the literature, in fact, it is possible to note that the multitemporal problems related to the very high resolution of the images have been faced mainly through two different approaches: (i) multiscale-based methods; and (ii) image transformation-based methods. In the first case a decomposition of the images at lower scales is at the base of the proposed techniques for the detection of changes. Different strategies are then joined to the

multiscale analysis for extracting the information about changes, without decreasing the resolution of the final CD results. In the second approach the images are transformed through standard methods (i.e. principal component analysis, independent component analysis, etc.) in order to overcome the limits of ineffective pre-processing. New change detection schemes are proposed that integrate a transformation of the images in the CD strategy allowing one to work with data less affected by noise, in which different sources of change can be identified. In the following a brief description on some of these works is reported.

The most common strategy in the definition of unsupervised change-detection techniques for VHR data is represented by the multiscale analysis. Examples of works in this direction are:

- F. Bovolo, *A multilevel parcel-based approach to change detection in very high resolution multitemporal images* [13]: this paper presents a novel parcel-based context- sensitive technique for unsupervised change detection in very high geometrical resolution images. In order to improve pixel-based change-detection performance, the author proposes to exploit the spatial-context information in the framework of a multilevel approach. The proposed technique models the scene (and hence changes) at different resolution levels defining multitemporal and multilevel "parcels" (i.e., small homogeneous regions shared by both original images). Change detection is achieved by applying a multilevel change vector analysis to each pixel of the considered images. The adaptive nature of multitemporal parcels and their multilevel representation allow one a proper modeling of complex objects in the investigated scene as well as borders and details of the changed areas.
- W. Wang et al., *Object-oriented change detection method based on multi-scale and multi-feature fusion* [34]: to overcome the limitations of traditional pixel-level change detection methods and the difficulties of change detection of high resolution remote sensing images based on object-oriented analysis method, this paper presents an innovative object-oriented CD method based on multi-scale and multi-feature fusion for high resolution remote sensing images. Due to the good use of main characters of object-oriented thinking, this novel method can give full play to the characteristics of high resolution data and get much better results than traditional methods for detecting changes from high resolution images.
- T. Celik et al., *Unsupervised change detection for satellite images using dual-tree complex wavelet transform* [35]: in this paper, an unsupervised change-detection method for multitemporal satellite images is proposed. The algorithm exploits the inherent multiscale structure of the dual-tree complex wavelet transform (DT-CWT) to individually decompose each input image into one low-pass subband and six directional high-pass subbands at each scale. A binary change-detection mask is formed for each subband through an unsupervised thresholding derived from a mixture statistical model, with a goal of minimizing the total error probability of change detection. Then all the produced subband masks are merged by using both the intrascale fusion and the interscale fusion to yield the final change-detection mask. Extensive simulation results clearly show that the proposed algorithm not only consistently provides more accurate detection of small changes but also demonstrates attractive robustness against noise interference under various noise types and noise levels.
- Y. Bazi et al., *Unsupervised change detection in multispectral remotely sensed imagery with level set methods* [36]: in this paper, the unsupervised change-detection problem in remote sensing images is formulated as a segmentation issue where the discrimination between changed and unchanged classes in the difference image is achieved by defining a proper energy functional. The minimization of this functional is carried out by means of a level set method which iteratively

seeks to find a global optimal contour splitting the image into two mutually exclusive regions associated with changed and unchanged classes, respectively. In order to increase the robustness of the method to noise and to the choice of the initial contour, a multiresolution implementation, which performs an analysis of the difference image at different resolution levels, is proposed.

- L. Cannavacciuolo et al., *A contextual change detection method for high-resolution optical images of urban areas* [28]: this paper presents a method for unsupervised change detection of multiresolution images. The approach is based on the concept of a reference resolution, corresponding to the highest resolution in the dataset. The spatial relationships between the class labels are specified through a Markov random field model defined at the reference resolution. The adopted technique is based on a Bayesian approach with unsupervised parameter estimation. Data at reference and coarser resolutions are related by a fully specified statistical model. The estimation of the model parameter is carried by EM and by the maximum pseudo-likelihood criterion, and the classification is based on the resulting multiscale model.
- M. Dalla Mura et al., *An unsupervised technique based on morphological filters for change detection in very high resolution images* [37]: in this work an unsupervised technique for change detection in very high geometrical resolution images is proposed, which is based on the use of morphological filters. This technique integrates the nonlinear and adaptive properties of the morphological filters with a change vector analysis (CVA) procedure. Different morphological operators are analyzed and compared with respect to the CD problem. Alternating sequential filters by reconstruction proved to be the most effective, permitting the preservation of the geometrical information of the structures in the scene while filtering the homogeneous areas.

An alternative solution to the CD problem is represented by image transformation. This approach has been implemented in some works, like:

- Niemeyer et al., *Change detection using the object features* [27]: in this work, the authors propose an unsupervised change detection and change classification approach based on the object features. Following the automatic pre-processing, image objects and their object features are extracted. Change detection is performed by the multivariate alteration detection, accompanied by the maximum autocorrelation factor transformation. The change objects are then classified using the fuzzy maximum likelihood estimation (FMLE). Finally the classification of changes is improved by probabilistic label relaxation.
- A. Nielsen et al., *Kernel principal component analysis for change detection* [38]: in this work, the authors introduce a kernel version of the principal component analysis (PCA) to detect changes over time. In particular, they use kernel PCA with a Gaussian kernel for detecting changes in data consisting of two variables which represents the same spectral band covering the same geographical region acquired at two times. Unlike ordinary PCA, kernel PCA with a Gaussian kernel successfully finds the change observations in cases where nonlinearities are present.

Finally other significant automatic approaches exist, like:

- F. Del Frate et al., *Automatic change detection in very high resolution images with pulse-coupled neural networks* [39]: a novel approach based on pulse-coupled neural network (PCNNs) for image change detection is presented in this work. These networks have many desirable properties and in particular they are unsupervised and context sensitive. Such aspects are particularly useful when very high geometrical resolution images are considered as, in this case, an object analysis might be more suitable than a pixel-based one. The two waves, one for each image, generated by the PCNN during each iteration of the algorithm create specific signatures of the scene which can be compared for deciding about the occurrence of change. Applying successively procedure to a

moving window allows one to process through the whole image. Some investigations on the robustness of the settings of the PCNN parameters are currently ongoing.

Most of these techniques implicitly assume that intrinsic differences between images due to the acquisition process can be neglected. They suppose that the images under investigation are radiometrically corrected and spatially co-registered. However, as previously pointed out, even after proper preprocessing, differences (particularly from a geometrical point of view) are significant and may strongly affect the quality of the change-detection map of the most of the presented methods. In greater detail, the unavoidable residual registration noise (misalignment) between images appears significantly higher in VHR images than in MR images. For this reason in order to obtain accurate CD results, it is important also to study effective techniques for the alignment of VHR data or to develop techniques robust to such kind of noise.

2.3. Registration techniques of VHR remote sensing images

Image registration is the process of aligning two or more images acquired over the same geographical area at different times, from different viewpoints, and/or by different sensors [12]. Let $\mathbf{X_1}$ and $\mathbf{X_2}$ be two multitemporal images acquired over the same geographical area at time t_1 and t_2, respectively. Let $\mathbf{X_1}$ be the reference image and $\mathbf{X_2}$ the moving one. The objective of a registration technique is to warp the moving image on the reference one in order to align them. This process is crucial in all image analysis tasks in which the final information is gained from the combination of various data sources like image fusion, change detection, and multichannel image restoration. The majority of the registration process consists of the following four steps: (i) feature detection (i.e. control points detection - CPs); (ii) feature matching; (iii) transform model estimation; and (iv) image resampling and transformation. In the first step salient objects are identified manually or automatically in the two images under investigation (the reference and the moving one) and then represented by their point representatives (centers of gravity, line endings, corners, etc.) which are called control points (CPs); in the second step the correspondences between the features detected in the moving images and those detected in the reference image are established according to different feature descriptors and similarity measures. Then in the third step type and parameters of the function for the alignment of the moving image to the reference one (the mapping function) are estimated on the basis of the correspondences retrieved in the previous step. Finally the moving image is transformed in the fourth step according to the mapping function. How to implement each step is strictly related to the kind of images under investigation and the specific application domain. For a survey of general image registration methods please refer to [12] and [40], in which the most relevant approaches to registration developed till 2003 are described.

In the following an overview on the most recent registration methods developed for high and very high resolution multitemporal optical remote sensing images is reported. As previously pointed out, geometric distortions, different view angles in the acquisition, such us radiometric differences make the process of registration of very high geometrical resolution images very critical. As for the CD techniques, also the registration techniques developed for MR images are less effective in aligning VHR images, for the same reasons. And this significantly affects most of the analysis conducted on multitemporal VHR data. The major problems in using registration techniques developed for MR images with high and very high resolution images are: (a) a precise location of the CPs is not as simple as with MR; (b) manually selecting the large number of CPs required for precise registration is tedious and time consuming; (c) high data volume will adversely affect the processing speed in the im-

age registration; and (d) local geometric distortions cannot be removed very well using traditional image registration methods even with enough CPs.

In order to face with these problems, in the literature some examples have been proposed for the registration of VHR data, often focused on specific applications and related to the kinds of data considered [41], [42], [43]. For example in [41] a registration techniques for high resolution data is proposed for the specific case of hilly area; in [42] a feature matching method especially suitable for pre and post event images (i.e. strongly inhomogeneous image pairs) is described; in [43] an automatic registration technique of urban VHR images is presented.

In general, the new proposed techniques present novel methods for feature extraction and matching, often based on multiscale [41], [44] and local [45],[46] analysis, and apply advanced non linear transformations [47] to the images for better handle the geometric problems proper of VHR images. Interesting works in this direction are:

- Y. Li et al., *Pixel-based invariant feature extraction and its application to radiometric co-registration for multi-temporal high-resolution satellite imagery* [44]: in this paper a robust fully automated method for relative radiometric co-registration is presented. First, a new low dimensional feature-point descriptor, called the Expanded Haar-Like Filter (EHLF) descriptor, is introduced. The EHLF has many desirable properties like flexible design, fast computation, and multiscale description, while also being insensitive to variations in image quality. Then, two spatial matching schemes are proposed for increasing the percentage of correctly matched feature points. The first is based on a global affine model and the second utilizes dynamic local template fuzzy distance matching. Finally, precise pixel-to-pixel invariant feature points are extracted from a diversity of image locations centered at matched local extrema points.
- G. Danchao et al., *Image registartion of high resolution remote sensing based on straight line feature* [47]: in this paper a registration algorithm based on line feature is described. First, the lines in both images are extracted; then a modified iterated Hough transform is introduced to develop the correspondences of the lines; finally, the parameters for an affine transformation are evaluated, based on a similarity measure of the distance of corresponding straight line segments.
- V. Arevalo et al., *Improving piecewise linear registration of high-resolution satellite images through mesh optimization* [46]: in this work the registration process of two images is obtained through an optimization of the local analysis based on triangular mesh; in particular, the optimization process consists in setting the appropriate topology upon the mesh vertices (once the mesh vertices position have been decided). In addition, the mutual information is used for measuring the registration consistency within the optimization process.
- N. Taleb et al., *An automatic image registration for applications in remote sensing* [45]: in this paper the registration process involves an edge-based selection of CPs in the reference image, followed by the searching of corresponding CPs in the moving one based on local similarity detection by means of template matching according to a combined invariants-based similarity measure. Finally the warping of the images is performed by using the thin-plate splines interpolation.

In some works the feature extraction step is implements as a road extraction problem, as in:

- X. Guo et al., *Automatic urban remote sensing images registration based on road networks* [43]: this paper proposes a method of automatic registration of urban remote sensing images that combines bilinear interpolation and road networks extraction. It comprises of extracting the road network in an urban area and computing the ground control points from the road junctions, then estimating the parameters of the mapping function and transforming the moving image.

- Y. Zhao et al., *Feature-based geometric registartion of high spatial resolution satellite imagery* [48]: this paper develops an improved feature-based geometric registration approach in which the CPs are efficiently selected automatically. First a modified watershed is used for image segmentation, then regions are represented by centers of gravity and road intersections are considered as the main target to perform the CPs extraction. Finally the extracted points are matched through spatial relations and the moving image is transformed according to the derived model.

In other works the registration process is conducted by generating the so-called disparity map (i.e. a map of the value of the displacement for each pixel), that is a particular case of estimation of spatial transform between two images where the transform cannot be represented analytically [49], and then using the information present in this map for transforming the image, like:

- M. di Bisceglie et al., *Image registration using non-linear diffusion* [50]: this work presents an image registration algorithm based on mutual information maximization and non-linear diffusion. It relies on a non-parametric estimation of the degree of dependency between reference and moving image which is intrinsically more robust against possible deformations due to imaging geometry and propagation disturbances. The approach based on non linear diffusion, nonetheless, has the advantage of producing a non-parametric discrete warping model which does not rely on a particular set of basis functions, and is therefore as much general as possible.
- Borzì et al., *Robust registration of satellite images with local distortion* [51]: a new method for registration of remote sensing images in the presence of local distortion is described in this paper. The template matching is performed using as a measure the Cumulative Residual Entropy, then the mapping of the moving image to the reference one is represented by a field of displacements vectors (the disparity map). Before warping the images a vector regularization based on a diffusion equation is applied to the displacement vector, in order to produce a more homogeneous displacement map, reducing the presence of anomalous patterns.

Finally some works have been proposed also for the registration of images acquired by different sensors, like[52], [53], [54], [55] or for the specific problem of aligning the panchromatic channel to the multispectral ones [56], [57].

2.4. Theoretical background

In this section the polar framework for Change Vector Analysis (Polar CVA) defined in [11] is described. This framework is at the base of most of the proposed analysis and methods of this thesis.
Let us consider two VHR multispectral images $\mathbf{X}_1$ and $\mathbf{X}_2$ acquired on the same geographical area at different times t_1 and t_2, respectively. Let X_1 and X_2 be two multidimensional random variables that represent the statistical distributions of pixels in images $\mathbf{X}_1$ and $\mathbf{X}_2$, respectively. Let $X_{b,t}$ be the random variable representing the bth (b=1,…,B) component of the multispectral image $\mathbf{X_t}$ (t=*1, 2*) in the considered feature space. Let us assume that these images do not show significant radiometric differences, in particular let us consider that the spectral channels at the two times have the same mean values (this can be easily obtained with very simple radiometric correction procedures) and are co-registered. Let $\Omega = \{\omega_n, \Omega_c\}$ be the set of classes of changed and no-changed pixels to be identified. In greater detail, ω_n represents the class of no-changed pixels, while $\Omega_c = \{\omega_{c_1}, ..., \omega_{c_K}\}$ the set of the K possible classes (kinds) of changes occurred in the considered area. As previously pointed out in order to detect changes between the two images a comparison should be performed according to a proper operator. When dealing with multispectral images, the comparison operator is usually the vec-

tor difference, which is applied to a *B*-dimensional feature space in order to give as input to the change-detection process all the relevant spectral information. This technique is known as CVA [58] and has been successfully used in many different application domains [59], [60], [61], [62]. CVA first computes a multispectral difference image ($\mathbf{X_D}$) subtracting the spectral feature vectors associated with each corresponding spatial position in the two considered images $\mathbf{X}_1$ and $\mathbf{X}_2$. Let $\mathrm{X_D}$ be the multidimensional random variable representing the spectral change vectors (SCVs) in the difference image obtained as follows [21]:

$$\mathrm{X_D} = \mathrm{X_2} - \mathrm{X_1} \tag{2.1}$$

In this treatment, for simplicity, we will assume that the CVA technique is applied only to two spectral channels of the considered multitemporal images, i.e., that a 2-D coordinate system is sufficient to completely describe the change-detection problem. However, the analysis can be generalized to the case of more spectral channels by considering more direction contributions for describing each SCV (see [11] for more details).

The spectral change vectors can be described through two different components: the magnitude and the direction, defined as:

$$\rho = \sqrt{(X_{1,D})^2 + (X_{2,D})^2} \quad \text{and} \quad \vartheta = \tan^{-1}\left(\frac{X_{1,D}}{X_{2,D}}\right) \tag{2.2}$$

where $X_{b,D}$ is the random variable representing the *b*th component (spectral channel) of $\mathbf{X}_D$ (b={1,2}).

However, the standard CVA technique considers only the magnitude component. In particular, in the standard CVA the *B*-dimensional problem described by $\mathrm{X_D}$ is reduced to a 1-dimensional problem by considering only the magnitude component of each SCVs.

According to the expression of ρ in (2.2), no-changed pixels present small magnitude values, whereas changed pixels show large values [11], [15]. Let $x_\rho(i, j)$ be a generic pixel in spatial position (i, j) in the magnitude image (i.e. the image reporting for each pixel the value of ρ of the corresponding SCV). The CD map Y where changed and no-changed pixels are separated can be computed according to the following decision rule:

$$y(i, j) = \begin{cases} \Omega_c & \text{if } x_\rho(i, j) \geq T \\ \omega_n & \text{if } x_\rho(i, j) < T \end{cases} \tag{2.3}$$

where $y(i, j)$ is the label associated to the pixel at spatial position (i, j) in Y, and T is the decision threshold. T can be defined either manually or automatically [15].

According to the given description it is clear that in the final change-detection map generated by the CVA approach all the pixels that have significant spectral differences in the two images under investigation are reported. For this reason it is important to have images very similar to each other; therefore effective pre-processing procedure (geometric and radiometric correction and registration) should be applied to them before CVA. In addition, no information about different kinds of change is provided.

In the literature, few examples exist that consider both the magnitude and the direction of the SCVs in the generation of the CD map [11], [60], [63] most of them carried out in an empirical way. This variable contains important information, especially for discriminating among different kinds of change.

In this thesis we consider the information given by both the variables, taking advantages from a 2D representation of the spectral change vectors in a polar domain presented in [11]. In the following a description of such polar framework is given.

According to the definition of magnitude and direction given in (2.2), let us define the magnitude-direction domain *MD* (in which all the SCVs of a given scene are included) as:

$$MD = \left\{ \rho \in \left[0, \rho_{\max}\right] \text{ and } \vartheta \in \left[0, 2\pi\right] \right\} \tag{2.4}$$

where ρ_{max} is the highest magnitude of SCVs in the considered multitemporal dataset.

According to the previous definitions, the change information for a generic pixels in spatial position (*i*,*j*) can be represented in the magnitude-direction domain with a vector z_{ij} having components ρ_{ij} and ϑ_{ij} computed according to (2.2).

From the theoretical analysis reported in [11] and under the above-mentioned assumptions, it is expected that in the polar representation no-changed and changed SCVs result in separated clusters. Unchanged SCVs show a low magnitude and are uniformly distributed with respect to the direction variable. In the polar domain the region associated with them is the *circle of no-changed pixels* C_n, defined as:

$$C_n = \left\{ \rho, \vartheta : 0 < \rho \le T \text{ and } 0 \le \vartheta < 2\pi \right\} \tag{2.5}$$

This circle is centered at the origin and has a radius equal to the optimal (in the sense of the theoretical Bayesian decision theory) threshold *T* that separates no-changed from changed pixels. On the opposite, changed SCVs are expected to show a high magnitude. The region associated with them in the polar domain is the *annulus of changed pixels* A_c, which is defined as:

$$A_c = \left\{ \rho, \vartheta : T \le \rho < \rho_{\max} \text{ and } 0 \le \vartheta < 2\pi \right\} \tag{2.6}$$

This annulus has inner radius *T* and outer radius given by the maximum among all possible magnitudes for the considered pair of images ($\rho_{\max}$). As changed SCVs show preferred directions according to the kind of change occurred on the ground, different kinds of changes can be isolated with a pair of threshold values (ϑ_{k_1} and ϑ_{k_2}) in the direction domain. Each pair of thresholds identifies an *annular sector* S_k *of change* $\omega_{c_k} \in \Omega_c$ in the *annulus of changed pixels* A_c defined as:

$$S_k = \left\{ \rho, \vartheta : \rho \ge T \text{ and } \vartheta_{k_1} \le \vartheta \le \vartheta_{k_2}, 0 \le \vartheta_{k_1} < \vartheta_{k_2} \le 2\pi \right\} \tag{2.7}$$

All the mentioned regions are depicted in Figure 2.2. Please refer to [11] for further details on both the polar framework and the general properties of SCVs in this kind of representation.

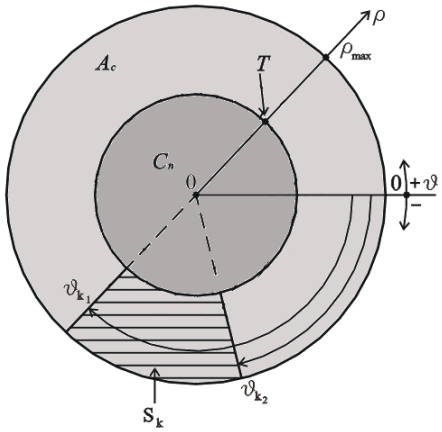

Figure 2.2. Representation of the regions of interest in the CVA polar framework

PART I:
REGISTRATION NOISE AND REGISTRATION TECHNIQUE

Chapter 3

3. Analysis and adaptive estimation of the registration noise distribution in multitemporal VHR images[1]

This chapter analyzes the problem of change detection in very high resolution (VHR) multitemporal images by studying the effects of residual misregistration (registration noise) between images acquired on the same geographical area at different times. In particular, according to an experimental analysis driven from a theoretical study, the main effects of registration noise on VHR images are identified and some important properties are derived and described within the polar framework for change vector analysis (see section 2.4). In addition, a technique for an adaptive and unsupervised explicit estimation of the registration noise distribution in the polar domain is proposed. This technique derives the registration noise distribution according to both a multiscale analysis of the distribution of spectral change vectors and the Parzen windows method. Experimental results obtained on simulated and real images confirm the validity of the proposed analysis, the reliability of the derived properties on registration noise, and the effectiveness of the proposed estimation technique. This technique represents a very promising tool for the definition of change-detection methods for VHR multitemporal images robust to registration noise.

3.1. Introduction

The ever increasing availability of remote sensing images regularly acquired by satellites over the same geographical area makes the analysis of multitemporal data (and the related applications) one of the most interesting research topics for the remote sensing community. Multitemporal images represent a valuable information source for performing the detection of changes occurred on the Earth surface at different scales. Change-detection techniques generally compare two images acquired at different times by assuming that they are similar to each other except for the presence of changes occurred on the ground. Unfortunately, this assumption is seldom completely satisfied due to differences in atmospheric and sunlight conditions, as well as in the sensor acquisition geometry. In order to satisfy the similarity assumption, pre-processing steps are required, including: image co-registration, radi-

[1] This chapter is published on *IEEE Transaction on Geoscience and Remote Sensing*, Vol. 47, no. 8, 2009, pp. 2658-2671. Title: "Analysis and Adaptive Estimation of the Registration Noise Distribution in Multitemporal VHR Images". Authors: F. Bovolo, L. Bruzzone and S. Marchesi.

ometric and geometric corrections, and noise reduction. Among the others, co-registration plays a fundamental role as it allows one to obtain a pair of images where corresponding pixels are associated with the same position on the ground. However, in practice, it is not possible to obtain a perfect alignment between images acquired at different times. This may significantly affect the accuracy of the change-detection process. The co-registration procedure becomes more complex and critical (and therefore intrinsically less accurate) when very high resolution (VHR) images acquired by the last generation sensors (e.g. WorldView, Ikonos, Eros, Quickbird, SPOT-5) are considered. These images can be acquired with different view angles and often show different geometrical distortions that, even after proper geometric corrections, strongly affect the precision of the registration process, thus resulting in a significant residual registration noise (RN). This noise sharply decreases the accuracy of the change-detection process.

In the literature large attention has been devoted to the development of advanced registration techniques, especially for what concerns medium resolution multitemporal and multisensor images [12], [40], [64], [65], [66]. Moreover, some studies exist on the effects of misregistration on the change-detection accuracy [8], [14], [67], [68], [69], [70] and on the development of change-detection techniques less sensitive to problems due to misregistration [71], [72]. Nonetheless, in our knowledge few attentions have been devoted to study the effects and the properties of registration noise in VHR images.

This work aims at analyzing the properties of registration noise in multitemporal VHR images in order to formulate an adaptive technique for the explicit estimation of the distribution of residual RN between multitemporal images. This distribution is a starting point for the development of novel change-detection techniques robust to such source of noise. The present study is developed within a polar framework for change vector analysis (CVA) recently introduced in the literature for change detection in medium resolution multispectral images [11]. The definition of this framework is based on the analysis of the distribution of spectral change vectors (SCVs) computed according to the CVA technique in the polar domain. In this context, the novel contributions of this work consist in: i) the analysis of the effects of registration noise in multitemporal and multispectral VHR images according to the study of the statistical distribution of SCVs; ii) the definition of the properties of registration noise in VHR images; and iii) the formulation of an adaptive and distribution-free technique for the estimation of the distribution of the registration noise in the polar domain. This last technique exploits the Parzen windows estimation procedure and takes advantage from both a multiscale decomposition of multitemporal images and the properties derived in the first part of this work. The experiments carried out on simulated and real multitemporal images confirm the validity of the theoretical analysis and the effectiveness of the proposed technique, which represents a valuable tool for the development of reliable change-detection techniques for multitemporal and multispectral VHR images. It is worth noting that the proposed method can be suitable also for the analysis of optical data at lower resolution, however we consider only very high geometrical resolution images as the impact of misregistration on this kind of data is more relevant. For a description of the framework proposed in [11] and used in this chapter and for an overview on the notation used in the following sections please refer to section 2.4.

The chapter is organized into six sections. The next section describes the experimental setup for the study of the properties of registration noise on simulated multitemporal VHR images. Section 3.3 derives and defines the properties of registration noise. Section 3.4 illustrates the proposed approach to the estimation of the distribution of registration noise in the polar domain. Section 3.5 presents the validation on real multitemporal Quickbird images of both the derived properties and the proposed

technique for the estimation of the registration noise. Finally, section 3.6 draws the conclusions of this work.

3.2. Design of the analysis and experimental setup

The objective of this work is to study the effects of misregistration within the framework presented in section 2.4 in order to derive its properties and to define a procedure for an adaptive estimation of the distribution of registration noise. As previously mentioned, residual misregistration affects multitemporal data and represents an important source of noise. In particular, this noise becomes more relevant when dealing with VHR images, as the process of co-registration is more complex and critical. Indeed, images acquired by VHR sensors of the last generation can be acquired with different view angles and often show different geometrical distortions that strongly affect the registration process. Thus, they result in a significant amount of residual registration noise. For this reason, it is very important to study the properties of registration noise and to define techniques for estimating its distribution (which is a valuable information to be given as input to CD methods).

RN is due to the comparison of pixels that do not represent the same area on the ground in images acquired over the same geographical area at different times. In particular, the most critical component of RN is related to the pixels that at the two dates belong to different objects/classes on the ground (as discussed in the next section) due to the misalignment between the two images. In fact, these pixels show a behavior similar to the one of real changes, causing misclassification effects in the change-detection process. It follows that it is important to identify these pixels and separate them from pixels associated with real changes in the multitemporal data analysis.

The residual registration noise can be modeled as the effect of different types of transformations between the images, such as scale variation, rotation, translation and skew [8]. In this section, for space constraints, only examples modeling the registration noise as a translational effect are reported; however this choice is reasonable as, according to [8], non-translational effects show (from a statistical viewpoint) a behavior similar to that of the translational ones. This behavior is confirmed by experimental results obtained with misregistered datasets generated considering relative rotation and roto-translation, which are not reported here for space constraints.

In order to study the registration noise in the polar CVA domain several data sets have been selected by considering: (i) very high geometrical resolution images acquired by different sensors (i.e., Quickbird, Ikonos, and Pleiades simulator); and (ii) areas with different characteristics, representative of the most frequent land-cover types (i.e., urban, rural, and forestry). Three different experiments have been defined to understand the behavior of RN on unchanged and changed pixels when the misalignment between images increases and the resolution level decreases. To avoid intrinsic differences between images typical of real multitemporal data sets (e.g., atmospheric differences, *etc.*), in the first phase of the analysis a single-date image has been considered for each data set, while the second acquisition has been simulated. The analysis carried out on the single-date data sets is then extended to real multitemporal images in section 3.5.

In the following we describe the experiments considering the analysis conducted on a Quickbird image acquired on the city of Trento (Italy) in July 2006 ($\mathbf{X}_1$). The selected test site is a section of a full scene including both rural and urban areas (Figure 3.1 (a)). Results obtained on other data sets (which contain areas with other characteristics and images acquired by other sensors) are very similar to those reported here, and thus omitted for space constraints. In the following, after an accurate preliminary analysis, among the four available spectral channels, only the red and the near infrared ones were considered for analyzing the distributions in the polar domain, as they demonstrated to be the most effec-

tive in emphasizing the properties of RN (with respect to both changed and unchanged pixels) on the adopted data set. Different choices led to poorer visual representations but to similar conclusions.

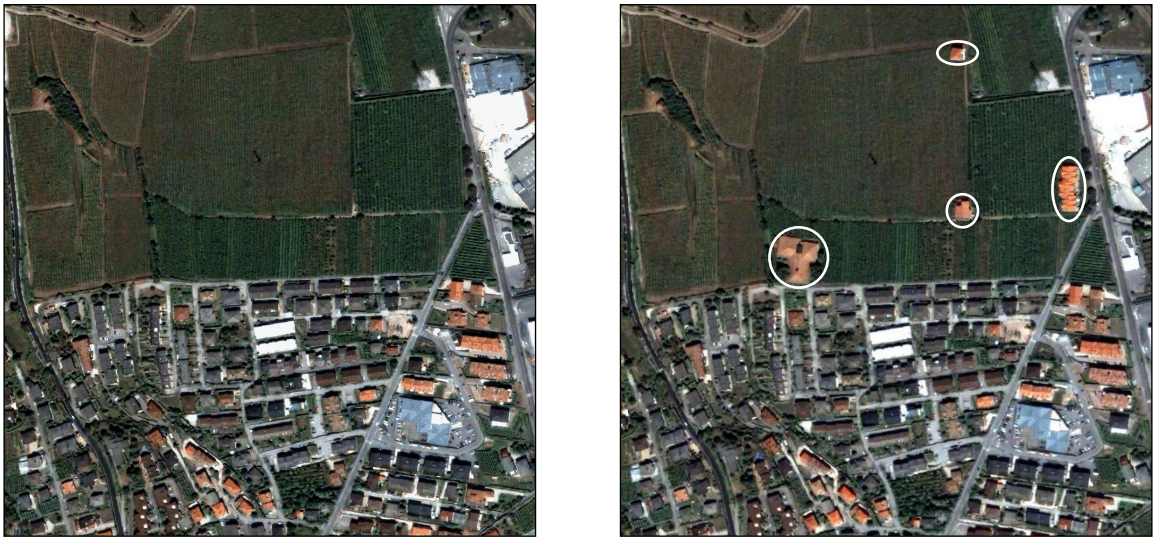

(a) (b)

Figure 3.1True color composition of pansharpened image of the city of Trento (Italy) acquired by the Quickbird VHR multispectral sensor in July 2006 (a) original image without simulated changes, (b) original image with simulated changes (pointed out with white circles).

3.2.1 Experiment 1: effects of increasing misregistration on unchanged pixels

From the considered image $\mathbf{X}_1$ different simulated images $\mathbf{X}_2$ have been generated introducing some pixels of misregistration according to translations in several directions. This resulted in different multitemporal data sets made up of the original image $\mathbf{X}_1$ and of its shifted versions $\mathbf{X}_2$. In particular, we considered misregistration between 1 and 6 pixels, which are possible values when taking into account large VHR images acquired with different view angles and/or in complex areas. After the application of the CVA, the SCV distributions were analyzed in the polar scatterograms in order to derive the properties of RN on unchanged pixels. It is worth noting that the application of the CVA technique to $\mathbf{X}_1$ and a copy of itself when images are perfectly co-registered leads to a multispectral difference image made up of SCVs with all zero components. Thus the representation in polar coordinates of SCVs collapses in a single point at the origin. This is no longer valid if the CVA is applied to misregistered images; in this case the distribution of SCVs in the polar domain corresponds to the distribution of registration noise (as no changes are present in the considered data set). Figure 3.2 shows an example of the behaviors of scatterograms obtained by applying the CVA technique to $\mathbf{X}_1$ and its 2- and 6-pixels shifted versions, respectively. An analysis of these scatterograms allows us to derive the properties of registration noise when no changes are present between the considered images (see section 3.3).

3.2.2 Experiment 2: effects of increasing misregistration on changed pixels

From the considered image $\mathbf{X}_1$ a new image $\mathbf{X}_2$ has been generated by adding simulated changes. These changes have been accurately introduced in order to be as similar as possible to real changes. In particular, some buildings have been added to the scene [see regions marked with white circles in Figure 3.1(b)] taking their geometrical structures and spectral signatures from other real buildings present in the image. All the mentioned buildings have similar spectral signatures and are located on agricultural fields. Therefore the solution to the simulated change-detection problem requires the iden

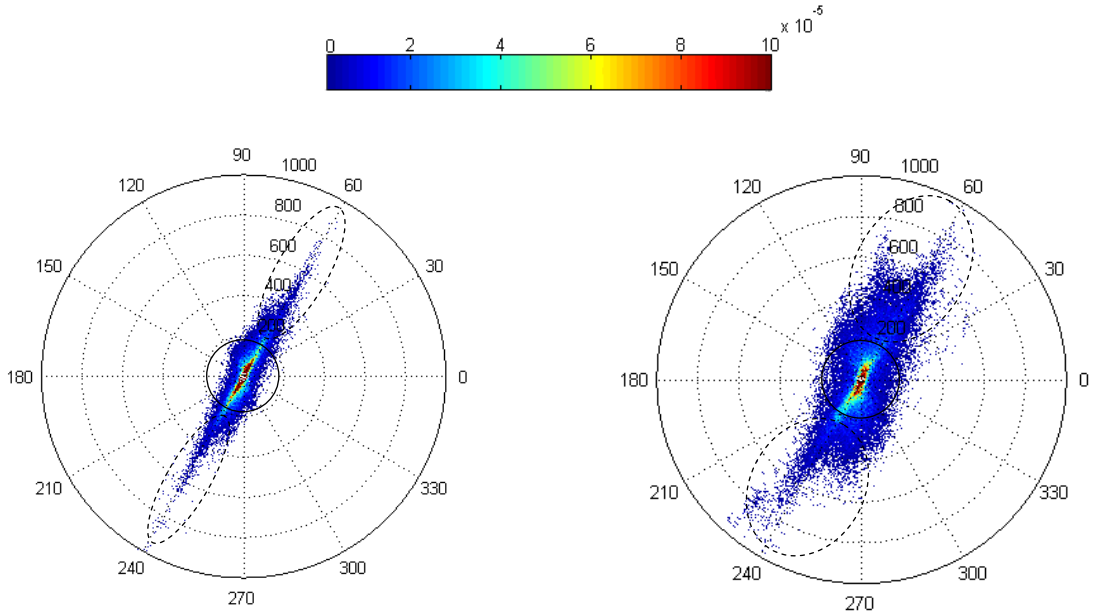

(a) (b)

Figure 3.2. Scatterograms in the polar coordinate system obtained by applying CVA to the simulated multitemporal data sets (which do not contain any change) that show (a) 2 pixels, and (b) 6 pixels of residual misregistration (Experiment 1).

tification of a single class of changed pixels (ω_{c_1}). As in the first experiment, from the simulated image six new images have been generated introducing some pixels of residual misregistration. This resulted in seven multitemporal data sets made up of the original image ($\mathbf{X}_1$) and one of the simulated images ($\mathbf{X}_2$). In particular, the two images in the first data set are perfectly aligned and differ only for the simulated changes, while the images in the other data sets show also a residual misregistration between 1 and 6 pixels. It is worth noting that when the images are perfectly co-registered the application of the CVA technique to $\mathbf{X}_1$ and to the image obtained introducing simulated changes leads to a multispectral difference image made up of SCVs with non-zero values only for the simulated changes. Other non-zero SCVs (associated with RN) appear if we compute the scatterograms of pair of misregistered images. Figure 3.3 shows an example of the behaviors of such scatterograms obtained by applying the CVA technique to the image $\mathbf{X}_1$ and: (a) the simulated image perfectly aligned; (b) the simulated image with 2 pixels of residual misregistration; and (c) the simulated image with 6 pixels of residual misregistration. An analysis of these scatterograms (and of the others obtained for different values of misregistration) allowed us to derive the properties of the registration noise on the class of changed pixels (see section 3.3).

3.2.3 Experiment 3: effects of misregistration at different scales

Further data sets have been generated from the considered image ($\mathbf{X}_1$) and the simulated image including changes with a four-pixel misregistration ($\mathbf{X}_2$) by applying to them a decomposition filter. In this manner two sets of images ($\mathbf{X}_1^n$ and $\mathbf{X}_2^n$, n=1,2…,N) have been generated that have lower scale (resolution) than the original ones. These images show a consistent decrease in detail content. In order to obtain the multiscale representation of the images, in the experimental phase different decomposition approaches have been used, as Laplacian/Gaussian pyramid decomposition, iterative sliding window low pass filter, recursively upsampled bicubic filter, wavelet transform. All these approaches provided similar results. For this reason we report only the analysis obtained by applying to $\mathbf{X}_1$ and $\mathbf{X}_2$

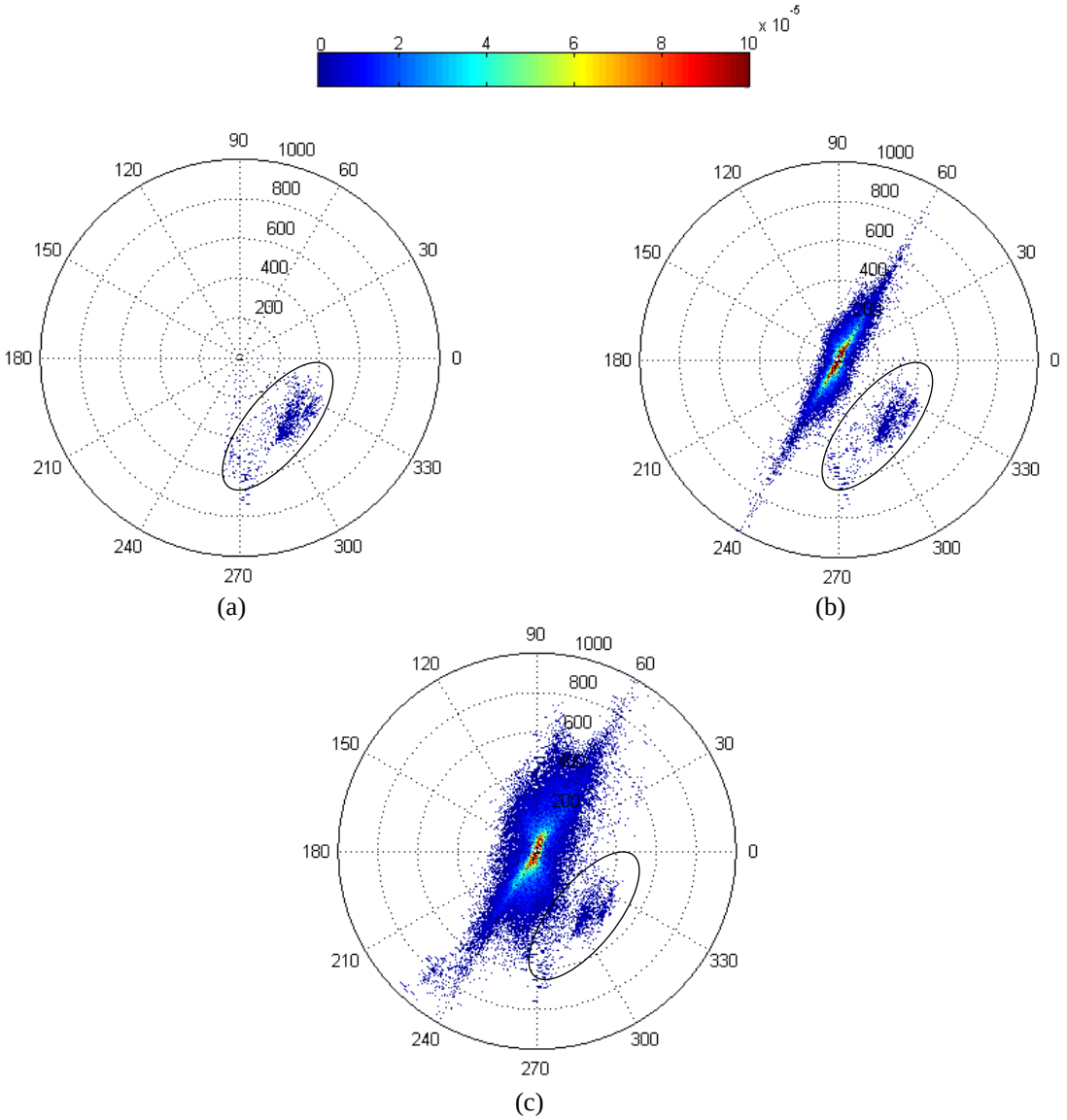

Figure 3.3. Scatterograms in the polar coordinate system obtained by applying CVA to the simulated data sets containing changes in the case of (a) perfect alignment between images, (b) 2 pixels of residual misregistration, and (c) 6 pixels of residual misregistration (Experiment 2).

the *Daubechies-4* stationary wavelet transform [73], [74]. In the following, as an example, the results achieved considering the pair of images obtained at the third decomposition level (n=3) are reported. It is worth noting that the choice of the level of decomposition is strictly data and application dependent (see section VI for details). Figure 3.4 reports the scatterograms obtained by applying the CVA technique to images $\mathbf{X}_1$ and $\mathbf{X}_2$ (full resolution) and to $\mathbf{X}_1^3$ and $\mathbf{X}_2^3$, respectively. By comparing these scatterograms (and the others obtained for different values of misregistration and at different resolution levels, which are not reported for space constraints) it is possible to study the effects of multiscale decomposition on the distribution of registration noise and of real changes (see section 3.3).

3.3. Properties of registration noise in VHR images

An analysis of the scatterograms obtained from the three sets of previously described experiments, and a study on the behavior of SCVs in the polar domain for each investigation setup allowed us to derive some important properties of the registration noise on both unchanged and changed pixels.

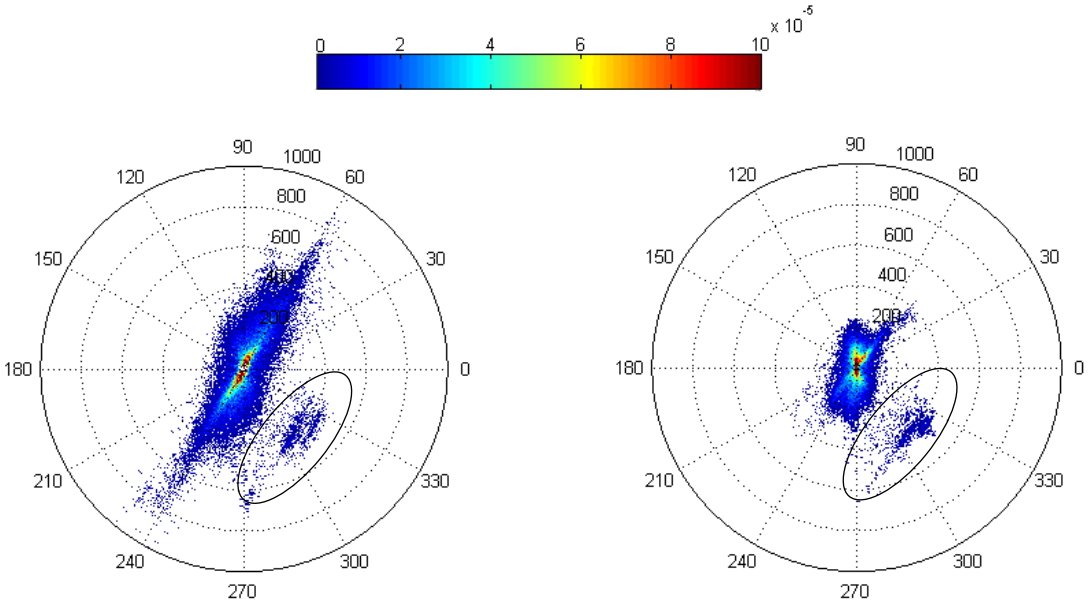

Figure 3.4. Scatterograms in the polar coordinate system obtained by applying the CVA technique to the simulated data sets containing changes (a) at full resolution, and (b) at a lower scale (level three) (Experiment 3).

Property 1. *RN affects unchanged pixels by: a) increasing the spread of the cluster in the circle of unchanged pixels C_n with respect to the case of perfectly aligned images; b) generating clusters of dominant registration noise in the annulus of changes A_c that have properties very similar to those of changed pixels.*

Experiment 1 makes it possible the study of the behavior of the distribution of registration noise (associated with the distribution of SCVs) versus different amounts of misregistration in the polar domain. As the misalignment increases, the number of multitemporal pixels having the same coordinates but that do not correspond to the same position on the ground at the two dates increases. Therefore, the CVA technique performs a comparison between pixels that are not associated to the same area on the ground due to the misalignment. This results in two different contributions to the distribution of RN in the polar domain: (i) the first one is related to the comparison of pixels that belong to the same object in the two images, but that are not associated with the same position on the ground due to misregistration (slightly different spectral signatures due to the heterogeneity of objects in VHR images); (ii) the second one comes from the comparison between pixels that belong to different objects in the two images (pixels associated with details and border regions). These contributions result in: (a) an increase of the standard deviation of the cluster of unchanged pixels when RN increases, and (b) the generation of cluster of unchanged pixels with properties very similar to those of real changes.

Sub-property 1.a. *The spread of the cluster in C_n increases by increasing the misalignment.*

Let us consider at first only the effect of the spectral differences between misaligned pixels of the same object. This effect can be observed in the scatterograms of Figure 3.2, where some SCVs associated with unchanged pixels that should stay in C_n fall in A_c. Nevertheless, they still show a relative low magnitude and a rather uniform distribution along the direction variable, as it happens for medium resolution images [11] (see regions marked with the continuous line circle in Figure 3.2). We can observe that the spread of the cluster of unchanged pixels increases, exhibiting an effect that is sharply amplified with respect to medium resolution images, due to the higher spectral heterogeneity within the objects. It is worth noting that the rather uniform distribution of SCVs along the direction is

due to the fact that the structures of objects are usually different for different elements in the scene.

A quantitative analysis carried out on both the magnitude and the direction of SCVs shows that the standard deviation σ_{ω_n} of the class of unchanged patterns ω_n increases in a non-linear way by increasing the misalignment (see Figure 3.5) and, as expected, it tends to saturate when the residual registration noise is over a given threshold.

Statistically, as reported in [11] for the class of unchanged pixels, registration noise generated by the comparison of pixels that belong to the same object can be modeled as a mixture of Gaussian distributions with the same mean values (as the distributions at the two dates are related to the same class) in the Cartesian domain, which corresponds to a Rayleigh distribution along the magnitude variable of the polar domain and to a uniform distribution along the direction variable.

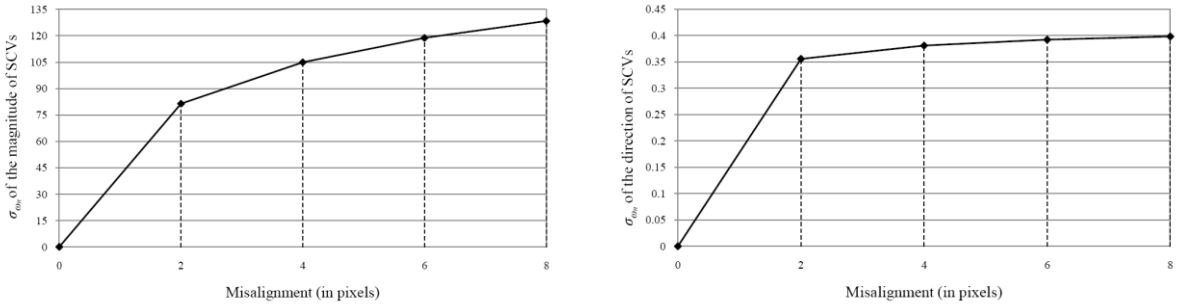

(a) (b)

Figure 3.5. Behaviors of the standard deviation of (a) the magnitude and (b) the direction of the SCVs in the cluster of unchanged pixels versus the number of pixels of misalignment(Experiment 1).

Sub-property 1.b. *The clusters of dominant registration noise in A_c have properties very similar to those of real changes and are made up of a number of patterns that increases by increasing the misalignment.*

Let us now consider the effects of pixels that at the two acquisition dates belong to different objects on the ground. In this case significantly different spectral signatures are compared leading to SCVs with large magnitude values. This behavior can be observed in the scatterograms of Figure 3.2 where it is possible to note that a large number of unchanged SCVs show a magnitude significantly higher than expected, thus falling in A_c (see regions marked with dashed circles in Figure 3.2). In the medium resolution case the distribution of such SCVs is nearly uniform along the direction [11]. On the contrary, when dealing with VHR images, their distribution has preferential directions, resulting in clusters of pixels of registration noise in A_c that exhibit properties very similar to those of changed pixels. Such an effect is mainly due to the comparison of misaligned pixels belonging to different objects with similar structures in different positions of the images. This can be explained, for example, with the regular structure of the urban areas and of the crop rows, as well as with the high frequency content of the VHR images. The number of SCVs composing these clusters increases by increasing the amount of RN. It is worth noting that, on the contrary, when dealing with medium resolution images, the number of misregistered pixels belonging to different objects is small and the effects of registration noise less evident and more uniformly distributed along the direction variable. This is due to both the small amount of geometrical details contained in such images, and the intrinsic effectiveness of classic registration algorithm on medium resolution data. We define the annular sectors in the polar domain associated with these clusters as *sectors of dominant registration noise* $S^D_{RN_i}$:

$$S_{RN_i}^{D} = \left\{ \rho, \vartheta : \rho \geq T \text{ and } \vartheta_{i_1} \leq \vartheta \leq \vartheta_{i_2}, 0 \leq \vartheta_{i_1} < \vartheta_{i_2} < 2\pi \right\} \tag{3.1}$$

Each $S_{RN_i}^{D}$ can be represented in the polar domain as a sector within A_c bounded from two angular thresholds ϑ_{i_1} and ϑ_{i_2}. This is not surprising as SCVs due to misregistration, exactly as SCVs of true changes, are originated from the comparison of pixels that are associated with different objects on the ground at the two acquisition dates. It follows that sectors of dominant registration noise are very critical because at full resolution they cannot be distinguished from sectors of true changes, resulting in a significant false alarm rate in the change-detection process. Statistically, as reported in [11] for the class of changed pixels, registration noise generated by the comparison of pixels that belong to different classes can be modeled as a mixture of Gaussian distributions with different mean values in the Cartesian domain which corresponds to a Ricean distribution along the magnitude variable of the polar domain and to a non-uniform distribution along the direction variable.

Property 2. *Statistical properties of clusters associated with changed pixels in A_c slowly vary with the amount of misalignment.*

Experiment 2 points out the behaviors of SCVs associated with changed pixels versus the amount of misalignment that affects the considered simulated data sets. Observing Figure 3.3 it is possible to note that SCVs associated with the class of changed pixels ω_{c_1} are not significantly affected by an increase of the amount of misregistration between images. Indeed, the cluster of changed pixels can be easily identified in all the three scatterograms and shows quite stable behaviors (see regions marked with circles in Figure 3.3). The position of the annular sector S_1 (which identifies pixels belonging to ω_{c_1}) is almost invariant with the misregistration. This behavior allows one to conclude that the registration noise does not affect significantly the properties of the cluster of changed pixels. This is confirmed from a quantitative analysis of the behavior of the mean value μ_{ω_c} and standard deviation σ_{ω_c} of the magnitude of SCVs in the cluster of changed pixels ω_c (for simplicity of notation in the following ω_{c_1} will be indicated as ω_c) versus the amount of misregistration (in pixels). As can be seen from Figure 3.6, these behaviors do not show significant variations by increasing misregistration.

Nonetheless, the RN indirectly affects the detection of changed pixels (see Property 1) as: (i) the overlap between clusters of changed and unchanged pixels increases when the standard deviation of the patterns in C_n increases; (ii) the presence of sectors of dominant RN in A_c results in false alarms.

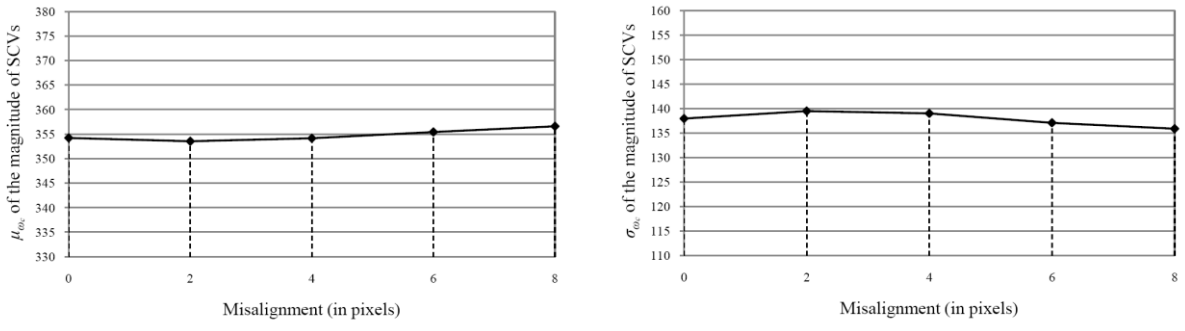

(a) (b)

Figure 3.6. Behaviors of (a) the mean value μ_{ω_c} and (d) the standard deviation σ_{ω_c} of the magnitude of SCVs in the cluster of changed pixels versus registration noise in the considered images (Experiment 2).

Property 3. *Clusters of dominant registration noise in A_c exhibit significant variations of properties versus the scale (resolution) of the images.*

From experiment 3 we can observe the effects of a multiscale decomposition of the images on pixels associated with both changed and unchanged areas. Let us first consider only unchanged pixels (changed pixels will be discussed in Property 4). As the resolution of the images decreases the presence of small and thin structures diminishes. This results in a reduced impact of registration noise at lower scales (resolutions) as the details and border regions are smoothed out from the low-pass effects associated with scale reduction. Comparing the scatterograms of Figure 3.4 (derived from experiment 3) it can be observed that reducing the scale, SCVs associated with registration noise tend to disappear. In other words, decreasing the resolution sectors of dominant registration noise tend to disappear, thus exhibiting a non stationary behavior with respect to the scale. In particular, such SCVs tend to collapse within C_n. This is confirmed from Figure 3.7, which reports the behavior of the mean value of the magnitude of SCVs associated with RN versus the resolution level (scale). As can be seen from the continuous line in the diagram, the mean value of RN clusters rapidly decreases by reducing the resolution. This property is very important in the definition of a strategy for estimating the distribution of RN in VHR images (see section 3.4).

Property 4. *Clusters associated with changed pixels in A_c exhibit slow varying statistical properties versus the scale (resolution) of the images.*

From experiment 3 it is also possible to observe the behavior of the cluster of changed pixels when the scale decreases. Observing regions marked with circles in Figure 3.4, it is possible to note that the cluster of pixels associated with true changes reduces its spread, but it is not completely smoothed out when the resolution decreases. In other words, it shows a nearby stationary behavior versus the resolution. This is confirmed by an analysis of the behavior of the mean value of the magnitude of SCVs associated with true changes versus the scale. As it can be seen from the dashed line in Figure 3.7, the mean value slightly varies with the resolution, but it decreases slower than the one of SCVs associated with registration noise (continuous line in Figure 3.7).

From properties 3 and 4 it follows that the behaviors of changed and unchanged (i.e., the ones due to RN) SCVs that fall in A_c versus the resolution are different: decreasing the resolution, sectors of changes, unlike sectors of dominant registration noise, are preserved. It is worth noting that this property is true under the reasonable and realistic assumption that given the very high geometrical resolution of the sensor, the true significant changes are associated with objects with a non-negligible size. This results in an intrinsic robustness of changes to the scale. On the contrary, misregistration appears in the difference image with linear (or non linear) and relatively thin structures having different orientations, that are smoothed out from the scale reduction process. Properties 3 and 4 can be exploited for defining an adaptive strategy for estimating the statistical distribution of registration noise. This strategy is described in the next section.

3.4. Proposed technique for the adaptive estimation of the RN distribution

The properties of RN described in the previous section suggest us to exploit the behaviors of SCVs in the polar domain at different resolution levels (scales) for explicitly estimating the statistical distribution of RN. In particular, properties 3 and 4 clearly show the usefulness of a multiresolution decomposition in identifying and separating annular sectors of dominant registration noise from annular sectors of real changes. Given the very high geometrical resolution of images, we assume that true

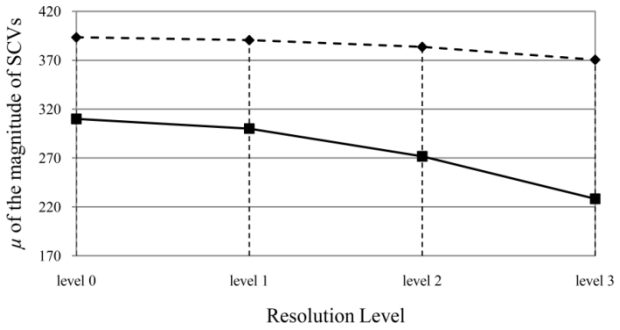

Figure 3.7. Behavior of the mean value of the magnitude of SCVs versus the resolution levels (scale) for clusters of change (dashed line) and of registration noise (continuous line).

significant changes are associated with objects with a non-negligible size. On the contrary, misregistration appears in the difference image with linear (or non linear) and relatively thin structures having different orientations. Therefore, if we reduce the resolution of images, we implicitly decrease the impact of the registration noise with respect to that on the original scene (Property 3), while true changes maintain a good stability (Property 4). In other words, the lower is the geometrical resolution, the lower is the probability of identifying in the polar representation annular sectors of dominant registration noise. This means that at low resolution, in the *annulus of changed pixels* mainly sectors (i.e., clusters) due to the presence of true changes on the ground are detected. Thus, by comparing the clusters present in the polar domain at full resolution and at reduced resolution, it is possible to identify annular sectors dominated from registration noise and separate them from annular sectors of changes. It is worth noting that this is made possible from the thin structures associated with RN that result in strong changes in the corresponding SCV clusters when the low pass effect of the scale reduction is considered.

On the basis of the aforementioned analysis, we propose an adaptive multiscale strategy that exploits the behaviors of SCVs to identify the distribution of the registration noise. The proposed technique compares the distribution of the SCVs at the highest resolution level with the one at a lower level in order to derive the distribution of registration noise at full resolution. In particular, first of all the two multitemporal images are decomposed according to a multiscale transformation (as described in section 3.2 different algorithms can be used, like stationary wavelet transform, recursively upsampled bicubic filter, etc.). In greater detail we applied the two-dimensional discrete stationary wavelet transform (2D-SWT); this decomposition technique is obtained as an extension of the one dimensional discrete stationary wavelet transform by applying one-dimensional filters independently along both dimensions of the considered image. In particular, two filters with different impulse responses are considered to built up the SWT filter bank: i) a low-pass filter with impulse response $l(.)$; and ii) a high-pass filter with impulse response $h(.)$. A one-step wavelet decomposition applies both filters separately, first along columns and then along rows. The original image $\mathbf{X}_i$ (i=1,2) is decomposed into a low resolution image (the approximation sub-band $\mathbf{X}_i^{LL}$), containing low spatial frequencies in both the horizontal and the vertical direction, and three detail images $\mathbf{X}_i^{LH}$, $\mathbf{X}_i^{HL}$ and $\mathbf{X}_i^{HH}$, which correspond to the horizontal, vertical and diagonal detail sub-bands at resolution level 1, respectively. Note that, superscripts *LL*, *LH*, *HL* and *HH* specify the order on which high- and low-pass filters have been applied to obtain the considered subband. The multiscale decomposition is obtained by recursively applying the described procedure to the approximation sub-band obtained at each scale 2^n. Thus the output at a generic resolution level *n* can be express analytically as follows:

$$\begin{aligned}
\mathbf{X}_i^{LL(n+1)}(i,j) &= \sum_{p=0}^{D^n-1}\sum_{q=0}^{D^n-1} l^n[p]l^n[q]\mathbf{X}_i^{LLn}(i+p,j+q) \\
\mathbf{X}_i^{LH(n+1)}(i,j) &= \sum_{p=0}^{D^n-1}\sum_{q=0}^{D^n-1} l^n[p]h^n[q]\mathbf{X}_i^{LLn}(i+p,j+q) \\
\mathbf{X}_i^{HL(n+1)}(i,j) &= \sum_{p=0}^{D^n-1}\sum_{q=0}^{D^n-1} h^n[p]l^n[q]\mathbf{X}_i^{LLn}(i+p,j+q) \\
\mathbf{X}_i^{HH(n+1)}(i,j) &= \sum_{p=0}^{D^n-1}\sum_{q=0}^{D^n-1} h^n[p]h^n[q]\mathbf{X}_i^{LLn}(i+p,j+q)
\end{aligned} \tag{3.2}$$

where D^n is the length of the wavelet filters at resolution level n. At each decomposition step, the length of the impulse response of both high- and low-pass filters is upsampled by a factor 2. Thus, filter coefficients for computing subbands at resolution level $n+1$ can be obtained by applying a dilation operation to the filter coefficients used to compute level n. In particular, 2^{n-1} zeros are inserted between the filter coefficients used to compute subbands at the lower resolution level. This allows a reduction in the bandwidth of the filters by a factor two between subsequent resolution levels. Filter coefficients of the first decomposition step for n=0 depend on the selected wavelet family and on the length of the chosen wavelet filter. To this purpose, we selected the *Daubechies* wavelet family and set the filter length to 8. The finite impulse response of the high-pass filter for the decomposition step is obtained by satisfying the properties of the quadrature mirror filters. This is done by reversing the order of the low-pass decomposition filter coefficient and by changing the sign of the even indexed coefficients [74].

In order to perform the proposed analysis, one must return to the original image domain. This is done by applying only to the approximation sub-bands the two dimensional inverse discrete stationary wavelet transform (2D-ISWT) at each resolution level independently. In this manner we obtain two sets of images $\mathbf{X}_{MS_i} = \left\{\mathbf{X}_i^0,...,\mathbf{X}_i^n,...,\mathbf{X}_i^{N-1}\right\}$ where the subscript i (i = 1,2) denotes the acquisition date, and the superscript n (n = 0,1,…, N-1) indicates the resolution level (note that $\mathbf{X}_i^0 \equiv \mathbf{X}_i$). Then the CVA technique is applied to each corresponding pair of images ($\mathbf{X}_1^n$, $\mathbf{X}_2^n$) and the distributions of the direction of SCVs at different resolution levels are analyzed. In particular, the behaviors of SCVs in A_c are studied. To this purpose, we compute the conditional density of the direction of pixels in A_c. In order to estimate this distribution we take advantages from the Parzen windows technique [75], [76], [77], [78], which is a basic and effective estimation method for one dimension problems. According to this technique the density estimation can be computed as:

$$\hat{p}_n(\vartheta \mid \rho \geq T) = \frac{1}{M_n}\sum_{m=1}^{M_n}\frac{1}{h_n}\gamma\left(\frac{\vartheta-\vartheta_m}{h_n}\right) \tag{3.3}$$

where T is the threshold value that separates the circle of unchanged pixels from the annulus of changed pixels (it can be retrieved either manually or in an automatic way through one of the algorithms proposed in the literature [11], [22], see section 2.4), n (n=0,1,…,N-1) denotes the resolution level at which the estimation is computed, ϑ_m represents the direction value of the mth SCV in A_c, M_n is the number of SCVs in A_c at scale n, $\gamma(.)$ is the kernel function used in the estimation process and h_n is the width of the kernel window (smoothing parameter) at scale n.

In particular, we used Gaussian kernel, so that the final estimation is given by:

$$\hat{p}_n(\vartheta \mid \rho \geq T) = \frac{1}{M_n} \sum_{m=1}^{M_n} \frac{1}{h_n \sqrt{2\pi}} \exp\left[-\frac{1}{2} \left(\frac{\vartheta - \vartheta_m}{h_n} \right)^2 \right] \tag{3.4}$$

For what concerns the smoothing parameter, which in our case is represented by the standard deviation of the Gaussian function, we propose to compute it as a function of the number of pixels that fall in A_c. In particular, considering a Gaussian kernel, the width value at scale n can be derived as in [75]:

$$h_n = sig * \left(\frac{4}{3M_n} \right)^{1/5} \tag{3.5}$$

where:

$$sig = \underset{m=1,\ldots,M_n}{median} \left| \vartheta_m - \underset{m=1,\ldots,M_n}{median}(\vartheta_m) \right| / 0.6745 \tag{3.6}$$

Then we observe the behaviors of $\hat{p}_n(\vartheta \mid \rho \geq T)$ versus the scale. According to the properties of RN, this density decreases at reduced resolutions in the *annular sectors of dominant registration noise* $S^D_{RN_i}$, whereas it remains nearby constant in the *annular sectors of true changes* S_k. On the basis of this analysis, we propose to estimate the conditional density of registration noise in the direction domain $\hat{p}_{RN}(\vartheta \mid \rho \geq T)$ as:

$$\hat{p}_{RN}(\vartheta \mid \rho \geq T) = C\left[P_0(\rho \geq T)\hat{p}_0(\vartheta \mid \rho \geq T) - P_{N-1}(\rho \geq T)\hat{p}_{N-1}(\vartheta \mid \rho \geq T) \right] \tag{3.7}$$

where $P_n(\rho \geq T)$ is the probability of SCVs to be in A_c at scale n, $\hat{p}_0(\vartheta \mid \rho \geq T)$ and $\hat{p}_{N-1}(\vartheta \mid \rho \geq T)$ are the marginal conditional densities of the direction of pixels in A_c at the full resolution and at the lowest considered resolution level (N-1), respectively, and C is a constant defined such that $\int_{-\infty}^{+\infty} \hat{p}_{RN}(\vartheta \mid \rho \geq T) d\vartheta = 1$. The term $P_n(\rho \geq T)$ in (3.7) is necessary in order to obtain a reliable comparison between distributions at different resolution levels.

In this way we obtain an explicit estimation of the distribution of registration noise that is adaptive (in the sense that it intrinsically takes into account the properties of the considered images). It is worth noting that this estimated distribution represents the behavior of RN at full scale (resolution). In the proposed technique the analysis at the lowest resolution is only used for separating the RN contribution from that of true changes (and of other possible sources of noise). The sensitivity of the estimation depends on the lowest level N-1 of decomposition considered. The lower the level is, the greater the sensitivity of the estimated distribution to the minor components of registration noise is. Nonetheless, considering applications like change-detection, it is important to choose the lowest scale according to the smallest size of expected changes, as they must be preserved in the degraded image in order to be detected.

3.5. Experimental Results

This section presents an experimental analysis on both the reliability of the derived properties of RN and the effectiveness of the proposed method to estimate the distribution of RN on real multitemporal images. The investigation was conducted on two different test areas of a pair of Quickbird images acquired on the Trento city (Italy) in October 2005 and July 2006. For both test areas the final data set is made up of two pansharpened radiometrically corrected multitemporal and multispectral

images of 984×984 pixels, with a geometrical resolution of 0.7 m, which after pre-processing show a residual misregistration of about 1 pixel on ground control points[2].

For applying the proposed method to the estimation of registration noise, the original images $\mathbf{X}_1$ and $\mathbf{X}_2$ were transformed to lower scales through a four-step stationary wavelet transform [73],[79] using 4th order orthogonal filters of the *Daubechies* family. The maximum level of decomposition was selected according to a tradeoff between the degree of sensitivity desired in the RN estimation and the size of the expected main change structures present in the images. Then the CVA technique was applied to the images at different scales. In order to separate the c*ircle of unchanged pixels* (C_n) from the *annulus of changed pixels* (A_c), for each data set a proper threshold value T on the magnitude variable was retrieved according to a trial-and-error procedure (we did not use an automatic technique for avoiding biases introduced from the threshold selection method in the evaluation of the effectiveness of the proposed method. However, at an operational level, one of the thresholding algorithms proposed in the literature can be used [15], [80]). In greater detail, in order to find the optimal threshold for our purposes, the whole analysis for the estimation of the RN distribution has been conducted for different values of the thresholds T in a consistent range of the magnitude valules. All of them provided similar results in the estimation of registration noise. For space constraints, in the following only the results obtained with a single threshold value for each dataset are reported. The marginal conditional densities of the directions of pixels in A_c at the highest resolution and at a lower resolution levels were computed according to (3.4), and finally the conditional density of registration noise was estimated according to (3.7). In order to assess the effectiveness of the proposed technique for the identification of the distribution of RN, such a distribution was thresholded and the direction intervals in A_c where $\hat{p}_{RN}(\vartheta \mid \rho \geq T)$ was higher than a given threshold were recognized as dominated from registration noise. Then the registration-noise maps were derived on the basis of the results obtained by thresholding $\hat{p}_{RN}(\vartheta \mid \rho \geq T)$ and a qualitative analysis was performed in order to assess the effectiveness of the proposed estimation technique.

3.5.1 Test site 1: urban and rural areas

The first test site considered (see Figure 3.8) covers both an urban area and a rural one. Between the two acquisition two kinds of changes occurred: (i) simulated changes (see section 0 on the procedure adopted to simulate them) that consist of new houses introduced on the rural area; (ii) real changes that consist of some roofs rebuilt in the urban area. In order to assess the reliability of the proposed technique the previously described procedure was applied to the two images. Figure 3.9 shows the behaviors of the marginal conditional densities of the direction in A_c [$\hat{p}_n(\vartheta \mid \rho \geq T)$] computed according to (3.4) and corrected by the term $P_n(\rho \geq T)$, after applying the CVA technique to the red and near infrared spectral channels of: (a) the original images at full resolution (continuous line in Figure 3.9); and (b) the low resolution images yielded at level four of the *Daubechies* stationary wavelet decomposition (dashed line in Figure 3.9). As previously mentioned, red and near infrared spectral channels were considered as they better represent changes occurred between the two dates. The estimation of the marginal conditional density of registration noise $\hat{p}_{RN}(\vartheta \mid \rho \geq T)$ was derived from the two aforementioned densities according to (3.7) (see Figure 3.10). From an analysis of the behavior of $\hat{p}_{RN}(\vartheta \mid \rho \geq T)$ it is possible to identify three main modes, which potentially define sectors where the

[2] It is worth noting that we carried out all the analysis using pansharpened images, as we expect that the pansharpening process can emphasized the effects of misregistration. However, similar results can be obtained on original multispectral images at lower resolution (2.4 [m]). We refer the reader to [91] for greater details on the effects of pansharpening on change detection.

registration noise is dominant. A comparison between the scatterograms at full and at low resolution (see Figure 3.11) points out that in the sectors corresponding to the three modes of $\hat{p}_{RN}(\vartheta \mid \rho \geq T)$ the density of the magnitude of SCVs in the annulus of changed pixel reduces significantly when the resolution decreases, whereas in the others it is nearly constant. In particular, it is possible to verify that the sectors in which the behavior of SCVs is quite stable correspond to sectors of true changes (continuous circles in Figure 3.11). This behavior also confirms the properties derived from the simulated data sets.

(a) (b)

Figure 3.8. True color composition of pansharpened images of the Trento city (Italy) acquired by the Quickbird VHR multispectral sensor in: (a) October 2005; and (b) July 2006 (Test site 1).

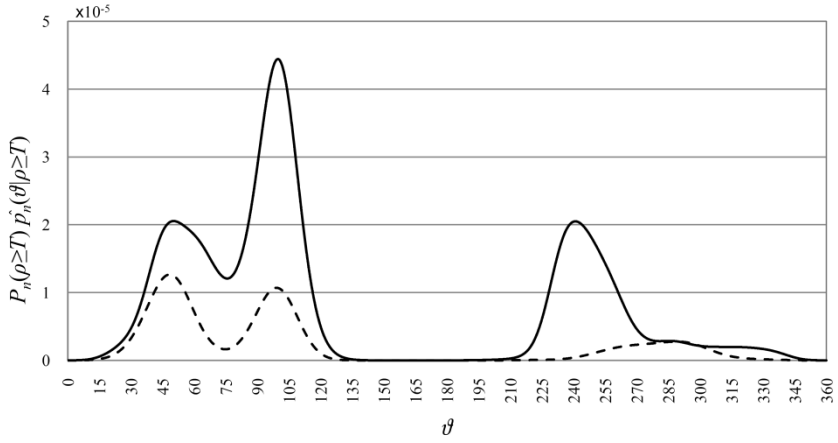

Figure 3.9. Marginal weighted conditional densities $P_n(\rho \geq T)\hat{p}_n(\vartheta \mid \rho \geq T)$ of the direction in A_c at full resolution (continuous line) and at level four of the *Daubechies* stationary wavelet transform (dashed line) (Test site 1).

To further understand the effectiveness of the proposed estimation technique, we applied a threshold to $\hat{p}_{RN}(\vartheta \mid \rho \geq T)$ to identify sectors of dominant registration noise. The threshold value was empirically fixed equal to $1\text{x}10^{-4}$. Thus, in the annulus of changed pixels (defined by applying a threshold T=310 to the magnitude of SCVs), the sectors of dominant registration noise were identified between 35° and 115° and between 225° and 265°. In order to perform a qualitative analysis of the estimation, Figure 3.12 reports the map of pixels associated with the estimated sectors of dominant RN. A

visual analysis of this map confirms that the regions identified as registration noise by the proposed technique are associated with areas that show the effects of misregistration between the multitemporal images, as they mainly refer to border regions of buildings located in the urban area, to roads and to crop rows. In addition, it is possible to note that the regions identified in the registration-noise map do not belong to areas of changes. This behavior confirms the effectiveness of the proposed technique that properly distinguishes between registration noise and true changes contributions in the estimation of $\hat{p}_{RN}(\vartheta \mid \rho \geq T)$. It is worth noting that the proposed technique marks as registration noise the boundaries of the four simulated changes. This happens as, in order to make the changes more realistic, together with the roofs also some pixels surrounding buildings have been copied; these pixels result in changes with thin structure and small size with respect to the sensor resolution. Thus, they do not satisfy the basic assumption that true significant changes are associated with objects with non-negligible size, and consequently appear correctly as registration noise.

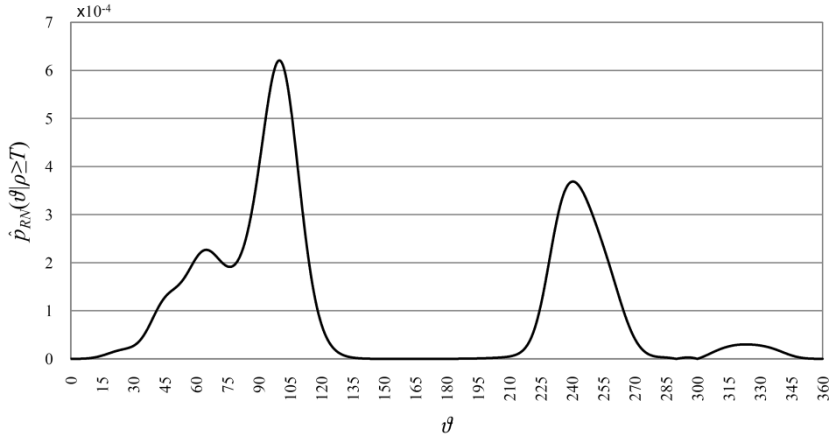

Figure 3.10. Estimated conditional density $\hat{p}_{RN}(\vartheta \mid \rho \geq T)$ of registration noise obtained with the proposed technique (Test site 1).

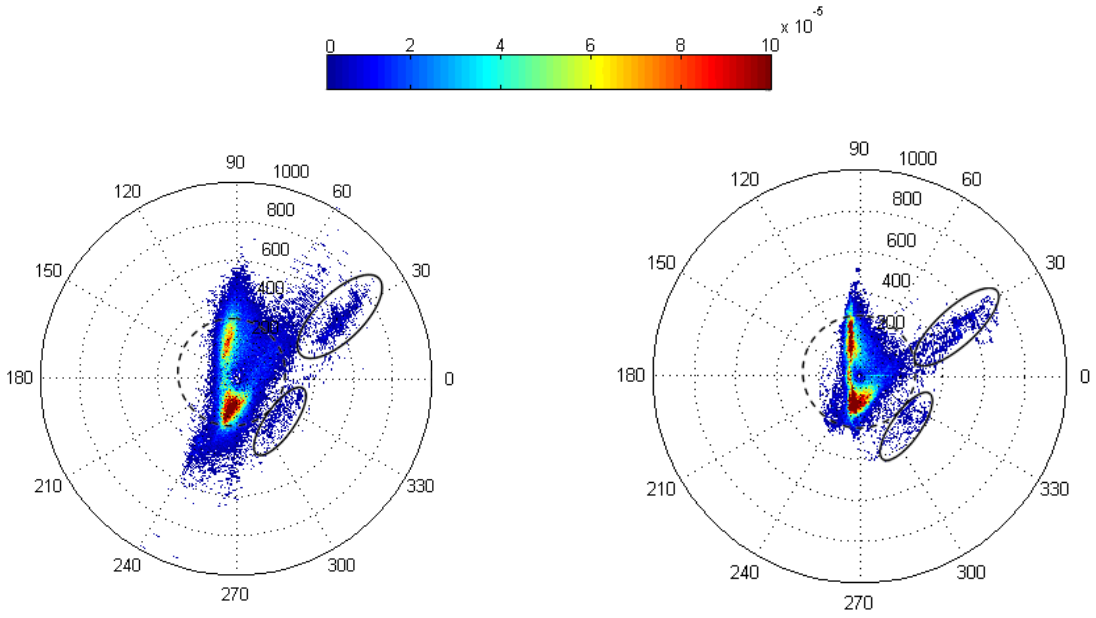

(a) (b)

Figure 3.11. Scatterograms in the polar coordinate system of (a) the full resolution original difference image $\mathbf{x}_D^0$, and (b) the low resolution image $\mathbf{x}_D^4$ obtained at level four of the wavelet decomposition (Test site 1). Dashed circles separate C_n from A_c, while continuous circles indicate sectors of true changes.

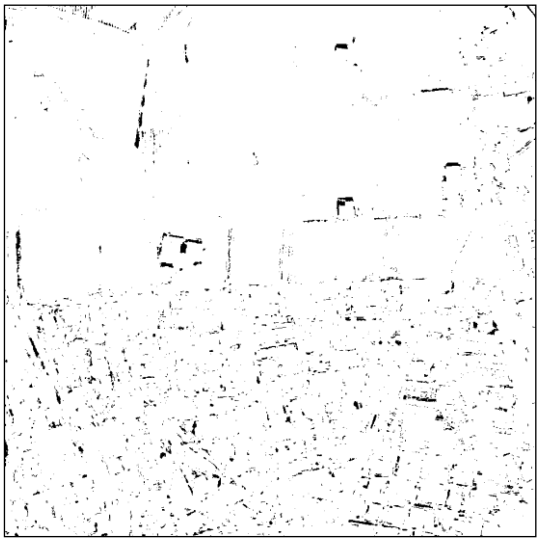

Figure 3.12. Registration-noise map obtained by thresholding the $\hat{p}_{RN}(\vartheta \mid \rho \geq T)$ obtained with the proposed technique (Test site 1).

3.5.2 Test site 2: industrial and rural areas

The second test site considered (see Figure 3.13) mainly covers an industrial area. Also in this case two kinds of changes occurred in the two images: (i) natural changes of the land cover in rural areas and along the river bank; and (ii) man made changes in the roofs of the industrial area. As for the previous data set, the marginal conditional densities of the direction in A_c were computed according to (3.4) after applying the CVA technique to the red and near infrared spectral channels of the original images at full resolution (continuous line in Figure 3.14) and the low resolution images yielded at level four of the *Daubechies* stationary wavelet decomposition (dashed line in Figure 3.14). From these distributions the $\hat{p}_{RN}(\vartheta \mid \rho \geq T)$ was estimated according to (3.7) (Figure 3.15). Also in this case from an analysis of the behavior of this distribution it is possible to identify three main modes, which represent the estimated sectors of dominant registration noise (this is confirmed from a visual analysis of polar scatterograms not reported for space constraints).

We applied a threshold to the density of RN in order to estimate sectors of dominant registration noise. With a threshold equal to $1\text{x}10^{-4}$ applied to $\hat{p}_{RN}(\vartheta \mid \rho \geq T)$, and a threshold in the magnitude domain T=310 the sectors of dominant registration noise were identified between 35° and 70°, between 90° and 120°, and between 220° and 250°. Figure 3.16 reports the map of registration noise pattern obtained by thresholding $\hat{p}_{RN}(\vartheta \mid \rho \geq T)$ with the proposed strategy. As for the previous test site, from a visual analysis of this map it is possible to conclude that the regions identified as registration-noise corresponds to areas of a misregistration, as they are mainly located in border of buildings, along the riverside and along the roads. In addition, also in this case, it is possible to note that the proposed technique allows one to properly distinguish between registration noise and true changes contributions in the estimation of $\hat{p}_{RN}(\vartheta \mid \rho \geq T)$.

3.6. Discussion and conclusion

In this chapter we have analyzed the properties of registration noise (RN) in very high resolution (VHR) remote sensing images. This analysis was carried out in the context of a polar framework for change vector analysis (CVA), where both the magnitude and the direction information of SCVs are

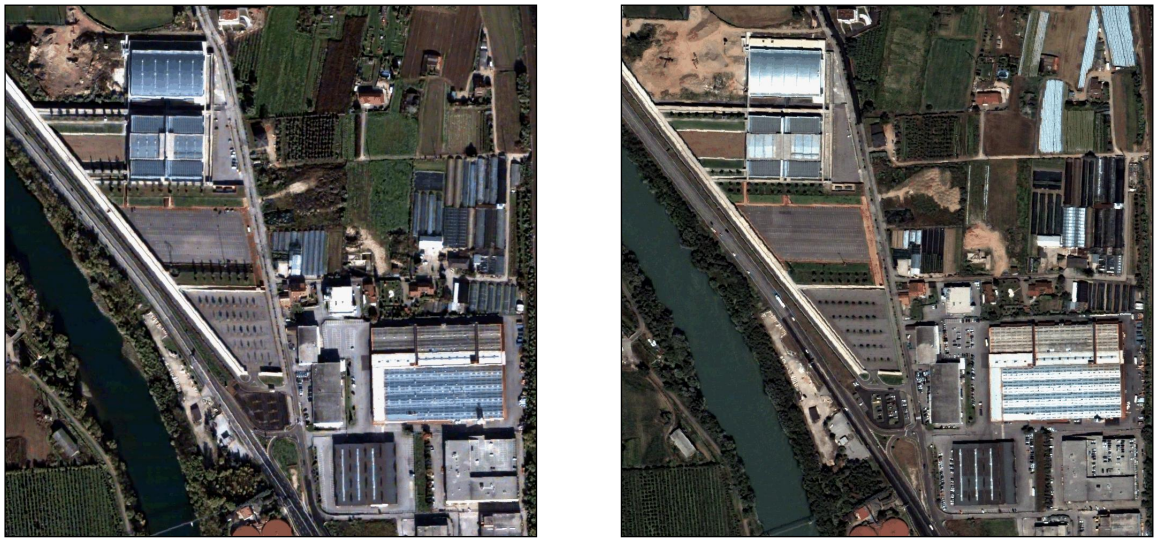

(a) (b)

Figure 3.13. Pansharpened images of the city of Trento (Italy) acquired by the Quickbird VHR multispectral sensor in October 2005 (a) and in July 2006 (b). Continuous white lines evidence changes in field crop, while the dashed lines mark changes in roofs (Test site 2).

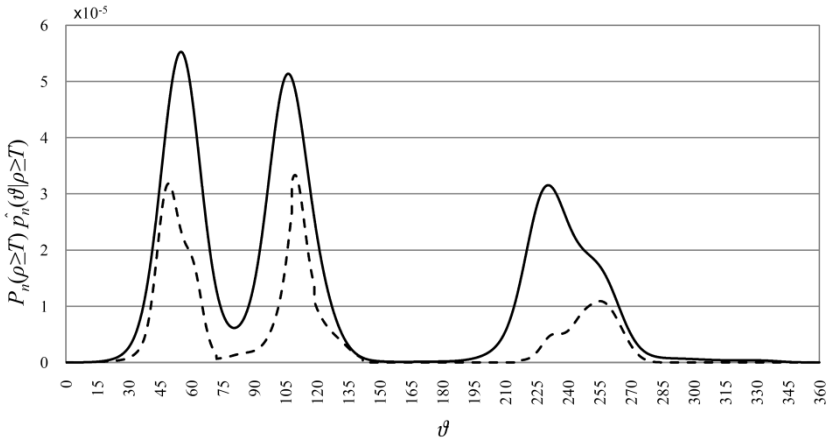

Figure 3.14. Marginal weighted conditional densities $P_n(\rho \geq T)\hat{p}_n(\vartheta \mid \rho \geq T)$ of the direction in A_c at full resolution (continuous line) and at level four of the *Daubechies* stationary wavelet transform (dashed line) (Test site 2).

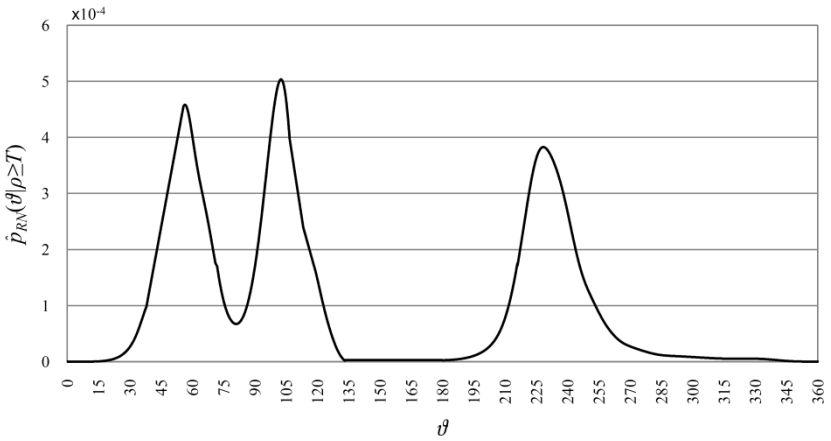

Figure 3.15. Estimated conditional density $\hat{p}_{RN}(\vartheta \mid \rho \geq T)$ of registration noise obtained with the proposed technique (Test site 2).

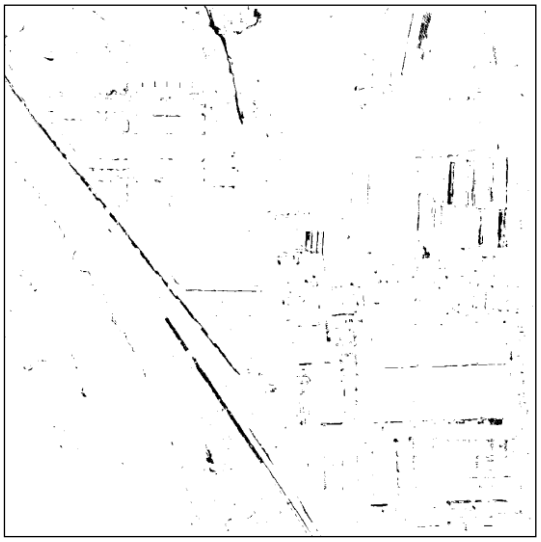

Figure 3.16. Registration-noise map obtained by thresholding the $\hat{p}_{RN}(\vartheta \mid \rho \geq T)$ obtained with the proposed technique (Test site 2).

represented. On the basis of the derived properties, a novel method for an adaptive estimation of the statistical distribution of RN in multitemporal VHR images has been proposed.

Images acquired by several sensors and with different land-cover types were considered in the analysis. From them, some simulated data sets have been generated in order to study the effects of RN when: (i) the misregistration between the two considered images increases; and (ii) the resolution of the original images decreases. From this analysis four different properties of the RN in VHR images have been derived, associated with both unchanged and changed pixels. These properties point out that misregistration may significantly affect the accuracy of change detection and show some important effects due to this specific kind of noise on VHR images. It is worth noting that on the basis of the conducted analysis, we can conclude that the properties of RN in VHR multispectral images are significantly different from those on high or medium resolution images. These differences should be properly understood and exploited in the mitigation of the effects of such a kind of noise in the definition of change-detection algorithms.

The analysis of the properties of registration noise resulted also in the definition of an adaptive technique for the estimation of the RN distribution in the polar domain. The proposed technique estimates the conditional density of RN with respect to the direction variable in the annulus of changed pixels, thus providing valuable information for the design of a change-detection procedure. In order to assess the reliability of the proposed estimation technique we performed an analysis of the results obtained with the estimation method on a couple of test sites made up of two real multitemporal images acquired by the Quickbird sensor. These results confirm the effectiveness of the proposed technique in identifying and modeling RN also in presence of real multitemporal noisy images acquired under different conditions.

Even if the proposed technique exploits a multiscale decomposition for identifying RN and modeling its conditional distribution, the resulting estimate represents the behavior of the RN at full resolution. Thus the estimated distribution can be used for analyzing the images at full scale, as the low-pass component used in the proposed strategy does not affect the scale of the estimation.

It is worth noting that depending on the considered scene, a slight relative shift effect (bias) on the direction variable between the distributions of the SCVs in the annulus of changed pixels at full and reduced resolution might be observed. This is due to the low-pass operation associated with the down-

scaling process. Even if this shift in general is not expected to be critical for the estimation technique, a simple correction procedure could be applied to the distributions before deriving the RN estimation.

The proposed strategy focuses on the estimation of the distribution of registration noise in the annulus of changed pixels and neglects the components of registration noise in the circle of unchanged pixels (whose properties are however identified in section 3.3). Nonetheless, this is not critical because only the registration noise components in the annulus of changed pixels affect the change-detection map resulting in a significant false-alarm rate.

As a final remark, it is important to observe that the proposed strategy can be considered also for estimating the registration noise on medium and high resolution multispectral images. Indeed, even if the typical uniform distribution of registration noise in the annulus of changed pixels obtained with such kind of data [11] is against the assumption to have well-defined clusters of dominant registration noise in the annulus of changed pixels, the rationale inspiring the proposed estimation strategy is still valid.

From this analysis, exploiting both the derived properties and the technique for the estimation of the registration noise distribution we have developed: i) effective change-detection methods for VHR images based on both the Bayesian decision theory and context-sensitive strategies (see chapter 5); ii) adaptive co-registration strategies based on the estimated local behavior of the registration noise (see chapter 4).

Chapter 4

4. A registration noise driven technique for the alignment of VHR images[3]

In this chapter a novel method for registration of multitemporal very high geometrical resolution (VHR) remote sensing images is presented. It relies on the extraction of a large set of control points (CPs) used for the estimation of a disparity map exploited for the registration process. CPs are automatically identified in both the images through the estimation and analysis of the distribution of registration noise (RN) described in the previous chapter and used together with an interpolation procedure in the definition of the disparity map. This map contains for each pixel the estimated value of the displacement between the reference and the moving image. The warping of the moving image is performed according to the disparity map by using thin plate spline interpolation. Results obtained on simulated and real VHR data confirm the validity of the proposed technique, which is effective both in identifying CPs and in performing the image alignment.

4.1. Introduction

Image registration is one of the most important steps in the analysis of multitemporal remote sensing images. Many applications (e.g., change detection, image fusion, etc.) require aligned images where corresponding pixels are associated with the same position on the ground (i.e. registered images). The co-registration procedure becomes critical when very high resolution (VHR) images of the last generation sensors are considered. These images can be acquired with different view angles and often show different geometrical local distortions that decrease the effectiveness of standard techniques developed for the registration of medium resolution images. In the literature only few automatic techniques have been proposed for the registration of high and very high resolution remote sensing images, which are often focused on specific applications [48], [50]. For an analysis of the state of the art of registration techniques effective on VHR images, please refer to section 2.3.

This chapter proposes a novel technique for a robust and accurate registration of VHR images, which is especially suitable for change-detection applications. The proposed technique follows the

[3] This chapter is published on *IGARSS, Proceedings of IEEE International Geoscience and Remote Sensing Symposium*, Honolulu, Hawaii, USA, July 25-30 2010, pp. 1023-1026. Title: "A registration-noise driven technique for the alignment of VHR remote sensing images". Authors: S. Marchesi and L. Bruzzone.

standard scheme of the registration process [12]: (i) feature (i.e. CPs) extraction; (ii) feature matching and transform model estimation; and (iii) image resampling and transformation. In particular, the presented method automatically extracts the CPs, estimates the disparity map that represents the non-parametric spatial transformation to be applied to the image and finally warps the moving image on the reference one. The proposed method takes advantages from the technique for the estimation of the distribution of registration noise (RN) presented in chapter 3 [81], which is exploited for automatically extracting and matching the CPs. Unlike standard registration methods, the proposed procedure: (i) is effective in obtaining good registration accuracy on the most critical points of the images where misregistration has a high probability to results in the detection of false changes; and (ii) is not affected by the presence of changes between the two images.

4.2. Proposed methodology

Let $\mathbf{X}_1$ and $\mathbf{X}_2$ be two multitemporal VHR images acquired over the same geographical area at different times that should be registered. Let $\mathbf{X}_1$ be the reference image and $\mathbf{X}_2$ the moving one. The objective of a registration technique is to warp the moving image on the reference one in order to align them. To this purpose, we propose a registration method for VHR images based on the following main steps (see[12]): (i) automatic extraction of CPs based on the registration noise distribution; (ii) CPs matching and transform model estimation by the generation of a complete disparity map; and (iii) image resampling and transformation. In the following a detailed description of each step is given.

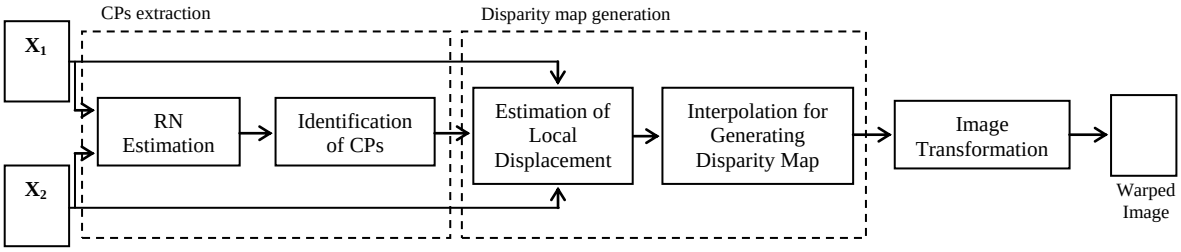

Figure 4.1. Block scheme of the proposed method

4.2.1 Automatic extraction of control points

The control points extraction and matching represents the most novel part of the proposed work. In greater details, we automatically extract as CPs the pixels that have the highest probability to be corrupted by registration noise and thus result in false alarms in the CD process. It is worth nothing that the term registration noise indicates the effects of a non perfect alignment between the multitemporal images under investigation. The most critical components of this noise are related to the pixels that at the two dates belong to different objects (i.e. border regions of objects or high frequency areas in the images).

In chapter 3[81] we have presented the analysis on the properties of RN on VHR images that resulted in the possibility to detect pixels affected by RN through a multiscale analysis in the context of a polar framework based on change vector analysis (CVA). Considering that misregistration appears in the difference image with linear (or non linear) and relatively thin structures having different orientations, it is expected that reducing the resolution the impact of RN decreases with respect to the one on the original scene. According to this observation, the conditional density of RN (which gives us information about the distribution of RN in the images) has been derived as [see also (3.7)]:

$$\hat{p}_{RN}(\vartheta \mid \rho \geq T) = C\left[P_0(\rho \geq T)\hat{p}_0(\vartheta \mid \rho \geq T) - P_N(\rho \geq T)\hat{p}_N(\vartheta \mid \rho \geq T)\right] \quad (4.1)$$

where ρ and ϑ indicate the magnitude and direction components, respectively, of the Spectral Change Vectors (SCVs) evaluated according to the polar CVA (see section 2.4); $P_0(\rho \geq T)$ and $P_N(\rho \geq T)$ are the probabilities of SCVs to have values in the magnitude domain higher than a predefined threshold T (i.e. to be pixels related to changes) at resolution level 0 and at the lowest level N, respectively; $\hat{p}_0(\vartheta \mid \rho \geq T)$ and $\hat{p}_N(\vartheta \mid \rho \geq T)$ are the marginal conditional densities of the direction of the same SCVs at resolution level 0 and N, respectively; and C is a constant defined such that $\int_{-\infty}^{+\infty} \hat{p}^{RN}(\vartheta \mid \rho \geq T)d\vartheta = 1$. Please refer to chapter 3 for further details. It is worth noting that a high value of $\hat{p}_{RN}(\vartheta \mid \rho \geq T)$ corresponds to a high probability to have pixels corrupted by registration noise (i.e. high differences in the distributions at different resolution levels). Accordingly, these pixels are the ones considered as CPs by the proposed technique. Thus, in order to extract them we apply a threshold T_{RN} to the conditional density of RN and then label as dominated by RN all the SCVs falling in direction intervals where $\hat{p}_{RN}(\vartheta \mid \rho \geq T)$ has values higher than T_{RN}. Pixels corresponding to these SCVs are then considered CPs for the proposed method. It is worth noting that the threshold T_{RN} intrinsically excludes from CPs pixels related to real changes occurred on the ground. As discussed in chapter 3, these pixels are quite stable with respect to the resolution, thus they usually have values of $\hat{p}^{RN}(\vartheta \mid \rho \geq T)$ smaller than T_{RN}. This aspect makes the proposed method robust to the presence of real changes, as the CPs automatically derived do not include changed pixels. It is worth noting that the proposed strategy, driving the registration process directly with critical pixels strongly affected by RN, reduces false alarms due to this noise allowing one to obtain higher accuracy in the change-detection process. Once the CPs are extracted, in order to perform the matching between them, we generate a registration noise map where all the pixels extracted as CPs are reported and have associated the value of the conditional density of RN of the corresponding SCVs.

4.2.2 Generation of the disparity map

In order to estimate the displacement of each CP between the two images, we perform a local analysis using as metric the value of the conditional density of RN. The analysis is made up of two main steps: (i) evaluation of the displacement for each CP; and (ii) interpolation of the displacement values for creating a complete disparity map.

In greater detail, in order to evaluate the displacement for each CP, we: (a) generate the registration noise map for different displacements; and (b) split the RN map and make a quantitative analysis based on the distribution of RN in each split. At first we create a set of possible displacements of the original image by taking the moving image and translating/rotating it according to a predefined set of misalignment values. Let Ω_d (d=1,…, D) be the set of the D different displacements $(\Delta x, \Delta y)_d$ considered. Then for each combination of the original fixed image and one of the D displaced moving images we derive the conditional density of registration noise $\hat{p}^d_{RN}(\vartheta \mid \rho \geq T)$ and we generate the registration noise maps M_d. In order to estimate the displacement of each pixel, we perform a local analysis of the D obtained M_d. At first we divide the RN maps into L sub-images of dimension hxh, then for a generic split l subject to a displacement d we evaluate the estimated amount of misregistration AM^l_d in the considered area as:

$$AM_d^l = \sum_{\substack{1\le i\le h \\ 1\le j\le h}} m_d^l(i,j) \tag{4.2}$$

where $m_d^l(i,j)$ is the variable that model the estimated misregistration for the pixel with coordinates *(i,j)* in the *l*-th split of the *d*-th RN map. It is worth noting that contributions to AM_d^l value are given only from pixels extracted as CPs as they are the only with non–zero value. Finally the displacement value is explicitly derived for all the splits that contain at least one CP (i.e. split with non-zero value of AM_d^l at the initial condition) according to the value of AM_d^l. Each split is associated to the displacement that results in the lowest value of AM_d^l with respect to *d.* In particular, for a generic split *l* the displacement value d_l is assigned according to:

$$d_l = \arg\min_d \left\{ AM_d^l \right\} \tag{4.3}$$

For simplicity, all the pixels belonging to a split are assumed to have the same displacement (this is equivalent to a quantization of the misregistration effects). In this manner we estimate the residual misalignment for all the splits containing at least one CPs. A bilinear interpolation is then applied in order to estimate the misalignment for all the splits of the image and thus to generate a disparity map. It is worth noting that trough this procedure we obtain a complete disparity map that shows for each pixel the estimated displacement vector. This disparity map corresponds to a discrete (quantized) representation of the image transformation necessary for registering the two original images. It has the advantage of making it possible to apply a general non-parametric warping [49].

4.2.3 Image transformation

The last step of the proposed method consists in the warping of the moving image to the reference one on the basis of the obtained disparity map. For data with non linear or local geometric distortion (such as VHR images) simple translation or affine transformations are not effective. Thus more complex transformation are needed to produce good interpolation results also at a local level. In this work, the warping of the moving image is performed by applying the thin plate spline (TPS) [82] interpolation function to the retrieved disparity map. This transformation is very flexible and allows one rotation, translation, scaling and skewing, permitting to represent a large number of transformations. One of the most important attributes of thin-plate spline is its ability to decompose a space transformation into a global affine transformation and a local non-affine warping component [83], [84]. Under the restriction of corresponding points (i.e. CPs and their relative displacements), matching matrixes and mapping parameters can all be achieved. Assuming that there are two sets of corresponding points *U* and *V*, which are represented as $\{u_a,\ a=1,2,...,n\}$ and $\{v_a,\ a=1,2,...,n\}$ and are extracted from images $\mathbf{X}_1$ and $\mathbf{X}_2$, respectively. Then the energy function of thin-plate spline can be defined as:

$$E_{TPS(f)} = \sum_{a=1}^{n} \left\| u_a - f(v_a) \right\|^2 + \lambda \iint \left[\left(\frac{\partial^2 f}{\partial x^2} \right)^2 + 2\left(\frac{\partial^2 f}{\partial x \partial y} \right)^2 + \left(\frac{\partial^2 f}{\partial y^2} \right)^2 \right] dxdy \tag{4.4}$$

where f is the mapping function between the point sets u_a and v_a. $(1, u_{ax}, u_{ay})$ and $(1, v_{ax}, v_{ay})$ are the homogeneous coordinates of u_a and v_a respectively. The first term in the above equation is the approaching probability between point sets u_a and v_a. The second term, on the other hand, is a smoothness constraint. Different λ means different degree of warping. When λ is close to zero, corresponding points are matched exactly.

According to this energy function, there exists a minimizing function $f(v), v \subset R^2$ for any fixed λ which can be represented as:

$$f(v) = v \cdot h + \phi(v) \cdot w \tag{4.5}$$

where v is the calculated point sets, h is a 3×3 affine transformation matrix, w is a $n\times3$ non-affine warping coefficient matrix, $\phi(v)$ is a $1\times n$ vector decided by thin-plate spline kernel. For each point of v, there exists a $\phi_a(v)$, which can be defined as: $\phi_a(v) = c\|v - v_a\|^2 \log\|v - v_a\|$, where c is a constant. When the solution of (4.5) is substituted into (4.4), we have:

$$E_{TPS}(d, w) = \|U - Vd - \Phi w\|^2 + \lambda trace\left(w^T \Phi w\right) \tag{4.6}$$

where U and V are concatenated point sets of v_a and u_a, Φ is an $n\times n$ matrix formed from the $\phi(v_a)$. Then, QR decomposition is used to separate the affine and non-affine warping space.

$$V = [Q_1 Q_2]\begin{pmatrix} R \\ 0 \end{pmatrix} \tag{4.7}$$

where Q_1 and Q_2 are ortho-normal matrices, R is upper triangular. The final solution for w and d can be written as:

$$w = Q_2\left(Q_2^T \Phi Q_2 + \lambda I_{(N-3)}\right)^{-1} Q_2^T U \tag{4.8}$$

$$d = R^{-1}\left(Q_1^T V - \Phi w\right) \tag{4.9}$$

From the generated disparity map a set of corresponding points is obtained (at least one for each split), which is extracted from the reference and moving images. Then the moving image is warped to the reference one by thin-plate spline based on these point pairs, which has the maximization of similarity or minimization of non-similarity. Thus the global elastic registration is achieved.

4.3. Experimental results

In order to assess the effectiveness of the proposed registration technique, we carried out experiments on a pair of Quickbird images. In greater detail, in the following we report the results obtained on: (a) a simulated data set generated from an image acquired by the Quickbird sensor over the city of Trento (Italy) in July 2006; and (b) a real data set made up of the same VHR image and an image acquired over the same geographical area by the same sensor in October 2005. In the following the data set are described and the results obtained on each of them are reported and analyzed.

4.3.1 Simulated data set

The first data set is made up of an image of 400x400 pixels acquired over the city of Trento (Italy) in July 2006 by the Quickbird satellite, which was used as the reference one and a copy of it distorted and containing simulated changes, used as the moving image (see Figure 4.2 (a) and (b), respectively). In particular, the simulated changes (new houses, see regions marked with white circles in Figure 4.2 (b)) have been accurately introduced taking their geometrical structure and spectral signatures from other real buildings present in the image. Concerning the distortion, we applied different deformation both in vertical and horizontal domain. However, for space constraints, in the following results obtained with a sinusoidal deformation in vertical direction with 3-pixels amplitude and 150-pixels period are reported.

(a) (b)

Figure 4.2. True color composition of the image acquired over the city of Trento by the Quickbird sensor. (a) Original image acquired in July 2006. (b) Image with simulated changes (pointed out with white circles) and sinusoid geometric deformation..

At first the procedure for the extraction of CPs was applied. To this purpose the two images were decomposed through *Daubechies-4* stationary wavelet transform. Then the CVA was applied and the conditional density of registration noise was derived according to (4.1) (*T* was set equal to 100) (see Figure 4.3). In order to extract the CPs a threshold $T_{RN} = 1\text{x}10^{-4}$ was applied to the RN. Figure 4.4 (a) shows the map containing all the extracted CPs. As one can see, CPs are mainly related to areas that show the effects of misregistration, i.e. they mainly refer to border regions of buildings located in the urban area and to crop rows (high frequency in the image). In addition, it is possible to note that the identified CPs do not belong to changed areas, thus confirming the capability of the proposed method to be insensitive to changes often present in multitemporal images.

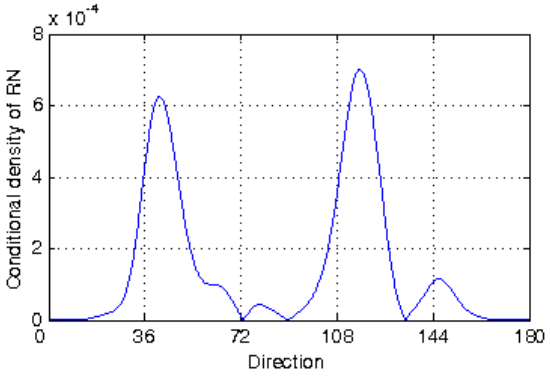

Figure 4.3. Conditional density of registration noise $\hat{p}_{RN}(\vartheta \mid \rho \geq T)$ evaluated on the original data set. (Simulated data set)

The second step was to derive the disparity map. To this purpose a set of displacement values Ω_d was defined by rotating and translating the moving image in an interval of [0;5] pixels for both step Δx and Δy. Then $\hat{p}_{RN}(\vartheta \mid \rho \geq T)$ was evaluated and the M_d was derived for each displacement vector. Afterwards the maps were divided into splits of dimension 10×10 (note that different values of *h* provided very similar results) and for each split *l* of each M_d we evaluated AM_d^l. Then for each split we compared the values AM_d^l and associated to the CPs belonging to the split the displacement $(\Delta x, \Delta y)_d$ that minimized AM_d^l. The final disparity map was retrieved applying bilinear interpolation to splits that did not contain any CP (see Figure 4.4 (b)). A visual analysis of this map confirms the validity of the displacement estimation, as the areas in which the sinusoid has its peak (both negative and positive) correspond to the lowest and highest values of the displacement (black and white re-

gions). Finally, in the last step the warping of the image was performed according to TPS transformation on the basis of the obtained disparity map. To this purpose, we consider as CPs the first pixels of each split (upper left corner). Please note that different choices in the position of the extracted CPs result in very small differences in the registration results, as all the pixels of each split are associated to the same displacement. Figure 4.5 reports the difference image evaluated before (Figure 4.5(a)) and after (Figure 4.5(b)) the registration process, for a visual analysis of the obtained results. As one can see, in regions where the sinusoid used for the deformation has its peaks, the effects of misregistration are clearly visible in the image before the registration both in urban and rural areas, whereas in the difference image obtained after applying the proposed registration method the effects are very smoothed. This confirms the ability of the method in performing an effective registration. In addition, changes are correctly reported without distortion and are not considered as CPs, proving the effectiveness of the method also when changes are present between the images. Similar results were obtained with different distortions.

In order to retrieve quantitative results, the Root Mean-Square Error (RMSE) and its standard deviation (STD) computed on twenty CPs randomly extracted from the fixed and moving images before and after the registration process, as well as the Mutual Information (MI) values between images have been evaluated and reported in Table 4.1. In addition, a comparison is performed with the results achieved by both the co-registration tool present in the ENVI package (manual extraction of CPs and warping according to a polynomial interpolation), and an automatic technique that automatically extracts CPs according to a minimum square error metric and warps the image through a simple transformation (only scale, rotation and translation are admitted). As for the qualitative analysis, observing the numerical results it is possible to confirm the effectiveness of the proposed automatic registration technique. One can observe that the values of RMSE and MI obtained by the proposed automatic method are very similar to those yielded with the manual approach. It is worth noting that using simulated data, like in this case, it is easier to manually retrieve GCPs than for real cases, as the spectral dynamics of the two considered images are the same. Consequently, through a simple visual analysis it is simple to extract corresponding control points. Differently to what happens with real data (see next section), the results provided by the standard automatic approach are not effective in this case. This is due to the strong non linear deformation modeled in simulated data, which reduce the effectiveness of warping algorithms based on linear transformations.

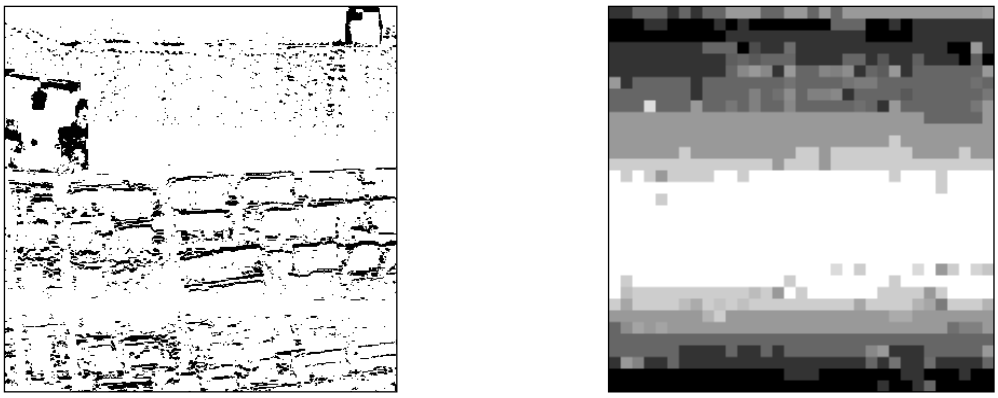

(a) (b)

Figure 4.4. (a) Map containing the extracted control points; and (b) disparity map obtained on the basis of the extracted CPs. (Simulated data set)

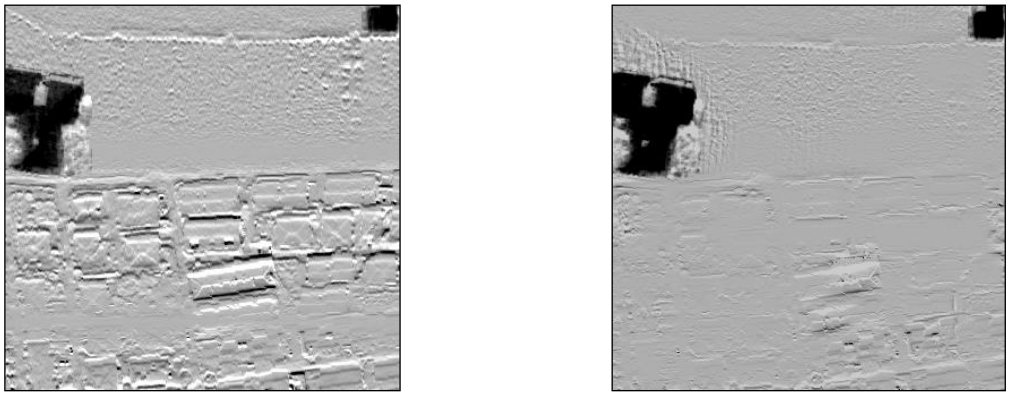

(a) (b)

Figure 4.5. Difference images obtained (a) on the original data set and (b) after the registration process. (Simulated data set)

TABLE 4.1. RESULTS OBTAINED BEFORE AND AFTER THE REGISTRATION WITH THE PROPOSED TECHNIQUE, THE MANUAL ONE AND THE AUTOMATIC RIGID APPROACH FOR THE SIMULATED DATA.

Registration method	RMSE (pixels)	STD (pixels)	MI (bits)
No registration	2.53	1.13	1.364
Proposed automatic approach	1.32	0.69	2.010
Manual approach	1.25	0.60	1.658
Standard automatic approach	2.44	1.18	1.371

4.3.2 Real VHR multitemporal data set

To further validate the proposed technique, experiments were carried out on a couple of real VHR multitemporal images. The considered data set is made up of the Quickbird image used in the simulation phase (Figure 4.2 (b)) and of a second image acquired on the same area in October 2005 (Figure 4.2 (c)). As for the simulated data set, in order to register the two images, the procedure described in section 4.2 was applied to the reference and moving images. In particular, the CPs were extracted after computing and thresholding the conditional density of registration noise (see Figure 4.7). Figure 4.6 (b) shows the CPs map obtained thresholding $\hat{p}_{RN}(\vartheta \mid \rho \geq T)$ with T_{RN} set equal to 1.5×10^{-4}; as for the previous example, the extracted CPs are mainly related to border regions of buildings and to crop rows. Then, the disparity map was generated, adopting the same set parameters of the previous described experiment (i.e. same set of displacement values, same splits). Finally, the moving image was warped according to the TPS transformation. As for the previous experiment, a quantitative analysis was performed in order to evaluate the effectiveness of the proposed method. Table 4.2 reports the numerical results achieved on these real data by the proposed method and the two techniques previously considered. An analysis of the numerical results points out the effectiveness of the proposed automatic technique, which allows one to accurately register the images obtaining RMSE slightly smaller and MI slightly greater than the ones reached by the manual registration technique. Moreover, the proposed method performs better in terms of both RMSE and MI than the automatic technique that uses the MSE as metric and linear transformation. This confirms the effectiveness of both the strategy for CPs extraction and the applied transformation. It is worth noting that the proposed method can achieve a more uniform accuracy on the image thanks to the local analysis carried out according to the disparity map. This is confirmed by the standard deviation values of the RMSE, that for the proposed approach are smaller than those related to other methods considered.

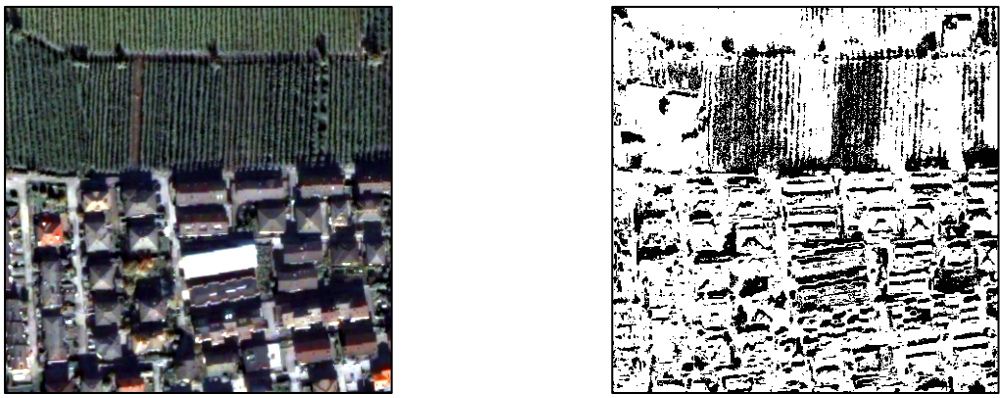

(a) (b)

Figure 4.6. (a) True color composition of the image acquired over the city of Trento by the Quickbird sensor in October 2005. (b) map containing the extracted control points. (Real data set)

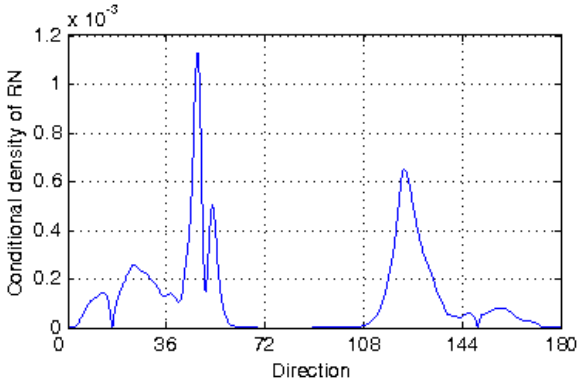

Figure 4.7. Conditional density of registration noise $\hat{p}_{RN}(\vartheta \mid \rho \geq T)$ evaluated on the original data set. (Real data set)

TABLE 4.2. RESULTS OBTAINED BEFORE AND AFTER THE REGISTRATION WITH THE PROPOSED TECHNIQUE, THE MANUAL ONE AND THE AUTOMATIC RIGID APPROACH FOR THE REAL DATA

Registration method	RMSE (pixels)	STD (pixels)	MI (bits)
No registration	3.56	1.81	0.564
Proposed automatic approach	1.38	0.59	0.652
Manual approach	1.41	0.62	0.646
Standard automatic approach	1.75	0.98	0.611

4.4. Discussion and conclusion

In this paper a novel method for the registration of VHR remote sensing images has been presented, which is especially effective for change-detection applications. The proposed method automatically extracts CPs that are associated with the most critical effects of the misalignment in image comparison. These points are identified by estimating RN distribution according to a multiscale analysis of the SCVs distribution. CPs are used to derive the disparity map that is exploited for the warping of the moving image through the well-known thin-plate spline transformation method. The proposed method exhibits the following properties: (i) automatic identification of CPs associated with the most critical points of the images where misregistration has a high probability to results in the detection of false changes; (ii) robustness to the presence of changes between the images.

Results obtained on both simulated and real data confirm the validity of the proposed method in identifying effective CPs, in estimating the disparity map and in performing the final co-registration between the considered images.

As future development of this work we plan to: (i) optimize the strategy for the searching of the displacement value; (ii) extend the analysis to other images (and larger images) acquired also by other VHR sensors; and (iii) compare the proposed method with existing more advanced registration methods.

PART II:
CHANGE-DETECTION METHODS

Chapter 5

5. A context-sensitive technique robust to registration noise for change detection in VHR multispectral images[4]

This chapter presents an automatic context-sensitive technique robust to registration noise (RN) for change detection (CD) in multitemporal very high geometrical resolution (VHR) remote sensing images. Exploiting the properties of RN in VHR images, the proposed technique analyzes the distribution of the spectral change vectors (SCVs) computed according to the change vector analysis (CVA) in a quantized polar domain. The method studies the SCVs falling into each quantization cell at different resolution levels (scales) to automatically identify the effects of RN in the polar domain. This information is jointly exploited with the spatial context information contained in the neighborhood of each pixel for generating the final CD map. The spatial context information is modeled through the definition of adaptive regions homogeneous both in spatial and temporal domain (parcels). Experimental results obtained on real VHR remote sensing multitemporal images confirm the effectiveness of the proposed technique.

5.1. Introduction

Unsupervised change detection plays an important role in many application domains related to the exploitation of multitemporal images. Depending on the considered application, the change-detection problem has different properties and peculiarities, and should satisfy specific constraints. In some domains, the priority constraint is related to the need to guarantee a real time detection of changes (e.g., in video surveillance [85], [86], [87], [88], motion detection [89], [90], etc.). In other applications, the time constraint can be relaxed and the precision of the change-detection result (also at the cost of a high computational complexity) plays the most important role (e.g. remote sensing [9], [91], biomedical applications [92], [93], etc). For some domains, the change-detection problem can require multidimensional (or multichannel) images: this is for instance the case of data simultaneously acquired in different bands of the electromagnetic spectrum (multispectral images) or taken with multimodal acquisition protocols (multimodal images). In this perspective, the change-detection procedure

[4] This chapter is published on *IEEE Transaction on Image Processing*, Vol. 19, no. 7, 2010, pp. 1877-1889. Title: "A Context-Sensitive Technique Robust to Registration Noise for Change Detection in VHR Multitspectral Images". Authors: S. Marchesi, F. Bovolo and L. Bruzzone.

is more complex and should be able to recognize the presence of changes by analyzing multidimensional vectors associated with each pixel of the investigated multitemporal images. Typical applications related to the above-mentioned data are in the remote sensing and the biomedical domains.

In this chapter we focus the attention on unsupervised change-detection techniques for multitemporal and multispectral remote sensing images. In greater detail, we consider very high geometrical resolution multispectral images acquired by the last generation of satellite sensors (e.g. Ikonos, Quickbird, EROS, GeoEye-1, WorldView-2). These sensors can acquire both multispectral and/or panchromatic images with a geometrical resolution on the ground which varies from few meters to 0.41[m] in the best case (at the time of writing). In the literature, several unsupervised change-detection methods for multidimensional remote sensing images have been proposed [11], [15], [17], [18], [21], [94], [95]. These techniques have been successfully employed in many different application domains related to land cover monitoring, like analysis of growth of urban areas, cadastral map updating, risk analysis, damage assessment, etc. However, the most of the available methods are optimized for the analysis of images acquired by medium resolution (MR) and high resolution (HR) sensors, and result ineffective when dealing with images showing metric or submetric resolution. Therefore it is necessary to develop novel methodologies capable to exploit the properties of VHR images in detecting changes between multitemporal images.

Change-detection techniques developed in other application domains for the specific analysis of VHR images result ineffective when applied to remote sensing images. The main problems are related to the different conditions in which the remote sensing images can be acquired, and in particular to differences in: (i) sunlight and atmospheric conditions; (ii) sensor acquisition geometry [21], [67], [91]; (iii) spectral signatures of vegetation due to seasonal effects. In order to reduce the impact of these conditions on CD maps, pre-processing steps are required as: co-registration, radiometric and geometric corrections, and noise reduction. Among them, co-registration plays a fundamental role and becomes more complex and critical (and therefore intrinsically less accurate), when the geometrical resolution increases. In practice, a perfect alignment between images is impossible as differences in the acquisition view angles and in geometrical distortions cannot be compensated, then causing a significant residual registration noise which sharply impacts on CD [8], [67], [68].

Another important problem in change detection on VHR images concerns the modeling of the spatial context information of the scene. Most of the classical change-detection techniques generally assume spatial independence among pixels, which is not reasonable in high geometrical resolution data. In order to better exploit the spatial correlation among neighboring pixels and to get accurate and reliable CD maps (both in regions corresponding to border or geometrical details and in homogeneous areas), it is necessary to integrate the spectral information with the spatial one and to model the multiscale properties of the scene. In the literature only few techniques capable to exploit the above-mentioned concepts [13], [24], [27], [96] are available.

In order to overcome the aforementioned problems, this chapter presents an adaptive context-sensitive technique, which: i) reduces the impact of registration noise in change detection on VHR multispectral images through a multiscale strategy; ii) considers the spatial dependencies of neighborhood pixels through the definition of multitemporal parcels (i.e. homogeneous region both in space and time domain). The proposed technique is developed in the context of the polar framework for change vector analysis (CVA) introduced in [11] and described in section 2.4 for the analysis of MR and HR multispectral images, and is based on the analysis of the properties of registration noise presented in chapter 3 [81]. The experiments carried out on multitemporal VHR images confirm the validity of the theoretical analysis and the effectiveness of the proposed technique.

The chapter is organized into four sections. The next section illustrates the proposed multiscale and context-based approach for change detection on VHR images. Section 5.3 presents the experimental results obtained on two real multitemporal data sets made up of QuickBird images. Finally, section 5.4 draws the conclusions of this work.

For the notation used in this chapter, please refer to section 2.4, while for the background on the registration noise properties please refer specifically to the multiscale properties retrieved in chapter 3 and in particular to Property 3 (*Clusters of dominant registration noise in Ac exhibit significant variations of properties versus the scale (resolution) of the images.*) and Property 4 (*Clusters associated with changed pixels in Ac exhibit slow varying statistical properties versus the scale (resolution) of the images.*) described in section 3.3.

5.2. Methodology

The multiscale properties of registration noise (Property 3 and Property 4) described in section 3.3 are at the basis of the development of the change-detection technique based on the analysis of the behavior of the distribution of SCVs in the polar domain at different scales described in this chapter. As reported in section 3.3, we expect that true significant changes are associated with objects with a non negligible size (this assumption is reasonable and realistic when dealing with VHR images), while misregistration appears in the multispectral difference image with relatively thin structures having different orientations. Therefore, by reducing the resolution of images we implicitly decrease the impact of the registration noise with respect to that on the original scene, while the statistical properties of true changes maintain a good stability. In other words, the lower the geometrical resolution is, the lower the probability of identifying clusters associated with registration noise in the *annulus of changed pixels*. This means that at low resolution levels in the *annulus of changed pixels* mainly clusters due to the presence of true changes on the ground can be detected. However, in order to obtain a change-detection map characterized by a good geometrical fidelity, we should work at full resolution. On the basis of these considerations, we propose a change-detection technique that exploits a multiscale decomposition in order to extract information about registration noise, and generates the final change-detection map working at full resolution. In this way we preserve the high geometrical detail content of VHR images. In addition, in order to exploit the specific properties of VHR images, the proposed technique adaptively models also the spatial context information.

The proposed method can be divided into two main phases: (i) registration noise identification; and (ii) context-sensitive decision strategy for the generation of the final change-detection map. The main idea of the developed technique is to detect the regions of the polar framework where the registration noise is dominant according to a multiscale strategy, and to consider the spatial-context information through the definition of multitemporal parcels in order to generate the final change-detection map (see Figure 5.1). In the following details on the two phases are reported.

5.2.1 Registration noise identification

The first phase of the proposed technique aims at identifying the regions related to registration noise in the polar domain. To this purpose, we apply an analysis based on the following three steps: 1) CVA at full resolution (identification at full resolution of regions in the polar domain candidate to include registration noise SCVs, i.e. A_c); 2) quantization-based analysis of the SCV distributions at different resolution levels; and 3) adaptive identification of registration noise cells.

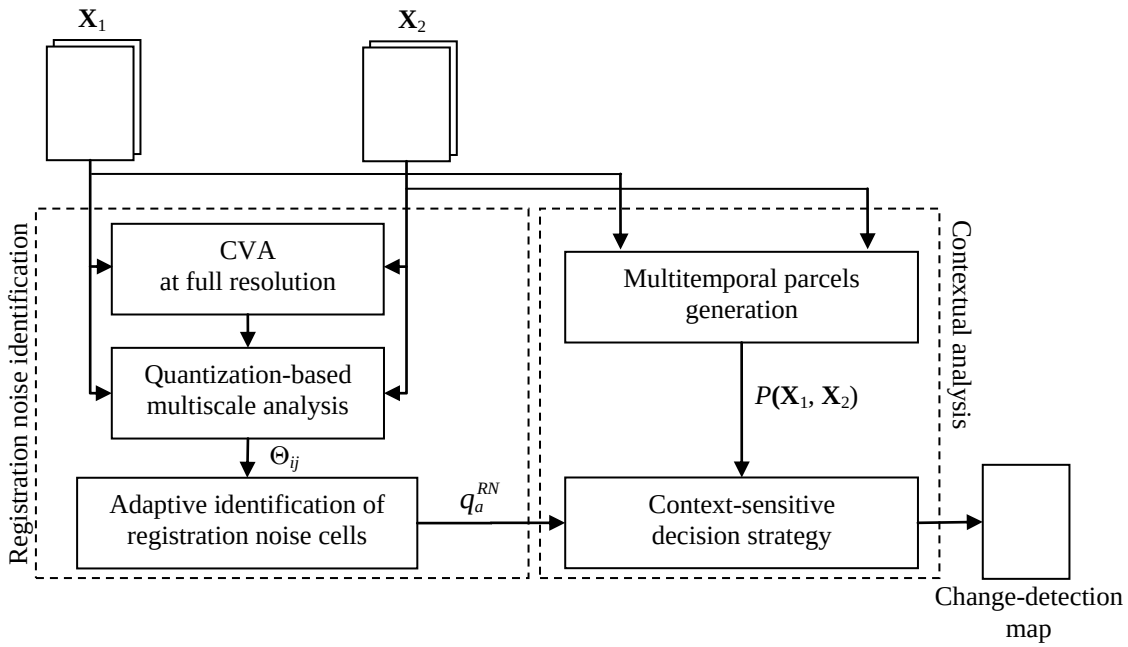

Figure 5.1. General architecture of the proposed multiscale and parcel-based change-detection technique.

In the first step the CVA technique is applied to the original images $\mathbf{X}_1$ and $\mathbf{X}_2$, and the threshold value T that separates the *circle of no-changed pixels* from the *annulus of changed pixels* is estimated. The value of T can be retrieved either by a manual *trial-and-error* procedure or by one of the automatic thresholding algorithms proposed in the literature[15], [80]. SCVs in C_n are labeled as no-changed SCVs, whereas pixels in A_c should be further analyzed in order to separate SCVs associated with registration noise from pixels of true changes.

To this end, in the second step, A_c is divided into M uniformly distributed quantization cells q_m (m=1,…,M) (A_c={q_1,q_2,…,q_M}) of fixed shape and size. Each cell is characterized by its extension $\Delta\rho$ and $\Delta\vartheta$ in the magnitude and in the direction coordinates respectively (see Figure 5.2). It is worth noting that the choice of the cell size can significantly affect the performance of the quantization-based registration-noise-identification process. The proposed method aims at overcoming this problem by exploiting different cell sizes in the identification of registration noise clusters in A_c (see the third step of the estimation procedure). Once cells have been defined, the two multitemporal images are decomposed according to a multiscale transformation obtaining two sets of images $\mathcal{X}_{MS_t} = \{\mathbf{X}_t^0, ..., \mathbf{X}_t^n, ..., \mathbf{X}_t^{N-1}\}$, where the subscript t (t=1,2) denotes the acquisition date, and the superscript n (n=0,1,…, N-1) indicates the resolution level ($\mathbf{X}_t^0 = \mathbf{X}_t$). The multiscale decomposition can be carried out by using different algorithms, like gaussian pyramid decomposition, wavelet transform, recursively upsampled bicubic filter, *etc.* Images in $\mathcal{X}_{MS_t}$ show different tradeoffs between registration noise and geometrical detail content. The CVA technique is applied to each corresponding pair ($\mathbf{X}_1^n, \mathbf{X}_2^n$), n=1,2,…, N-1, of low resolution images in $\mathcal{X}_{MS_1}$ and $\mathcal{X}_{MS_2}$. Then the distribution of SCVs within each cell is studied at different scales. In particular, for each set of pixels with SCVs falling in a given cell q_m (m=1,2,…,M) at full resolution, the behavior of the distribution of the same SCVs at resolution level N-1 (i.e., the lowest considered one) is analyzed in order to identify whether the cell is associated with registration noise or not. It is worth noting that the maximum level of decomposition N-1 has to be selected according to the size of expected main change structures in the considered images. The main idea of this procedure is to identify cells of registration noise through a comparison

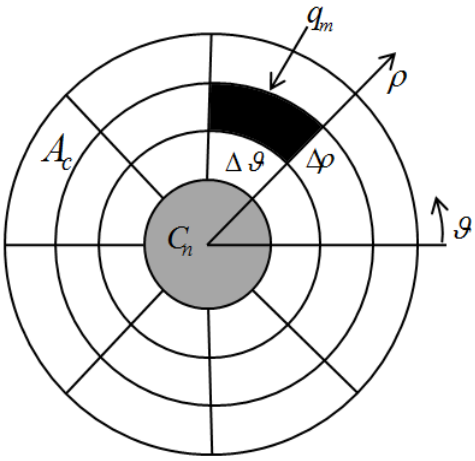

Figure 5.2. Quantized magnitude-direction polar domain

between the distribution of the magnitude of SCVs at full resolution and at the lowest consideredresolution. At this level pixels of registration noise tend to disappear given their properties that usually result in small and thin structures. To this purpose, according to the multiscale properties described in the previous section, the behavior of the mean value of SCVs on the magnitude variable at different resolutions is analyzed. In the proposed method the mean value $\mu_{q_m}^0$ of the magnitude ρ of SCVs that fall within a cell q_m at full resolution (level 0) is compared with the mean value $\mu_{q_m}^{N-1}$ that the same SCVs have at resolution level N-1[5]. A cell is associated with registration noise (*RN*) or not (*RNfree*) according to the following decision rule:

$$q_m \in \begin{cases} RNfree & \text{if } \left\{\left|\mu_{q_m}^0 - \mu_{q_m}^{N-1}\right| < K\right\} \\ RN & \text{if } \left\{\left|\mu_{q_m}^0 - \mu_{q_m}^{N-1}\right| \geq K\right\} \end{cases} \tag{5.1}$$

where K is a threshold value empirically set as equal to the difference between the mean value of all the SCVs falling in A_c at full resolution and the mean value of the corresponding SCVs at the lowest level, i.e.:

$$K = \left|\mu_{A_c}^0 - \mu_{A_c}^{N-1}\right| \tag{5.2}$$

It is worth noting that small variations of the threshold value around the automatic retrieved one do not significantly affect the identification of registration noise clusters.

Let q_m^{RN} be a generic cell q_m associated with registration noise according to (5.1). A generic SCV z_{ij} is associated with registration noise if it falls within a cell q_m^{RN}, i.e.

$$z_{ij} \in \begin{cases} RN & \text{if } z_{ij} \in q_m^{RN} \\ RNfree & \text{otherwise} \end{cases} \tag{5.3}$$

In this way we locate the SCVs affected by registration noise in the polar domain.

As pointed out previously, an important aspect to be considered is the choice of the quantization cell size. Slightly different results can be obtained with different quantization characterized by cell sizes in different ranges of parameters $\Delta\rho$ and $\Delta\vartheta$. Therefore in the third step we adopt a strategy

[5] It is worth noting that in order to identify cells of registration noise we do not analyze the behavior of SCVs that fall within the same cell at different resolution levels, but we consider SCVs that at the highest resolution fall within a cell and the same SCVs at the lowest considered level. This approach allows us to follow the low-pass effect of the decomposition filter, which causes a migration of SCVs toward the origin of the polar domain.

capable to take advantage of different cell sizes, in order to make the technique less affected from the choice of these parameters. First of all the *annulus of changed pixels* is divided L times into uniformly distributed quantization cells with different size $\Delta\rho_l \times \Delta\vartheta_l$, ($l$=1,…,$L$).

Let us define the set $\boldsymbol{Q}$ of all the L considered quantizations as:

$$\boldsymbol{Q} = \left\{ Q_l \,\middle|\, l = 1,...,L \right\} \tag{5.4}$$

Q_l (l=1,…, L) is the lth quantization made up of a set of cells with the same size

$$Q_l = \left\{ q_m^l \;\middle|\; \bigcup_{m=1}^{M_l} q_m^l = A_c \,,\; q_m^l = \Delta\rho_l \times \Delta\vartheta_l \right\} \tag{5.5}$$

where M_l indicates the number of cells that results from the quantization process, given $\Delta\rho_l$ and $\Delta\vartheta_l$.

For each quantization Q_l the previously described procedure is performed in order to obtain labels *RN* and *RNfree* for each cell of each quantization Q_l (l=1,…, L). Let Θ_{ij} be the set of L labels (one for each Q_l) associated to z_{ij} according to (5.3). Labels in Θ_{ij} can assume values in {*RN*, *RNfree*}. In order to determine if a spectral change vector z_{ij} is of registration noise or not, a majority voting rule is applied to Θ_{ij}. Therefore a spectral change vector z_{ij} is of registration noise if the most of the labels in Θ_{ij} is *RN*, i.e.,

$$z_{ij} \in \begin{cases} RN & \text{if } mode(\Theta_{ij}) = RN \\ RNfree & \text{if } mode(\Theta_{ij}) = RNfree \end{cases} \tag{5.6}$$

where *mode*(.) is the mathematical operator that returns the element that occurs most often in a set of elements. In other words, a generic region of A_c covered by cells (one for each Q_l) that are mostly associated to registration noise according to (5.1) is defined as registration noise region, otherwise it is registration noise free. Actually, this procedure implicitly results in a quantization Q_A of the *annulus of changed pixels* made up of regions with different shapes and sizes. Each region is labeled as *RN* or *RNfree*. We refer to these regions as adaptive cells q_a (a=1,…, M_a), and Q_A results defined as:

$$Q_A = \left\{ q_a \;\middle|\; \bigcup_{a=1}^{M_a} q_a = A_c \right\} \tag{5.7}$$

Let q_a^{RN} (a=1,…,M_a) be a generic adaptive cell which includes contiguous SCVs in the magnitude-direction domain that have been associated to label *RN* according to (5.6). Taking into account this notation, the rule (5.6) can be rewritten as:

$$z_{ij} \in \begin{cases} RN & \text{if } \; z_{ij} \in q_a^{RN} \\ RNfree & \text{otherwise} \end{cases} \tag{5.8}$$

5.2.2 Context-sensitive decision strategy for the generation of the final change-detection map

The retrieved information on each adaptive cell is used for properly driving the generation of the final change-detection map according to a context-sensitive parcel-based procedure. Parcels are defined as regions that adaptively characterize the local neighborhood of each pixel in the considered scene and are homogeneous in both temporal images [13], [79]. The adaptive nature of multitemporal parcels allows one to model complex objects in the investigated scene as well as borders of the changed areas and geometrical details. In order to generate multitemporal parcels from the two original images we first compute two segmentation maps $P(\mathbf{X}_1)$ and $P(\mathbf{X}_2)$ applying a segmentation algorithm separately to images $\mathbf{X}_1$ and $\mathbf{X}_2$, respectively. In this work a region growing segmentation algorithm was considered, however any different kind of technique can be adopted. Each $P(\mathbf{X}_t)$ represents a partition of image $\mathbf{X}_t$ (t=1,2) in disjoint regions of spatially contiguous pixels. Each single region in

both partitions satisfies a homogeneity measure $H(.)$ that involves spectral and spatial properties [97], [98]. The desired representation of the spatio-temporal context of the considered scene is obtained merging the two segmentations. The final output is a partition $P(\mathbf{X}_1,\mathbf{X}_2)$ shared by both considered images made of N regions p_r (r=1,…, R) called parcels. The defined multitemporal parcels satisfy the following conditions:

$$\begin{gathered} H[\mathbf{X}_1(p_r)] = true \quad \text{AND} \quad H[\mathbf{X}_2(p_r)] = true \\ H[\mathbf{X}_1(p_r) \cup \mathbf{X}_1(p_k)] = false \quad \text{OR} \quad H[\mathbf{X}_2(p_r) \cup \mathbf{X}_2(p_k)] = false \\ \forall \quad r,k = 1,...,R \text{ and } r \neq k \end{gathered} \tag{5.9}$$

where $\mathbf{X}_t(p_r)$ represent the portion of image $\mathbf{X}_t$ (t=1,2) covered by parcel p_r (r=1,..., R) and p_r and p_k are adjacent.

The spatial-context information associated to each parcel is integrated to the information about presence or absence of registration noise retrieved from the multiscale analysis in the previous phase. Let Z_r be the set of spectral change vectors corresponding to the pixels included in parcel p_r, i.e. $Z_r = \{z_{ij} \,|\, z_{ij} \in p_r\}$. Each SCV in Z_r can assume one out of three labels. Therefore the SCVs (i.e., the pixels) in a generic parcel p_r can be divided into three subsets: i) Z_r^{RN} which includes SCVs of registration noise labeled according to (5.8); ii) Z_r^{RNfree} which includes SCVs that are not affected by registration noise according to (5.8); and iii) $Z_r^{\omega_n}$ which includes SCVs that fall into C_n. According to this notation, all the SCVs in a generic parcel p_r (and thus the parcel itself) are classified as changed or no-changed according to the following majority rule:

$$p_r \in \begin{cases} \omega_n & \text{if } \dfrac{\left|Z_r^{RN}\right| + \left|Z_r^{\omega_n}\right|}{\left|Z_r\right|} \geq 0.5 \\ \Omega_c & \text{otherwise} \end{cases} \tag{5.10}$$

where $|.|$ is the mathematical operator that returns the cardinality of sets. In other words a parcel p_r (and therefore all the pixels in it) is labeled as no-changed if the most of the SCVs belonging to it either have been classified as SCVs affected by registration noise according to (5.8) or fall into C_n. It is worth noting that the proposed approach allows us to create a relationship between the RN information retrieved in the polar domain (related to spectral change vectors) and the spatial information of the original images (related to pixels and parcels). The final change-detection map is obtained at full resolution, as low resolution components extracted from the multiscale analysis are used only for detecting quantization cells associated with registration noise. Thus the obtained change-detection map adequately models geometrical details present in the analyzed VHR images, reproducing accurately both border and homogeneous changed regions.

5.3. Experimental results

In this section the experimental analysis conducted on real data is presented. First of all the data sets are described, then the multiscale properties presented in section 3.3 are analyzed on the considered data. Finally the proposed multiscale and parcel-based technique is applied to the images and results are discussed.

5.3.1 Data set description

In order to assess the effectiveness of the proposed technique, two multitemporal data sets were considered. In particular, two different portions of two images acquired on the city of Trento (Italy)

by the Quickbird multispectral sensor in October 2005 and July 2006 were analyzed. The Quickbird sensor collects panchromatic images at 0.7 [m] resolution and multispectral images with 4 spectral channels (blue (450-520[nm]), green (520-600[nm]), red (630-690[nm]) and near-IR (760-900[nm])) at 2.8 [m] resolution. In the pre-processing phase the two images were: i) pan-sharpened; ii) radiometrically corrected; and iii) co-registered. In particular, we considered pan-sharpened images as we expect that the pan-sharpening process can improve the results of the change-detection process, as demonstrated in previous work [99]. To this purpose we applied to the images the Gram-Schmidt procedure implemented in the ENVI software package [100] to the panchromatic channel and the four bands of the multispectral images. Concerning radiometric corrections, we simply normalized the images by subtracting from each spectral channel of the two considered images its mean value.

The two different data sets were selected with the following rationale: i) the first data set (Data Set 1), which is made up of images of 984 x 984 pixels, is a small portion of the investigated scene for which we have a complete and detailed knowledge of the changes occurred on the ground. This allowed us to perform a quantitative detailed analysis under completely controlled conditions; ii) the second data set (Data Set 2), which is made up of images of 5000 x 5000 pixels, is related to the largest portions of the two available Quickbird images that correspond to the same area on the ground. These large images allowed us to perform a less detailed quantitative analysis (based on a spatial random sampling as we did not have a complete knowledge of the changes occurred on the ground) but an important qualitative analysis on the effectiveness and robustness of the proposed technique in real operational conditions on large scenes. The registration process was carried out by using a polynomial function of order 2 according to 14 ground control points (GCPs) for the first data set and according to 20 GCPs for the second one, and by applying a nearest neighbor interpolation [100]. In our experiments we did not use more advanced registration techniques and procedures for geometric corrections for better assessing the robustness of the proposed method to the residual registration noise.

Figure 5.3(a) and Figure 5.3(b) show a true color composition of the pansharpened images $\mathbf{X}_1$ and $\mathbf{X}_2$, respectively, related to the Data Set 1 (984 x 984 pixels). Between the two acquisitions two kinds of changes occurred: (i) simulated changes that consist of new houses introduced on the rural area (continuous circles in Figure 5.3(b)); and (ii) real changes that consist of some roofs rebuilt in the urban area (dashed circles in Figure 5.3(b)). It is worth noting that simulated changes have been introduced in a completely realistic way in order to include a second type of change in the analysis. In particular, simulated buildings have been added to the scene taking their geometrical structures and spectral signatures from other real buildings present in other portions of the available full scene in order to take into account the image dynamic and noise properties. Moreover, between the two dates other spectral changes that depend on differences in the vegetation phenology and have not a semantic meaning are present, due to the different acquisition seasons (i.e., summer and autumn) of the images under investigation. To perform a quantitative assessment of the effectiveness of the proposed method, a reference map (which includes 20602 changed pixels and 968256 no-changed pixels) was defined according to both the available prior knowledge on the considered area and to a visual analysis of images (see Figure 5.3(c)). According to the previous observation, the reference map does not report changes due to seasonal variations of the vegetation phenology. However, if these changes show significant intesity in the magnitude domain, they will appear in the final change-detection map, even if, from a semantic point of view, the related area is not changed.

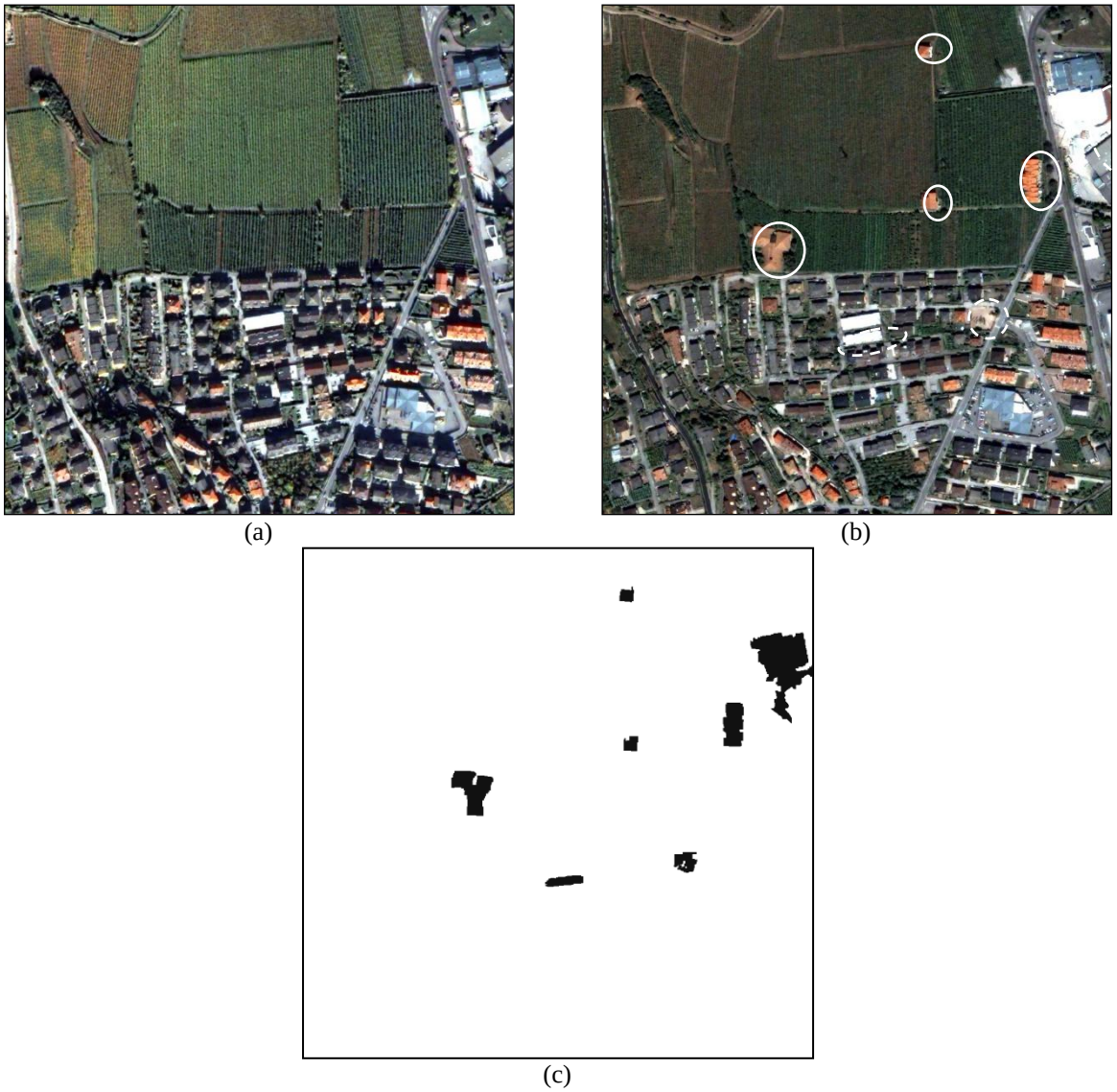

Figure 5.3. True color composition of Data Set 1 (small images) made up of pansharpened images of the Trento city (Italy) acquired by the Quickbird VHR multispectral sensor in: (a) October 2005; and (b) July 2006 (simulated changes appear in the regions marked with continuous circle, while real changes occurred between the two acquisition dates appear in regions marked with dashed circles). (c) Change-detection reference map.

Figure 5.4(a) and Figure 5.4(b) show the true color compositions of the pansharpened images $\mathbf{X}_1$ and $\mathbf{X}_2$, respectively, related to the Data Set 2 (5000 x 5000 pixels). Between the two acquisitions different kinds of changes occurred on the ground affecting urban, industrial, rural and forest areas. From a visual analysis it is possible to note: i) differences in some roofs of the urban and industrial areas; ii) differences in the bank of the river due to a reduction of the water level; iii) significant differences due to shadows in the forest area; and iv) differences in the cultivated fields due to different kinds of farming. Considering the extent of the scene and the fact that we have no a priori information on the whole area under investigation, in this case it was not possible to derive a complete reference map. The magnitude image obtained according to (2.2) points out the main spectral differences present between the two dates (Figure 5.4(c)). To perform a quantitative assessment of the effectiveness of the proposed method on these large images, a set of points were randomly collected in the scene and each of them was labeled as changed or non-changed according to a careful visual analysis. In particular, 2300 points were collected (245 labeled as change and 2055 as no-change). It is worth

noting that in this case there are some semantic changes in the crops (i.e. changes in the type of cultivation), which are considered as changes in the reference map and thus in the quantitative analysis. Finally, also in this second data set changes related to different phenology of the vegetation are considered as false alarms, since they have not any semantic meaning.

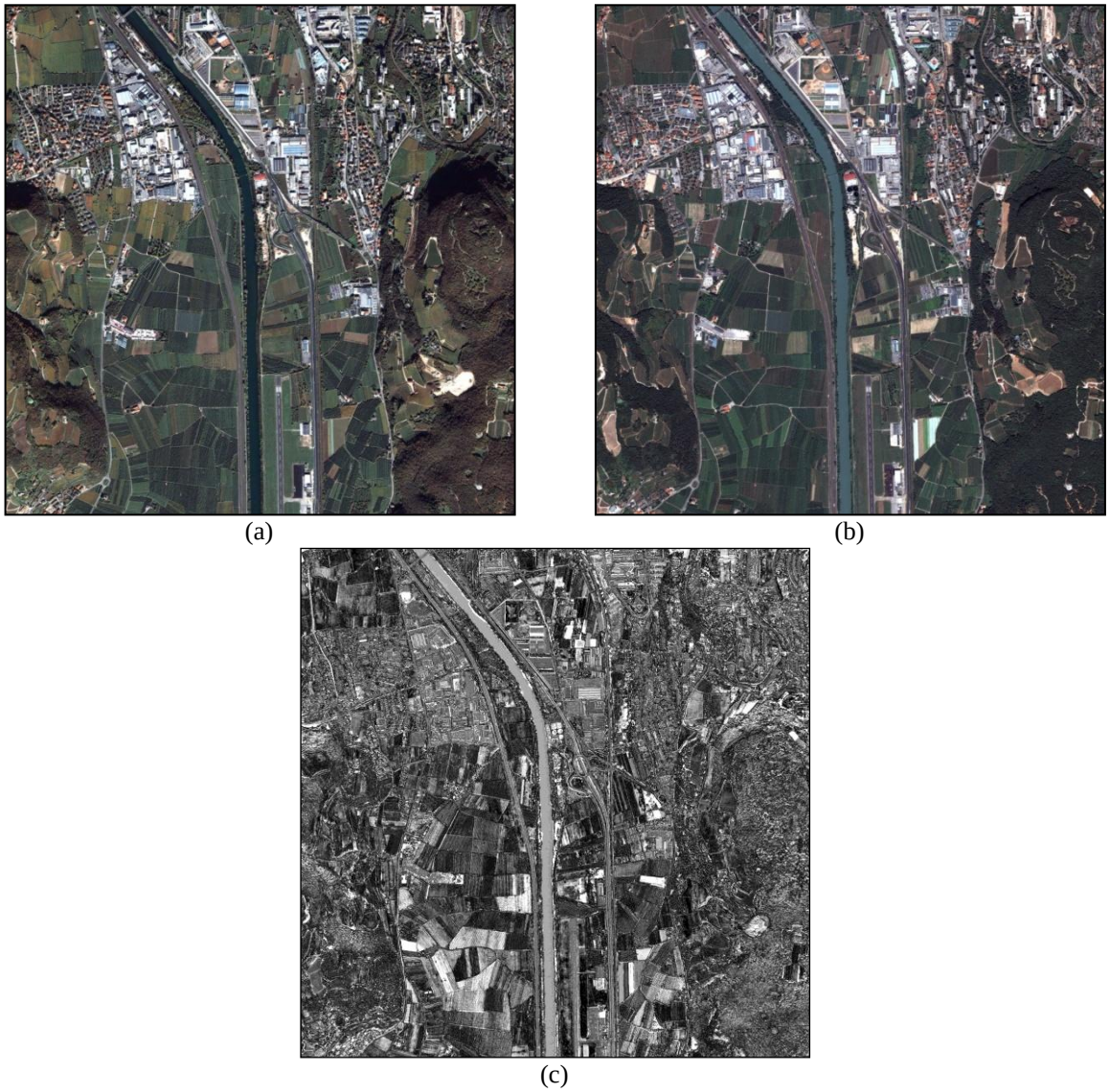

(a) (b) (c)

Figure 5.4. True color composition of Data Set 2 (large images) made up of pansharpened images of the Trento city (Italy) acquired by the Quickbird VHR multispectral sensor in: (a) October 2005 and (b) July 2006; (c) magnitude image.

5.3.2 Results: multiscale properties

To confirm the validity of the fundaments of the proposed technique, we carried out an analysis on the multiscale properties of registration noise on the considered images. This analysis was conducted only on Data Set 1, as a complete reference map on the investigated area was available only for the small images. The aim of this analysis was to show that the properties derived on simulated data are effective also for real data. To this purpose, as done for simulated data in [81] and reported in this thesis in chapter 3 from the Quickbird multitemporal images $\mathbf{X}_1$ and $\mathbf{X}_2$ we generated images at different scales by applying the *Daubechies-4* stationary wavelet transform [73] to the multitemporal images $\mathbf{X}_1$ and $\mathbf{X}_2$. To show the effect of the multiscale decomposition in the polar domain, we applied the

CVA technique to the original images and to the dataset at lowest resolution. We considered only the red and near infrared spectral channels, as they revealed to be the most effective in emphasizing the changes occurred on the area of interest. Figure 5.5 reports the scatterograms obtained on both the images at full resolution and the images at the fourth level of the decomposition. Comparing these scatterograms (and the other ones obtained at different resolution level, which are not reported for space constraints) it is possible to observe that, decreasing the resolution, clusters associated with changed pixels (see regions marked with continuous circles in Figure 5.5) only reduce their spread, without being completely smoothed out. On the contrary, clusters associated with RN tend to disappear (dashed circles in Figure 5.5 (a)), collapsing within the *circle of no-changed pixels* (dotted circle in Figure 5.5 (a)). This behavior confirms what expected from the analysis presented in section 3.3, i.e. SCVs of real changes show a quite stable trend, while SCVs associated with registration noise have non stable properties versus the scale. These results were conducted also on other data sets.

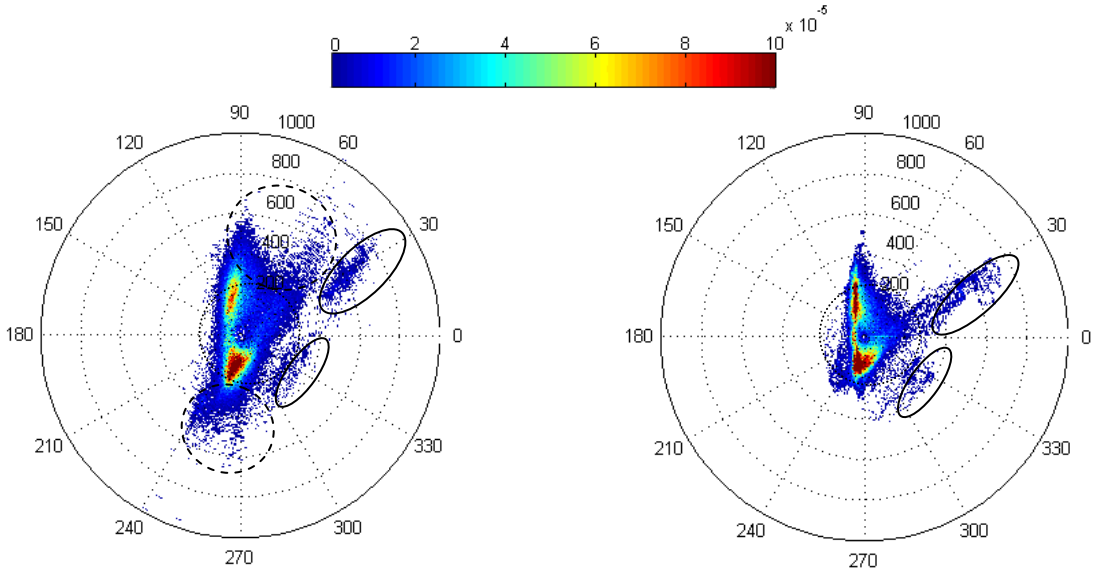

(a) (b)

Figure 5.5. Scatterograms in the polar coordinate system of (a) the full resolution original difference image, and (b) the low resolution image obtained at level four of the wavelet decomposition. Dotted circle separates C_n from A_c, continuous circles indicate sectors of true changes, while dashed circles identify regions of registration noise.

In greater detail, we studied the behavior of the mean values in the magnitude domain of SCVs related to registration noise and to real changes, when the resolution of the images decreases. Figure 5.6 reports the behavior of the mean value of the magnitude of SCVs versus the scale: the mean value of RN clusters rapidly decreases by reducing the scale (continuous line), while the mean value of SCVs associated with true changes slightly varies with the scale (dashed line), decreasing slower than the one of SCVs related to RN.

5.3.1 Results: change detection on Data Set 1 (small images)

The effectiveness of the proposed technique was firstly tested on the Data set 1. To this purpose cells of registration noise were identified according to the procedure described in section 5.2.1, and then the final change-detection map was generated according to section 5.2.2. According to the proposed technique, the first step aimed at identifying registration noise. To this purpose the change vector analysis technique was applied to images $\mathbf{X}_1$ and $\mathbf{X}_2$ and the decision threshold T that separates the *annulus of changed pixels* from the *circle of no-changed pixels* was computed.

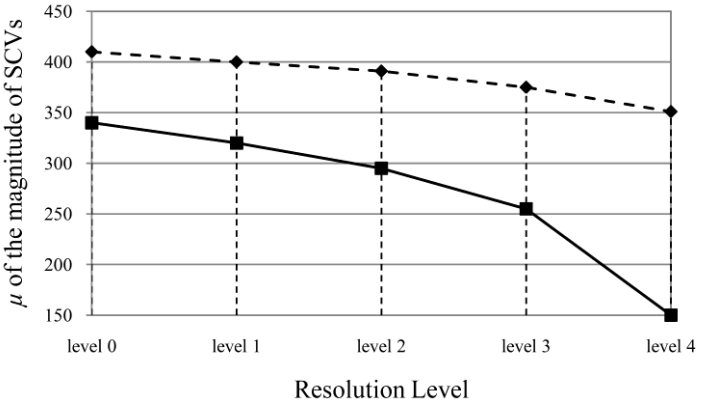

Figure 5.6. Behavior of the mean value of the magnitude of SCVs versus the resolution levels (scale) for the class of changes (dashed line) and of registration noise (continuous line).

The Bayes rule for minimum error [15], [80] with estimates obtained by the Expectation Maximization (EM) algorithm was used for retrieving a value T equal to 220. SCVs in C_n were labeled as no-changed SCVs. Five (L=5) different quantizations Q_l (l=1,...,5) were considered for the *annulus of changed pixels* with cells of size $\Delta\rho_l \times \Delta\vartheta_l$, where $\Delta\rho_l \in \{100, 200, 300, 400, 500\}$ and $\Delta\vartheta_l = 10°$ (for each l=1,..., 5). It is worth noting that different values for $\Delta\rho_l$ and $\Delta\vartheta_l$ can be selected according to the considered data set. Images $\mathbf{X}_1$ and $\mathbf{X}_2$ were decomposed according to the procedure described in section 5.3.2, and the CVA technique was applied to the full (i.e., level 0) and the lowest (i.e. level four of the wavelet transform) resolution images. Figure 5.5 shows the polar scatterograms obtained for the two mentioned resolution levels.

In order to identify whether a cell q_m^l (l=1,…, M_l) for a given Q_l (l=1,...,5) is of registration noise or not the difference in the mean values of the magnitude of SCVs between the resolution level 0 and 4 was computed. This value was compared with the threshold K derived according to (5.2) (for T equal to 220, the value of K resulted equal to 190). SCVs falling into cells in which the difference resulted to be higher than K were labeled as belonging to registration noise according to (5.3). At this stage, for comparison purposes, a set of five change-detection maps was generated (one for each considered quantization) by assigning SCVs in C_n and SCVs of registration noise to the class of no-changed pixels and all the others to the class of changed pixels (see Table 5.1). As one can see, for $\Delta\rho_l$ between 200 and 400 similar results were achieved, whereas higher or lower values resulted in slightly worse performance.

In order to reduce the impact of critical values of $\Delta\rho_l$ and $\Delta\vartheta_l$ on the changed-detection performance, we applied the proposed technique for adaptively modeling the cell shape and size involving in the decision step all the five quantization intervals. Each SCV was classified as belonging to registration noise or not according to (5.6). Even at this stage, for sake of comparison, a change-detection map was computed by assigning SCVs in C_n and SCVs of registration noise to the class of no-changed pixels and all the others to the class of changed pixels (see results for the pixel-based proposed technique in Table 5.2). Comparing these results with the ones in Table 5.1 it is possible to conclude that the joint use of quantization cells of different size makes the change-detection process more robust as results obtained with unreliable quantizations values are discarded thanks to the majority decision rule in (5.6).

Finally, the information about adaptive cells of registration noise was used within the parcel-based decision strategy for computing the final change-detection map according to the proposed strategy. To

TABLE 5.1. CHANGE-DETECTION RESULTS OBTAINED ON DATA SET 1 AT A PIXEL LEVEL WITH THE PROPOSED MULTISCALE TECHNIQUE WITHOUT THE ADAPTIVE ANALYSIS OF THE CELL DIMENSION.

Cell size $(\Delta\rho_l \times \Delta\vartheta_l)$	False alarms	Missed alarms	Overall error	Overall accuracy (%)
100x10	111279	17356	128635	86.72
200x10	61252	5123	66375	93.15
300x10	62867	4728	67595	93.02
400x10	63091	4644	67735	93.00
500x10	76614	17905	94519	90.24

this end, multitemporal parcels were generated as described in section 5.2.2 and SCVs in each parcel were labeled according to (5.10). As one can see from Table 5.2, the use of the spatial-context information significantly reduces both false and missed alarms. It is worth noting that the use of spatial-context information retrieved according the parcel-based strategy allows one to obtain a regularized change-detection map without affecting the geometrical details content of the map itself.

TABLE 5.2. CHANGE-DETECTION RESULTS OBTAINED ON DATA SET 1 (SMALL IMAGES) AT BOTH PIXEL AND PARCEL LEVEL BY THE PROPOSED ADAPTIVE AND MULTISCALE TECHNIQUE, THE STANDARD CVA TECHNIQUE AND THE MANUAL APPROACH.

Technique		False alarms	Missed alarms	Overall error	Overall accuracy (%)
Pixel-based	**Proposed**	61429	5061	66490	93.13
	Standard CVA	173676	1470	175146	81.91
	Manual (upperbound)	55984	5768	61752	93.62
Parcel-based	**Proposed**	28150	3870	32020	96.69
	Standard CVA	106580	734	107314	88.92
	Manual (upperbound)	23160	4192	27352	97.18

For a further assessment of the effectiveness of the proposed technique, change detection was performed according to the standard pixel-based [15] and parcel-based [79] change vector analysis ignoring the information about registration noise. In both cases (see Table 5.2) it is clear that standard methods are sharply affected by the presence of registration noise, which involves a high number of false alarms mainly located in the high frequency regions of the images. On the contrary, the proposed method significantly reduces false alarms both at pixel (from 17.94% to 6.34%) and at parcel level (from 11.01% to 2.91%), and generates change-detection maps characterized by high accuracy both in homogeneous and border areas. Figure 5.7 allows one a visual comparison between the change-detection map obtained at parcel level with the proposed technique (Figure 5.7 (a)) and the standard CVA (Figure 5.7 (b)).

A final comparison is made with the results achieved according to a manual trial-and-error approach. In this case the final change-detection map is computed assigning SCVs that fall into C_n to ω_n, and applying manual thresholds for isolating within A_c SCVs associated with changed pixels from those associated with registration noise on the basis of some prior information.

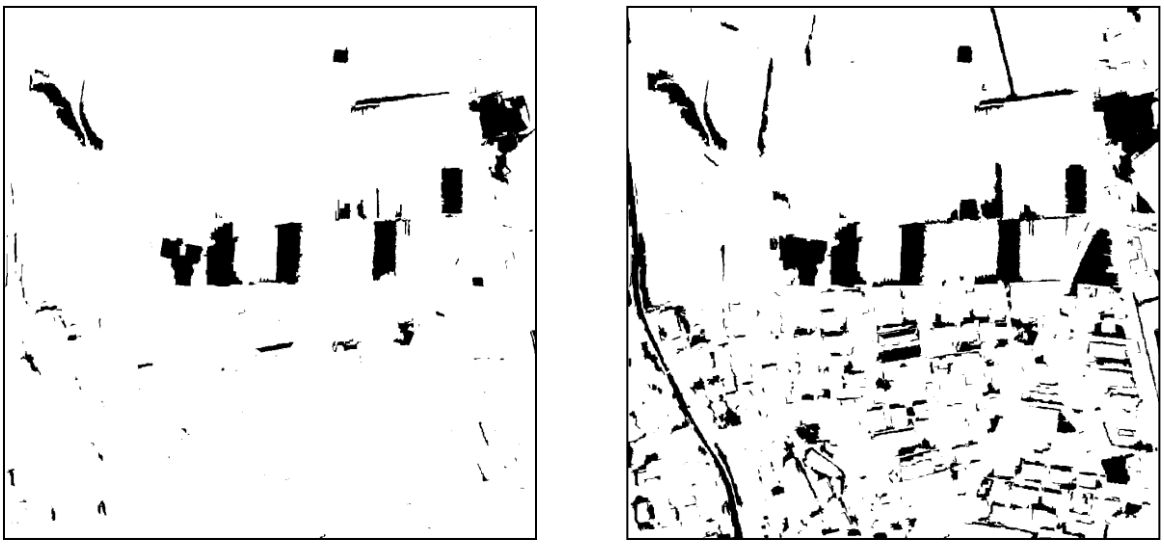

(a) (b)

Figure 5.7. Change-detection maps obtained on Data Set 1 with: (a) proposed multiscale approach with the adaptive estimation of the cell dimension at a parcel level; and (b) the standard parcel-based CVA.

Two maps were generated. The first considers the spatial-context information arising from multitemporal parcels while the second does not. Results yielded with this procedure can be considered as an upper bound for the proposed technique. Observing Table 5.2, one can conclude that the proposed method performs effectively both at a pixel and at a parcel level, as it exhibits overall accuracies that are close to those obtained by the manual (optimal) approach (i.e., 93.13% *vs.* 93.62% for the pixel-based case and 96.69% *vs.* 97.18% for the parcel-based one).

As final remark it is important to notice that the change-detection map derived by the proposed approach presents residual false alarms mainly due to the different acquisition seasons of the considered images (i.e., summer and autumn). This characteristic resulted in significant radiometric differences related to seasonal variations in the crop rows and in the shapes of shadows. The false alarms due to such acquisition conditions can be reduced only considering additional semantic information associated with changes. However, the overall accuracy achieved by the proposed context-sensitive technique robust to registration noise (i.e., 96.69%) due to sharp reduction of false alarms and the high fidelity in the reproduction of changed objects (both in uniform and contour regions) confirms its validity.

5.3.2 Results: change detection on Data Set 2 (large images)

In order to study the effectiveness of the proposed method in real operational conditions (where large images are considered), this sub-section reports the results obtained on the Data Set 2. As described for the previous data set, cells of registration noise were identified and then the final change-detection map was generated. In order to identify registration noise, we decomposed the images through the *Daubechies-4* stationary wavelet transform and we applied the CVA technique to the images $\mathbf{X}_1$ and $\mathbf{X}_2$ at full resolution and at the lowest considered level (fourth level of the wavelet transform). Also in this case the threshold value T (T=320) that separated A_c from C_n was retrieved according to the Bayes rule for minimum error. Five different quantization Q_l (l=1,...,5) of the *annulus of changed pixels* with cells of size $\Delta\rho_l \times \Delta\vartheta_l$, where $\Delta\rho_l \in \{100, 200, 300, 400, 500\}$ and $\Delta\vartheta_l = 5°$ (for each l=1,..., 5), were considered. Then the analysis on the difference in the mean values of the SCVs that fall within each cell at full resolution and at low resolution was performed and compared with the

threshold K derived according to (5.2) (K=98), in order to label each SCVs as belonging to RN or not according to (5.4). At this point the proposed technique for adaptively modeling the cell shape was applied to the five different considered quantizations Q_l and the final change-detection map at a pixel level was generated by assigning SCVs in C_n and SCVs of registration noise to the class of no-changed pixels and the others to the class of changes pixels (see results in Table 5.3).

Finally, the contextual information was exploited through the parcel-based proposed strategy and the final change-detection map at a parcel level was generated. Numerical results obtained on the test set described in section 5.3.1 are reported in Table 5.3. As one can observe, also in this case the number of false alarms is significantly reduced in the parcel-based strategy.

As for the Data Set 1, we compared the results obtained with the proposed method with the ones achieved by the standard CVA both at pixel and parcel level ignoring the information about registration noise. Observing Table 5.3, it is clear that in both cases the standard method is sharply affected by a high number of false alarms (mainly due to RN), whereas the proposed method exhibits a significant reduction of them, resulting in an overall change detection accuracy 6% higher than that achieved by the standard method (from 87.07% to 94.56% for the pixel-based case and from 91.25 % to 97.10% for the parcel-based case).

TABLE 5.3. CHANGE-DETECTION RESULTS OBTAINED ON DATA SET 2 (LARGE IMAGES) AT BOTH PIXEL AND PARCEL LEVEL BY THE PROPOSED ADAPTIVE AND MULTISCALE TECHNIQUE AND THE STANDARD CVA TECHNIQUE.

Technique		False alarms	Missed alarms	Overall error	Overall accuracy (%)
Pixel-based	**Proposed**	74	51	125	94.56
	Standard CVA	274	23	297	87.07
Parcel-based	**Proposed**	21	41	62	97.10
	Standard CVA	160	41	201	91.25

Figure 5.8 (a) and Figure 5.8 (b) report the change-detection maps obtained at a parcel level with the proposed method and with the standard CVA, respectively. A visual analysis of them confirms the effectiveness of the parcel-based method in representing correctly both homogeneous and border regions, and shows the sharp reduction of false alarms due to RN with the proposed method, especially in the urban area of the considered scene (upper left part of the image).

Results obtained on the large data set are very similar to the ones obtained on the small one. This proves the effectiveness of the proposed method also on large images which are a typical condition in real operational applications.

5.4. Conclusion

In this chapter we presented a context-sensitive multiscale technique robust to registration noise for change detection on very high geometrical resolution multispectral images.

When dealing with change detection in multitemporal VHR images one of the most significant sources of errors is registration noise. Such kind of noise is due to the impossibility to perfectly align multitemporal images even if accurate co-registration techniques are applied to the data. In order to understand how to reduce the impact of residual misregistration on the change-detection process, in this work we carried out an analysis of the behaviors of registration noise that affect multitemporal VHR data sets.

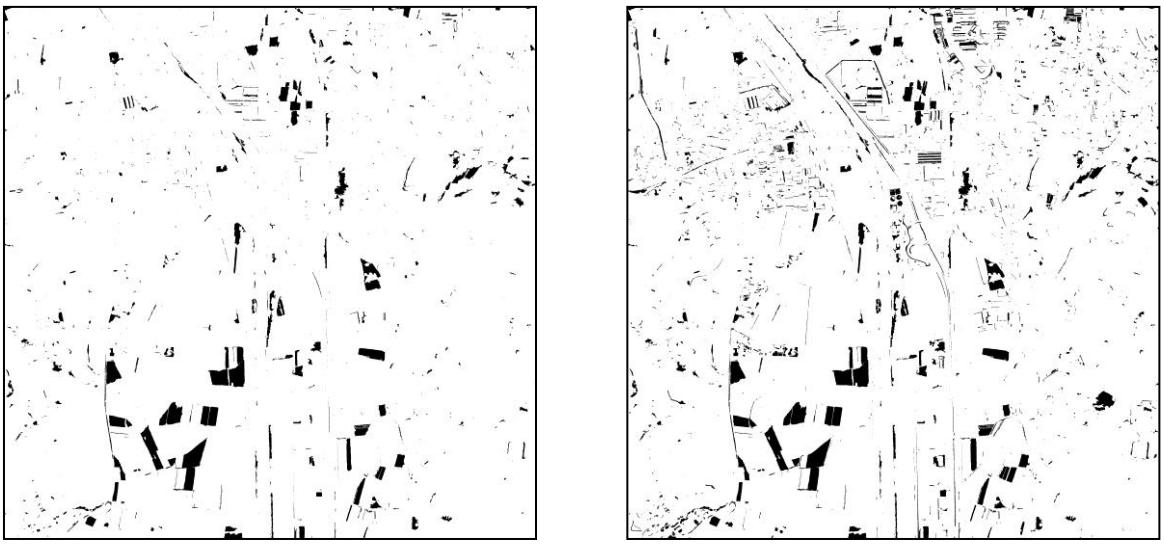

(a) (b)

Figure 5.8. Change-detection map obtained on Data Set 2 with: (a) proposed multiscale approach with adaptive estimation of the cell dimension at parcel level; and (b) the standard parcel-based CVA. (It is worth noting that the maps represent an area of 5000x5000 pixels and thus many changes are not clearly visible).

This analysis was developed in the context of a polar framework for change vector analysis. It was observed that SCVs that fall into the annulus of changed pixels but are associated with registration noise (and therefore are a possible source of false alarms) exhibit significant variations of statistical properties as the scale is reduced. According to this observation, the proposed approach performs a quantization-based multiscale analysis of SCVs in the magnitude-direction domain in order to identify SCVs associated with registration noise. The retrieved information on registration noise is then exploited in the framework of a parcel-based decision strategy that takes advantage of spatial-context information in defining the final change-detection map. This step is performed at full resolution in order to preserve all the high geometrical detail information characteristic of VHR images.

The qualitative and quantitative analysis of the results obtained on two data sets made up of a small and a large pair of Quickbird images point out that the proposed technique involves a low amount of false alarms in change-detection maps and a high accuracy in modeling both geometrical details and homogeneous areas. In greater detail, the achieved results are significantly better than the ones yielded by standard change-detection techniques. The effectiveness of the proposed technique was also tested on different data sets acquired by different remote sensing sensors (that are not reported for space constraint), which confirmed the conclusion drawn for the presented Quickbird data.

An additional remark concerns the residual false alarms present in the final change-detection map yielded by the proposed technique. These errors are mainly related to radiometric changes induced by seasonal variations which are not relevant to the considered application. Although we did not consider this aspect in this work, such false alarms can be reduced only considering additional semantic information about the kind of changes present on the ground.

It is worth noting that despite the proposed method was developed for VHR remote sensing images (as the impact of misregistration on this kind of data is more relevant), it can be suitable also for the analysis of optical data at lower resolution and, under given conditions, also for other kinds of images.

As a future work we plan to extensively test the proposed method on other multitemporal images acquired by different sensors representing different change-detection problems.

Chapter 6

6. Automatic and unsupervised detection of multiple changes in multitemporal images[6]

The detection of multiple changes (i.e., different kinds of change) in multitemporal remote sensing images both at medium and very high geometrical resolution is a complex problem. When multispectral images having B spectral bands are considered, an effective solution to this problem is to exploit all available spectral channels in the framework of supervised or partially supervised approaches. However, in many real applications it is difficult/impossible to collect ground truth information for either multitemporal or single date images. On the opposite, unsupervised methods available in the literature are not effective in handling the full information present in multispectral and multitemporal images. They usually consider a simplified sub-space of the original feature space having small dimensionality and thus characterized by a possible loss of change information. In this chapter we present a framework for the detection of multiple changes in multitemporal and multispectral remote sensing images both at medium and very high geometrical resolution that allows one to overcome the limits of standard unsupervised methods. The framework is based on: i) a compressed yet efficient 2-dimensional (2D) representation of the change information; and ii) a 2-step automatic decision strategy. The effectiveness of the proposed approach has been tested on two multitemporal and multispectral data sets having different properties. Results obtained on both data sets confirm the effectiveness of the proposed approach.

6.1. Introduction

In the literature, the problem of multiple-change detection (*i.e.*, the detection of different kinds of change) has been usually treated as a problem of explicitly detecting land-cover transitions according to (semi-, partially-) supervised methods [101], [102]. The easiest approach in such cases is Post-Classification Comparison (PCC), where two multitemporal images, acquired over the same area at different times, are independently classified and land-cover transitions are estimated according to a pixel-by-pixel comparison of classification maps [21]. The performance of this approach critically depends on the accuracies of the single classification maps and (under the assumption of independent

[6] This chapter is under revision for *IEEE Transaction on Geoscience and Remote Sensing*, under revision. Title: "A Framework for Automatic and Unsupervised Detection of Multiple Changes in Multitemporal Images". Authors: F. Bovolo, S. Marchesi and L. Bruzzone.

errors in the maps) it is close to the product of the accuracies yielded at the two times. This method has the drawback that it does not consider temporal correlation between available acquisitions. A possible alternative is given by Direct Multidate Classification (DMC) [21]. In this technique the two images acquired at different dates are simultaneously classified by stacking their feature vectors. Each possible transition is considered as a class, and thus a training set made up of pixels with labels for both available acquisitions should be defined. In real applications this represents a strong constraint. In order to overcome the drawbacks that affect the two aforementioned approaches, recently other methods have been developed in the context of partially supervised or domain adaptation techniques. These methods assume that ground truth information is available for only one acquisition date while it is not given for the second one. Information about class transitions is obtained by jointly exploiting unlabeled patterns from the second acquisition and labeled patterns available for the first one [9], [103],[104]. However, also these methods require the availability of ground truth information for at least one of the images to be analyzed. When dealing with real applications, the ground truth information collection requires a significant effort from the economical and practical viewpoint. Moreover, in many cases, due to real application constraints, it is almost impossible to retrieve such kind of information. In order to cope with these situations, unsupervised techniques have been developed, which do not require any prior information about land-cover classes. Exhaustive surveys of unsupervised change-detection methods for multispectral images acquired by passive sensors can be found in [17], [18], [21], [36], [39], [94], [105], [106], [107], [108], [109]. Despite these methods can perform change detection without prior information and with a reduced computational burden, most of them allow only the detection of presence/absence of changes but do not discriminate different kinds of change. In the literature some examples exist of methods that try to distinguish in an unsupervised way between different kinds of change [11]. However, often they require the selection of only 2 (or few) spectral channels among the available ones. This process may lead to a significant loss of information, a degradation of the accuracy of the change-detection process and a failure to identify some kinds of change. Moreover unsupervised methods for the detection of multiple changes at the state-of-art (included [11]) do not address the problem of the change information extraction in an automatic way, neither in the full-dimensional nor in a lower dimensional representation of SCVs. From this analysis it emerges a lack of unsupervised methods being able to properly detect the presence of multiple changes in a fully unsupervised and automatic way.

In this chapter we propose a framework for the detection of multiple changes in bi-temporal and multispectral remote sensing images, which allows one to overcome the limits of standard unsupervised methods. The framework is based on: i) a compressed yet efficient 2-dimensional (2D) representation of the change information; and ii) a 2-step automatic decision strategy. First the multidimensional feature space of SCVs is compressed into a 2-dimensional feature space without neglecting any available spectral band (and thus possible information about changes). This representation allows one to easily display and understand change information in a polar coordinates system. Second, an automatic 2-step method for separating unchanged from changed patterns, and distinguishing different kinds of change is presented. The first step separates changed from unchanged pixels. The second one takes into account only changed patterns and aims at distinguishing between different kinds of change.

The rest of the chapter is organized into six sections. The next section introduces mathematical notation and summarizes the background behind the proposed framework. Section 6.3 introduces the proposed compressed 2D representation and the characterization of the change information in bitemporal multispectral images. Section 6.4 presents the proposed technique for extracting multiple-

change information and computing the final change-detection map. Section 6.5 illustrates the experimental results obtained on two real multitemporal datasets acquired by Landsat-5 and Quickbird satellites multispectral sensors. Finally, section 6.6 draws the conclusion of this work.

6.2. Notation and background

Let us consider two co-registered multispectral images, $\mathbf{X}_1$ and $\mathbf{X}_2$ of size $I \times J$ acquired over the same geographical area at different times t_1 and t_2, respectively. Let $X_{b,t}$ be the image representing the bth (b=1,…,B) component of the multispectral image $\mathbf{X}_t$ (t=1,2). As explained in section 2.4, unsupervised change-detection methods usually starts computing the multispectral difference image $\mathbf{X}_D$ by subtracting the spectral feature vectors associated with each corresponding spatial position in the two considered images $\mathbf{X}_1$ and $\mathbf{X}_2$, *i.e.*,

$$\mathbf{X}_D = \mathbf{X}_2 - \mathbf{X}_1 \tag{6.1}$$

In the past several unsupervised approaches have been developed for exploiting the information present in $\mathbf{X}_D$ [17], [21], [94]. The most common and easiest one reduces the BD problem to a 1D problem [15], [35], [110] by considering only the magnitude ρ of spectral change vectors (SCVs). A simple thresholding of the magnitude variable allows one to obtain a change-detection map that highlights the presence/absence of changes [15], [35], [111], however, no information can be retrieved about possible different kinds of change (i.e., the presence of multiple changes).

The above mentioned drawback drove to the definition of more advanced techniques that try to solve the change-detection problem by including all available features in the decision process[7]. In this case the detection of changes requires the solution of a complex BD problem, where an unsupervised analysis would imply the application of clustering algorithms to BD vectors [11], [112]. However, in real applications, the data complexity and the noise present in the BD feature space (refer to [11] for further details on this issue) affect the performance of clustering procedure, which in many cases result in change-detection accuracies smaller than those provided by a simple thresholding of the 1D magnitude of SCVs [15], [21]. A further drawback of working in a BD space is that this space is difficult or impossible to visualize when the considered dimensions are more than 2. This implies that the process of understanding the change-detection problem structure when semi-automatic interactive solutions are investigated with the support of an expert can become rather complex.

A possible alternative to solve the BD problem with a limited loss of information is to split it in a set of $\binom{B}{2}$ 2D problems by considering all possible pairs of spectral channels. The obvious drawback of this approach is the need of defining an effective strategy for combining the $\binom{B}{2}$ solutions in the final decision step[8]. Therefore the most common practice is to select only one out of all the possible 2D problems[9] (*i.e.*, neglecting B-2 spectral bands) and to use this sub-optimal representation as the solution to the initial BD change-detection problem [59],[61]. In practice, the two selected spectral channels of $\mathbf{X}_D$ are commonly used to represent the change-detection problem in 2D polar coordinates (2D-CVA) according to the magnitude and direction variables, as described in2.4, defined as [see also (2.2)]:

[7] The BD feature space could be either the one of the multispectral difference image or an alternative multidimensional representation of it like for examples the one achieved by Principal Component Analysis (PCA).

[8] It is worth noting that in the literature it doesn't exist a change detection method based on this strategy. The definition of such an approach is out of the goals of the present work.

[9] This is also commonly done in PCA based change detection approaches where (often implicitly) only the first 2 (or few) principal components are selected for the solution of the BD problem[132].

$$\vartheta = \tan^{-1}\left(\frac{X_{1,D}}{X_{2,D}}\right) \quad \text{and} \quad \rho = \sqrt{(X_{1,D})^2 + (X_{2,D})^2} \tag{6.2}$$

Independently on the selected channels, the drawback of this strategy is that the change-detection solution is usually affected by a loss of information (except for simple cases) with respect to the original multitemporal and multispectral feature space (or to the *B*D SCVs feature space). To limit this effect, prior knowledge on the specific considered problem (*i.e.*, on the kinds of change occurred on the ground) could be employed to select the 2 most relevant channels [15],[91]. However, in most of the practical applications, prior information is not available and is not possible to assure that change information is constrained to only two channels (*e.g.*, there are different kinds of change that affect the spectral signatures of the land covers in different bands). Thus the 2D approach can result in poor change-detection performance. Nevertheless, it shows the advantages of being easy to visualize and analyze.

Table 6.1 summarizes advantages and disadvantages of the different representations present in the literature. From its analysis and recalling that different kinds of change have different effects on different features (*i.e.*, all spectral channels are potentially useful for solving the change-detection problem and no channel can be neglected a priori), it emerges therefore the need of defining a framework where the information about multiple changes can be easily managed in a 2 dimensional feature space without completely neglecting any spectral channel (and the information about changes in them). Moreover the framework should integrate effective change-detection techniques able to distinguish multiple changes in an unsupervised and automatic way.

TABLE 6.1. ADVANTAGES AND DISADVANTAGES OF THE DIFFERENT POSSIBLE REPRESENTATION OF THE *B*D CHANGE-DETECTION PROBLEM GIVEN BY THE MULTISPECTRAL DIFFERENCE IMAGE.

Representation	Unsupervised approach to CD	Advantages	Disadvantages
***B*D (*B*>2)**	*B*D clustering.	Information about multiple kinds of change is preserved.	Complex to manage. Change information cannot be to visualized. Clustering techniques are often not effective.
***B*D (sub-optimal) (*B*>2)**	Solve $\binom{B}{2}$ 2D problems. Combine $\binom{B}{2}$ solutions.	Information about multiple kinds of change is preserved.	Sub-optimal detection of changes. The combination of 2D solutions for generating the *B*D solution requires an additional step. Combination strategies are not available in the literature yet.
2D	Select 2 out of *B* bands. Threshold magnitude and direction variables.	Easy and intuitive to visualize. Different kinds of change can be detected.	Requires prior information about changes for band selection. Depending on selected bands some kinds of change can be lost.
1D	Threshold the magnitude variable.	Easy to manage and visualize.	Only information about presence/absence of changes can be extracted.

6.3. Proposed compressed representation of the change information

In order to preserve the most of the available information present in the *B*D feature space and to obtain a feature space easy to visualize and manage from a user point of view, here we propose a transformation that maps the *B*D feature space into a 2D feature space without the need of any prior information about the specific change-detection problem. The two considered features are: i) the magnitude of spectral change vectors, and ii) a direction variable that models the information about different kinds of change without rejecting any spectral channel. The two features define a space in which the change information can be effectively and intuitively represented and extracted.

6.3.1 Magnitude of Spectral Change Vectors

The first of the considered features is the well known and widely used magnitude ρ of multidimensional spectral change vectors in $\mathbf{X}_{\mathrm{D}}$ defined as:

$$\rho = \sqrt{\sum_{b=1}^{B} \mathrm{X}_{b,\mathrm{D}}^2} = \sqrt{\sum_{b=1}^{B} \left(\mathrm{X}_{b,2} - \mathrm{X}_{b,1}\right)^2}, \quad \rho \in [0, \rho_{max}] \tag{6.3}$$

where ρ_{max} is the maximum value assumed by the magnitude for the considered image pair. Theoretically ρ_{max} could tend to infinity, however in practical applications it is bounded by the digital nature of the data.

As widely known [15], [21], the magnitude carries information about the presence/absence of changes. On this feature changed pixels show a relative high value whereas unchanged pixels show a relatively low value [11], [15], [21], [111]. Despite the magnitude does not carry information about different kinds of change, it represents a valuable and robust variable for distinguishing changed from no-changed pixels. In the literature several automatic and unsupervised approaches to change detection that analyze the magnitude variable are available [17], [18], [21]. Among them the most widely used are automatic threshold selection techniques [15], [17], [111].

6.3.2 Direction of Spectral Change Vectors

As the magnitude of SCVs does not include any information about different kinds of change, a complementary feature is proposed to distinguish multiple changes. An angle measure α [alternative to ϑ, see eq. (6.2)] is proposed that effectively compresses the information about different kinds of change to a 1-dimensional variable. α is defined as an angle computed in radians between two multidimensional vectors *t* and *r*:

$$\alpha = \arccos\left(\sum_{b=1}^{B} \left(t_b r_b\right) \Big/ \sqrt{\sum_{b=1}^{B} t_b^2 \sum_{b=1}^{B} r_b^2} \right), \quad \alpha \in [0, \pi] \tag{6.4}$$

where t_b and r_b are the *b*th components of *B*D vectors *t* and *r*, respectively [113].

Such kind of measure has been already successfully employed in the context of: i) supervised approaches to geological mapping in high and very high geometrical resolution images [114],[115],[116]; ii) supervised classification and/or clustering of hyperspectral and multispectral images[117],[118]; iii) supervised change detection [119]; iv) spectral unmixing [120],[121]; v) target detection in hyperspectral images [122]; and vi) pansharpening quality assessment. In the mentioned applications the angle defined in (6.4) is used as a supervised similarity measure between a given spectral signature $\mathbf{X}$ and reference spectra $\mathbf{X}_{ref}$ (*i.e.*, spectral libraries or end-members stored in a database) and is commonly referred to as Spectral Angle Mapper (SAM)[123]. In such cases, equation (6.4) can be rewritten as:

$$\alpha = \arccos\left(\sum_{b=1}^{B}\left(\mathrm{X}_b \mathrm{X}_{b,ref}\right) \Big/ \sqrt{\sum_{b=1}^{B}\mathrm{X}_b^2 \sum_{b=1}^{B}\mathrm{X}_{b,ref}^2} \right), \quad \alpha \in [0,\pi] \tag{6.5}$$

where X_b and $\mathrm{X}_{b,ref}$ are the bth component of BD vectors $\mathbf{X}$ and $\mathbf{X}_{ref}$, respectively.

However, as we are dealing with an unsupervised approach to change detection no libraries for $\mathbf{X}_{ref}$ are available. Therefore in this work we propose an alternative way to use the angular distance measure defined in (6.4). In the BD feature space of the multispectral difference image $\mathbf{X}_\mathrm{D}$, we define vector t as the spectral change vector associated to each spatial position and r as a BD unit vector u with elements u_b (b=1,…,B) all equal to each other. The latter choice is suggested by the absence of prior information about changes occurred on the ground that makes it difficult to establish a relative relevance of spectral channels. Without loss of generality, in order to link u_b to a physical characteristic of the considered problem we set elements of u equal to $\sqrt{B}/B$. Therefore the desired angle variable can be written as:

$$\alpha = \arccos\left(\sum_{b=1}^{B}\left(\mathrm{X}_{b,\mathrm{D}} u_b\right) \Big/ \sqrt{\sum_{b=1}^{B}\mathrm{X}_{b,\mathrm{D}}^2 \sum_{b=1}^{B} u_b^2} \right) = \arccos\left[\frac{1}{\sqrt{B}} \left(\sum_{b=1}^{B}\mathrm{X}_{b,\mathrm{D}} \Big/ \sqrt{\sum_{b=1}^{B}\mathrm{X}_{b,\mathrm{D}}^2} \right) \right], \quad \alpha \in [0,\pi] \tag{6.6}$$

It is worth noting that if any information is available to establish a relative relevance of the spectral channels, different choices can be made for the elements of u.

6.3.3 Proposed Compressed Change Vector Analysis

Following an approach similar to the one in [11], recalled in section 2.4, the properties of the two features defined according to (6.2) and (6.6) can be exploited for defining a compressed polar representation of the change-detection problem represented by the multispectral SCVs in a 2D feature space. We call this feature space as Compressed CVA (C^2VA) domain. The C^2VA domain is bounded by the ranges of existence of ρ and α, *i.e.*,

$$\mathrm{C}^2\mathrm{VA} = \left\{ \rho \in [0, \rho_{max}] \text{ and } \alpha \in [0,\pi] \right\} \tag{6.7}$$

Eq. (6.7) represents a semi-circle that includes all SCVs of the considered images (see Figure 6.1). Within this domain, regions of interest can be identified associated to different classes in Ω. Since no-changed pixels are expected to have a magnitude close to zero, whereas changed pixels are expected to show a magnitude far from zero [11], [15], [21], the C^2VA domain can be divided into two regions with respect to the magnitude variable. The first region is associated with unchanged pixels, whereas the second one is associated with changed pixels. The two regions can be separated according to the optimal (in the sense of the theoretical Bayesian decision theory) threshold value T that separates pixels belonging to ω_n from pixel belonging to Ω_c (dark and light gray areas in Figure 6.1, respectively) [11], [15].

The first region is the *semicircle SC_n of no-changed pixels* (dark gray area in Figure 6.1) located close to the origin of the C^2VA domain. This region is defined mathematically as follows

$$SC_n = \left\{ \rho, \alpha : 0 \le \rho < T \text{ and } 0 \le \alpha \le \pi \right\} \tag{6.8}$$

The second region is the *semi-annulus of changed pixels SA_c* (light gray area in Figure 6.1) located far from the origin of the C^2VA domain, and is mathematically defined as

$$SA_c = \left\{ \rho, \alpha : T < \rho \le \rho_{\max} \text{ and } 0 \le \alpha \le \pi \right\} \tag{6.9}$$

Let us now consider the information carried out by the direction variable α. As it represents the similarity between each considered SCV and a reference vector, it is expected that different kinds of change will be characterized by different values of α. According to this observation, within the semi-

annulus of changed pixels different *annular sectors* S_k (k=1,…,K) *of the semi-annulus* SA_c can be detected along α, and defined as

$$S_k = \{\rho, \alpha : \rho \geq T \text{ and } \alpha_{k_1} \leq \alpha < \alpha_{k_2},\ 0 \leq \alpha_{k_1} < \alpha_{k_2} < \pi\} \tag{6.10}$$

where α_{k_1} and α_{k_2} are the two angular thresholds that bounds the sector S_k. Each sector (hatched area in Figure 6.1) can be associated in principle with a specific kind of change $\omega_{c_k} \in \Omega_c$ occurred on the ground.

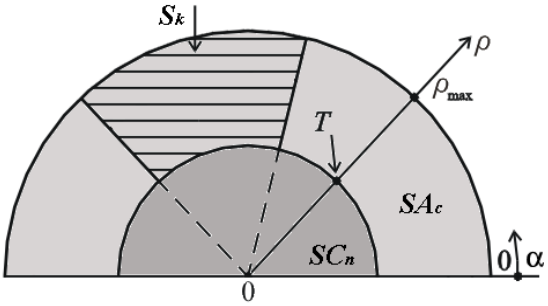

Figure 6.1. Regions of interest for the compressed 2D representation of the change-detection problem.

Despite the applied compression considers all spectral channels, some ambiguity rises from the process of information compression which is mainly due to the simplified representation given by the direction variable. The loss of information may result in similar values of α for different kinds of change. In this situation, each detected sector S_k must be associated to more kinds of change in Ω_c instead of only one. However, this is a drawback common to other low dimensional representations (*i.e.*, lower than the original one) usually adopted for unsupervised change detection. Nevertheless, the defined 2D feature space has two valuable advantages: i) the ambiguity does not affect the detection of changes but just the possible merging (in some specific cases) of different kinds of change; and ii) it considers in the solution of the change-detection problem all available spectral bands thus avoiding the need of prior information about relevant spectral bands (which is requested for a 2D standard CVA in polar coordinates). Moreover, the 2D representation makes it easy to visualize the change-detection problem for interaction with the end-user.

6.4. Proposed technique for the detection of multiple changes

The proposed 2D representation suggests a change-detection approach based on a 2-step procedure: i) identification of the *semicircle* SC_n *of no-changed pixels* and of the *semi-annulus* SA_c *of changed pixels* (*i.e.*, separation of changed and unchanged patterns) by the analysis of the distribution of the magnitude variable ρ; and ii) identification of *annular sectors* S_k (k=1,…,K) in the *semi-annulus* SA_c (*i.e.*, detection of different kinds of change within the set of changed patterns identified in the first step) by the analysis of the distribution of the direction variable α. It is worth noting that from a theoretical point of view the identification of the different regions in the C^2VA domain should be carried out by jointly analyzing ρ and α. Nonetheless we simplify the process by analyzing separately ρ and α thus implicitly assuming the independence between them.

6.4.1 Separation of changed from unchanged patterns

In the first step changed and unchanged pixels are distinguished from each other according to a well known ad widely used unsupervised technique based on the Expectation-Maximization algorithm[124],[125].

Let $P(\omega_n)$, $P(\Omega_c)$, $p(\rho|\omega_n)$ and $p(\rho|\Omega_c)$ be the prior probabilities and the conditional probability density functions of class ω_n and meta-class Ω_c, respectively. Let us assume that the distribution of the observed magnitude variable can be expressed as a mixture density distribution, *i.e.*:

$$p(\rho) = P(\omega_n)\, p(\rho \mid \omega_n) + P(\Omega_c)\, p(\rho \mid \Omega_c) \tag{6.11}$$

Under simple assumptions it is possible to prove that in the 2D case the magnitude of changed and unchanged classes can be modeled by a Rayleigh and a Rice density function, respectively (see [11] for greater details). However, in the considered case these hypotheses are not satisfied as: i) more than two spectral channels are involved in the calculus; ii) Ω_c can include in general more than one kind of change; and iii) no assumption is made on the statistical parameters of changed and unchanged pixels in the domain of the multispectral difference image. According to these considerations the assumption that $p(\rho|\omega_n)$ and $p(\rho|\Omega_c)$ follow a Gaussian distribution seems a reasonable and simple approximation. The threshold T that separates class ω_n and meta-class Ω_c can be computed according to the Bayes decision theory after retrieving the class prior probabilities $P(\omega_n)$ and $P(\Omega_c)$ and the class statistical parameters (the mean values μ_{ω_c} and μ_{ω_n} and variances $\sigma^2_{\omega_c}$ and $\sigma^2_{\omega_n}$ in the magnitude domain ρ of change and no-change classes, respectively). As change detection is approached in an unsupervised way, the well know Expectation-Maximization algorithm [124],[125] can be used for estimating these parameters. After initialization, the following iterative equations that allows us to solve the estimation problem under Gaussian assumption can be applied [15]:

$$P^{s+1}(\omega_n) = \frac{1}{IJ} \sum_{X_\rho(i,j) \in X_\rho} \frac{P^s(\omega_n)\, p^s(X_\rho(i,j)) | \omega_n)}{p^s(X_\rho(i,j))} \tag{6.12}$$

$$\mu^{s+1}_{\omega_n} = \frac{\sum_{X_\rho(i,j) \in X_\rho} \frac{P^s(\omega_n)\, p^s(X_\rho(i,j)) | \omega_n)}{p^s(X_\rho(i,j))} X_\rho(i,j)}{\sum_{X_\rho(i,j) \in X_\rho} \frac{P^s(\omega_n)\, p^s(X_\rho(i,j)) | \omega_n)}{p^s(X_\rho(i,j))}} \tag{6.13}$$

$$(\sigma^2_{\omega_n})^{s+1} = \frac{\sum_{X_\rho(i,j) \in X_\rho} \frac{P^s(\omega_n)\, p^s(X_\rho(i,j)) | \omega_n)}{p^s(X_\rho(i,j))} \left[X_\rho(i,j) - \mu^s_{\omega_n} \right]^2}{\sum_{X_\rho(i,j) \in X_\rho} \frac{P^s(\omega_n)\, p^s(X_\rho(i,j)) | \omega_n)}{p^s(X_\rho(i,j))}} \tag{6.14}$$

where $X_\rho(i,j)$ is the magnitude value of pixel in spatial position (i,j) within the magnitude image X_ρ. Superscript s indicates the iteration. Initial values for the statistical parameters of both classes are computed as sample mean and variance and relative frequency of pixels within a set of patterns with a high probability to belong to the two classes, respectively. Such sets are built by applying two thresholds for selecting the pixels with very high (meta-class Ω_c) or very low magnitude values (class ω_n) according to the well known properties of the ρ variable [15]. The iterative process stops when the likelihood function reaches a local maximum.

Once class statistical parameters are estimated, the Bayes decision rule can be used for pattern labeling, *i.e.*,

$$\omega_h = arg \max_{\omega_i \in \{\omega_n, \Omega_c\}} \{P(\omega_i \mid X_\rho(i,j))\} = arg \max_{\omega_i \in \{\omega_n, \Omega_c\}} \{P(\omega_i)\, p(X_\rho(i,j) | \omega_i)\} \tag{6.15}$$

The explicit solution of (6.15) leads to the definition of a Bayesian decision threshold T [15]. Thus each pixel $x(i,j)$ in spatial position (i,j) is assigned to the class of changed or unchanged pixels according to the following decision rule

$$x(i,j)\in\begin{cases}\omega_n & if \quad X_\rho(i,j)<T\\ \Omega_c & if \quad X_\rho(i,j)\geq T\end{cases} \tag{6.16}$$

6.4.2 Identification of different kinds of change

Once changed pixels have been separated from no-changed ones, the attention is focused on the set of changed pixels only. The aim of this step is to separate the contributions of possible different kinds of change within the meta-class Ω_c. This can be done by exploiting the direction variable.

Let $P(\omega_{ck}|\rho\geq T)$ and $p(\alpha|\omega_{ck},\rho\geq T)$ (k=1, …, K) be the prior probability and the conditional probability density function of the class $\omega_{ck}\in\Omega_c$, k=1,…,K, given that changes occurred (*i.e.*, given that the magnitude variable is higher than the threshold T). Under this hypothesis, the observed direction variable in the semi-annulus of changed pixels can be written as a mixture density distributions:

$$p(\alpha|\rho\geq T)=\sum_{k=1}^{K}P(\omega_{ck}|\rho\geq T)\,p(\alpha|\omega_{ck},\rho\geq T) \tag{6.17}$$

The derivation of the analytical expression for the conditional probability density function $p(\alpha|\omega_{ck},\rho\geq T)$ is a complex task [11] and results in distributions that are difficult to be used in the context of automatic techniques. Thus for simplicity, the statistical distribution of each class of change $\omega_{ck}\in\Omega_c$, k=1,…,K is approximated by a Gaussian function. Under this reasonable approximation, the generic class of change ω_{ck} can be statistically described with its class prior probability $P(\omega_{ck}|\rho\geq T)$, the mean value ($\mu_{ck}$) and the variance value (σ_{ck}^2) computed along the direction variable α. Once class statistical parameters have been estimated, also in this case the Bayes decision rule can be used for pattern labeling, *i.e.*,

$$\omega_h=\arg\max_{\omega_i\in\Omega_c}\{P[\omega_i|X_\alpha(i,j),\rho\geq T]\}=\arg\max_{\omega_i\in\Omega_c}\{P(\omega_i|\rho\geq T)\,p[X_\alpha(i,j)|\omega_i,\rho\geq T]\} \tag{6.18}$$

where $X_\alpha(i,j)$ is the direction value of pixel in spatial position (i,j) within the direction image X_α. Under the Gaussian distribution hypothesis, the statistical parameters of each class $\omega_i\in\Omega_c$ can be estimated with the EM algorithm applying the same iterative equations as in (6.12)-(6.14). However, unlike the case of the magnitude variable where a reasonable initial assumption can be done on the position of classes along the magnitude variable (*i.e.*, changed pixels show a high magnitude and no-changed pixels show a low magnitude), along the direction variable no hypotheses can be formulated on the location of the classes associated to different kinds of change. Therefore in this case a K-mean clustering [126] is applied in order to determine in an unsupervised way reasonable initial seeds for the iterative algorithm. The K-mean clustering algorithm requires the definition of the number of expected clusters, *i.e.*, the number K of expected kinds of change occurred on the ground. This information can be recovered according to: i) some prior knowledge on the considered problem; ii) interactions with the end-user; or iii) methods for validation of clustering results [127], [128], [129], [130].

The explicit solution of (6.18) leads to the definition in the direction domain of a pair of thresholds α_{k_1} and α_{k_2} for each kind of change. Each pixel $x(i,j)$ that falls to the SA_c (i.e., $X_\rho(i,j)>T$)is assigned to one of the detected kinds of change $\omega_{ck}\in\Omega_c$ according to the following the decision rule:

$$x(i,j)\in\begin{cases}\omega_{c_1} & if \quad \alpha_{1_1}<X_\alpha(i,j)\leq\alpha_{1_2}\\ \vdots & \qquad\vdots\\ \omega_{c_K} & if\,\alpha_{K_1}<X_\alpha(i,j)\leq\alpha_{K_2}\end{cases} \tag{6.19}$$

It is worth noting that the proposed technique for the detection of multiple changes can be also applied to the CVA polar framework under the assumption of selecting 2 out of B spectral channels for computing the SCVs [11].

6.5. Experimental results and discussion

In order to assess the reliability of both the proposed 2D representation in the C^2VA domain and the effectiveness of the proposed change-detection technique, several experiments were carried out on two multispectral and multitemporal datasets. The first data set is made up of two images acquired by the Thematic Mapper sensor mounted on the Landsat 5 satellite and represents a 6D problem. The second data set includes two very high geometrical resolution images of an area nearby the city of Trento (Italy) acquired by the multispectral sensor mounted on the Quickbird satellite and represents a 4D problem.

The reliability of the proposed C^2VA representation was studied by a comparison with the standard CVA polar framework [11]. We briefly recall here that the CVA framework is defined by the magnitude ρ ($\rho \in [0, \rho_{max}]$) and the direction ϑ ($\vartheta \in [0,2\pi)$) computed by selecting 2 out of B spectral channels according to (2.2) (it is worth stressing that the selection of 2 out of B spectral channels may result in a significant loss of information). Following [11], the domain of interest is represented by a circle with outer radius ρ_{max}. Within this domain one can identify: i) a circle of no-changed pixels (C_n); and ii) an annulus of changed pixels (A_c) separated by a threshold T. Within A_c, sectors of annuls S_k that correspond to different kinds of change occurred on the ground can be defined bounded by two angular thresholds ϑ_{k_1} and ϑ_{k_2} (see Figure 2.2). The magnitude ρ and direction variables ϑ observed in the CVA polar framework can be described as mixture of Gaussian distributed densities [i.e., $p(\rho)$ and $p(\vartheta|\rho \geq T)$, respectively], similarly to what done for ρ and α variables in the C^2VA domain. Thus, thanks to this similarity, the proposed automatic technique for the detection of multiple changes can be effectively applied also to the CVA polar framework.

In our experiments, for each data set, CVA in polar coordinates is applied to two different pairs of spectral channels: i) one made up of a couple of bands chosen in a random way (this simulates problems in which no prior information on the types of change is available); and ii) one made up of two spectral channels chosen according to some prior knowledge on the considered changes occurred on the ground.

The effectiveness of the proposed framework was evaluated according to: i) a qualitative comparison between the capabilities in representing the change information of the proposed C^2VA and the standard 2D CVA; ii) a quantitative analysis of the performance of the proposed technique for the detection of multiple changes (which was conducted according to an available reference map) applied to both the C^2VA and 2D CVA, and iii) a comparison of the performance obtained with the proposed automatic and unsupervised method with the ones achieved with a manual trial and error procedure (MTEP), *i.e.*, a procedure that selects the threshold values both along magnitude and direction by minimizing the overall error with respect to the available reference map.

6.5.1 Data set 1: Thematic Mapper images of Landsat-5

The first data set is made up of a couple of images acquired on the Sardinia Island (Italy) in September 1995 and July 1996, respectively, by the Thematic Mapper sensor mounted on the Landsat 5 satellite. This data set is characterized by a spatial resolution of 30m×30m. The selected area is a section (412×300 pixels) of two full scenes including Lake Mulargia. In the pre-processing phase the two images were radiometrically corrected and co-registered in order to make them as more comparable as

possible. As an example of the images used in this experiment, Figure 6.2 (a) and (b) show band 4 of the September and July images, respectively. Between the two acquisition dates three kinds of change occurred (K=3): i) an enlargement of an open quarry between the two branches of the lake (bottom right part of the scene, ω_{c1}); ii) a burned area (bottom left part of the scene, ω_{c2}) (this is a simulated change, refer to [11] for further details on how the change has been included in a realistic way); and iii) an enlargement of the lake surface associated to an increase of the water volume of Lake Mulargia (centre of the scene, ω_{c3}). A reference map of the analyzed site was defined according to a detailed visual analysis of the multitemporal images and some prior information. The obtained reference map contains 10180 changed pixels and 113492 unchanged pixels. In greater details, 214 pixels are related to ω_{c1}, 2414 to ω_{c2} and 7480 to ω_{c3} (see Figure 6.2 (c)).

First of all we represented the change information in the Compressed CVA (C^2VA) domain. To this purpose, according to the procedure described in Section 6.3, we reduced the dimension of the feature space from 6 (*i.e.*, the number of spectral channels of the TM images, excluding the thermal channel) to 2 computing the magnitude of the multispectral difference image according to (6.2) and the angle α according to (6.6). Elements of vector u were all set to $\sqrt{6}/6$. Figure 6.3 (a) shows the scatterogram in the C^2VA domain. Figure 6.3 (b) and (c) show the scatterogram in the polar domain obtained by applying CVA to two pairs of spectral channels: i) Figure 6.3 (b) is obtained from the analysis of bands 1 and 3 (which were randomly selected), whereas ii) Figure 6.3 (c) is obtained from the analysis of bands 4 and 7 (which were selected according to prior knowledge about changes related to water and burned areas). In the scatterogram obtained with the proposed representation (Figure 6.3 (a)) three main clusters can be easily identified showing a high magnitude and specific preferential values along α. As expected (and confirmed by our experimental analysis) in the other two representations (Figure 6.3 (b) and (c)), only two clusters can be clearly identified with a high magnitude and a preferred direction and therefore only two types of change can be detected. The proposed approach to multiple change detection estimated threshold value T (that separates along ρ pixels belonging to ω_n from pixels belonging to Ω_c) as equal to 45 when ρ was computed considering all spectral channels (C^2VA), whereas it was equal to 35 considering spectral channels 1 and 3, and to 31 considering bands 4 and 7 (2D CVA). As an example, Figure 6.4 reports the distribution of the SCVs along the magnitude variable. In particular, Figure 6.4 (a) shows the real distribution derived from the histogram ($h(\rho)$) of the magnitude of SCVs (grey line) and the distribution estimated as a mixture of Gaussians ($p(\rho)$), while Figure 6.4 (b) shows separately the distributions $P(\omega_n)p(\rho|\omega_n)$ of the class ω_n (black line) and the distribution $P(\Omega_c)p(\rho|\Omega_c)$ of the class Ω_c (grey line) estimated along the magnitude variable by the EM algorithm (eq. (6.12)-(6.14)) for the C^2VA. The fitting of the two distributions (the estimated and real ones) confirms the good approximation obtained with the Gaussian distributions [Figure 6.4 (a)].

Then we derived the distribution $p(\alpha|\rho \geq T)$ of SCVs along the direction variable considering only patterns labeled as changed. According to section 6.4, threshold values were identified in order to separate contributions from different kinds of change. Here, we inferred the information about K from a visual analysis of the scatterograms (Figure 6.3) and of the histograms along the direction variable of SCVs in the semi-annulus (or annulus for CVA) of changed pixels ($h(\alpha|\rho \geq T)$) (Figure 6.5). In the C^2VA domain K was set equal to 3 (three clusters having relatively high magnitude values are present in the scatterograms of Figure 6.3(a); thus, the histograms in Figure 6.5(a) presents 3 main peaks in positions corresponding to the ones of clusters in the scatterogram). Differently, in the two polar CVA representations the value of K was set equal to 2 (see Figure 6.3(b) and (c) and Figure 6.5 (b) and (c)).

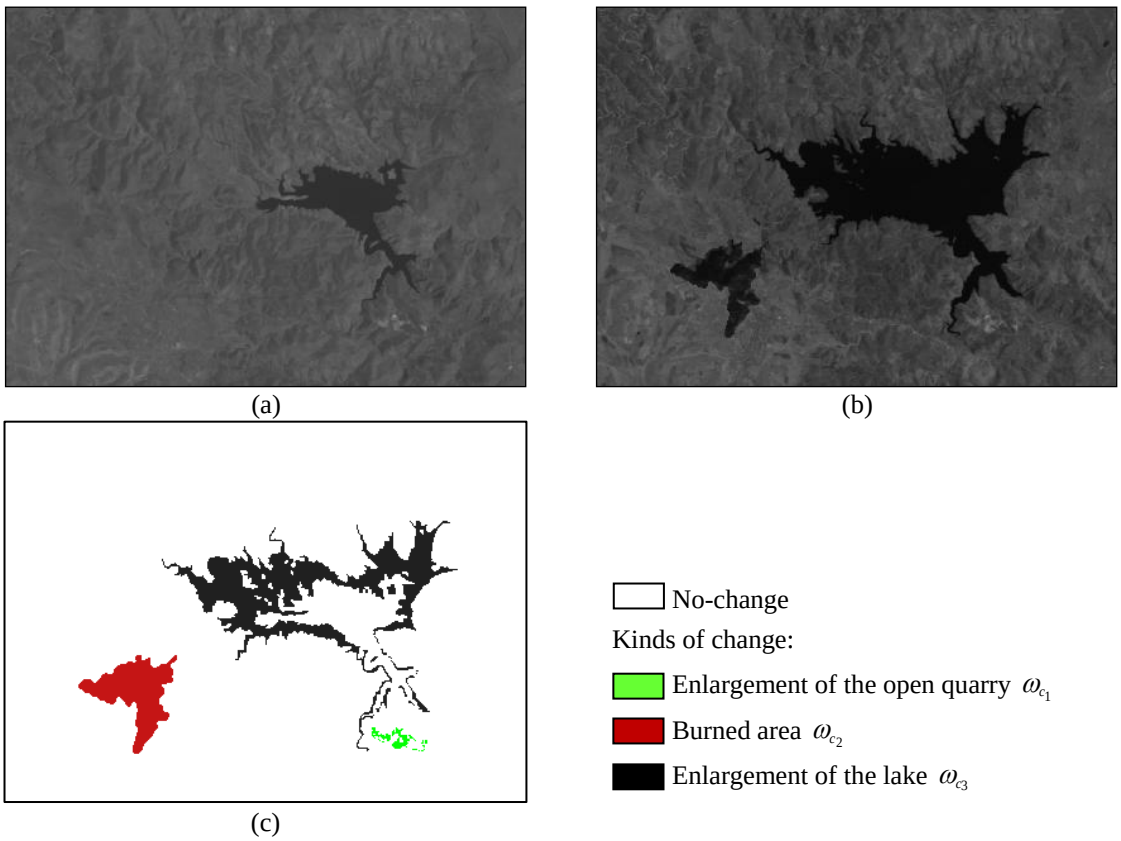

Figure 6.2. Images of Lake Mulargia (Italy) acquired by the Thematic Mapper sensor of the Landsat 5 satellite; (a) channel 4 of the image acquired in September 1995 and (b) channel 4 of the image acquired in July 1996; (c) reference map.

As one can see from Figure 6.5, the distribution estimated with the EM algorithm (black line Figure 6.5) matches well the real distribution of SCVs (grey line Figure 6.5), thus confirming the reasonable approximation with a Gaussian distribution. In order to improve the visual quality of Figure 6.5 (and of similar ones in the following) the level corresponding to zero occurrence was moved from the origin to a semicircle/circle (perimeter of the grey semicircle/circle) slightly shifted from the origin of the plot itself. This choice avoids the bias in the visualized information due to the collapse of probability density functions in the origin. The separation of the three different kinds of change is achieved by applying the Bayes decision rule in (6.19). This operation results in the identification of three threshold values and three annular sectors (S_1, S_2 and S_3) in SA_c corresponding to one of the different kinds of change. The first annular sector is defined as $S_1=\{\rho,\alpha : \rho\geq 45 \text{ and } 0°\leq \alpha\leq 70°\}$. All SCVs that fall into S_1 are labeled as ω_{c_1} and are associated to the change caused by the quarry enlargement. The second annular sector is defined as $S_2=\{\rho,\alpha : \rho\geq 45 \text{ and} 70°\leq \alpha\leq 142°\}$. All SCVs that fall into S_2 are labeled as ω_{c_2} (*i.e.*, forest fire). Finally, the third annular sector is defined as $S_3=\{\rho,\alpha : \rho\geq 45$ and $142°\leq \alpha\leq 180°\}$.All SCVs that fall into S_3 are labeled as ω_{c_3} and are associated to the change related to the enlargement of the lake surface. Concerning the 2D CVA approach the analysis of the first pair of channels (1 and 3), led to the identification of pixels belonging to ω_{c_1} (SCVs with $\vartheta\in[0°,182°)$, $\rho\geq 35$) and pixels belonging to ω_{c_3} ($\vartheta\in[182°,360°)$, $\rho\geq 35$). Considering bands 4 and 7, it is possible to isolate changes due to ω_{c_2} (SCVs with $\vartheta\in[323°,360°]\cup[0°,28°)$, $\rho\geq 31$) and to ω_{c_3} (SCVs with

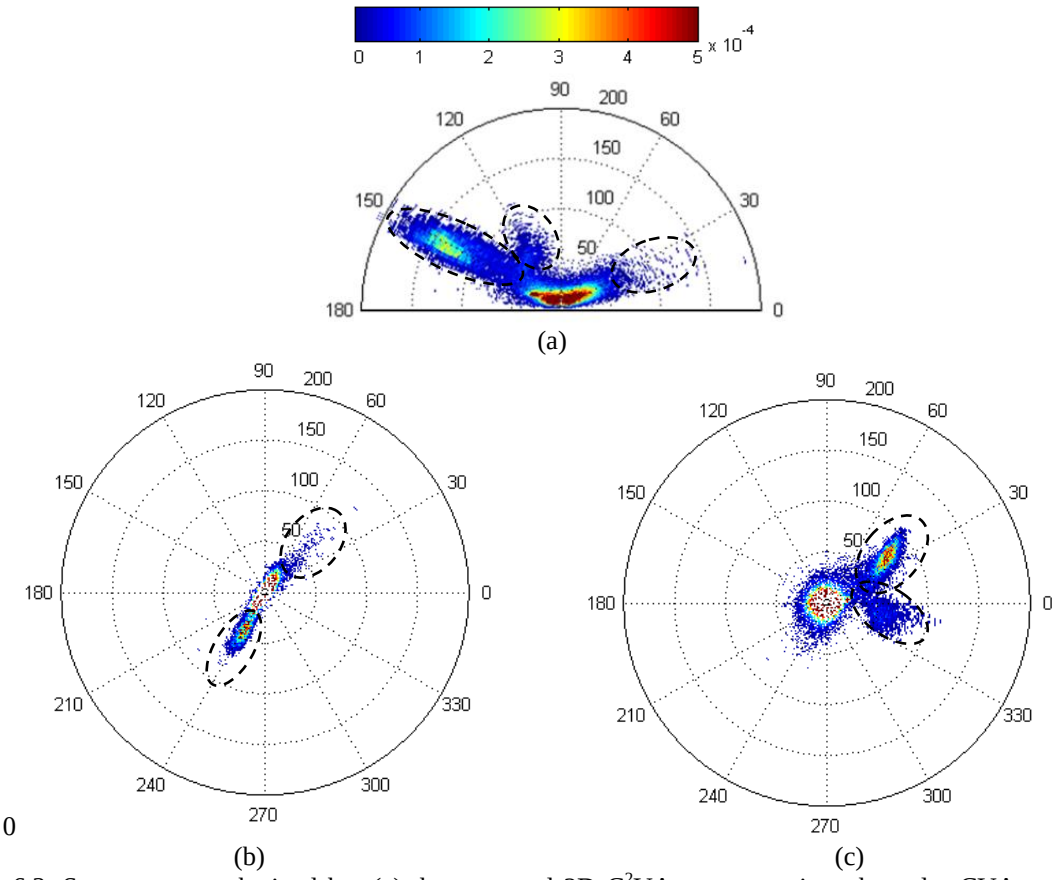

Figure 6.3. Scatterograms obtained by: (a) the proposed 2D C^2VA representation; the polar CVA applied to spectral channels (b) 1 and 3, and (c) 4 and 7 (Landsat 5 dataset).

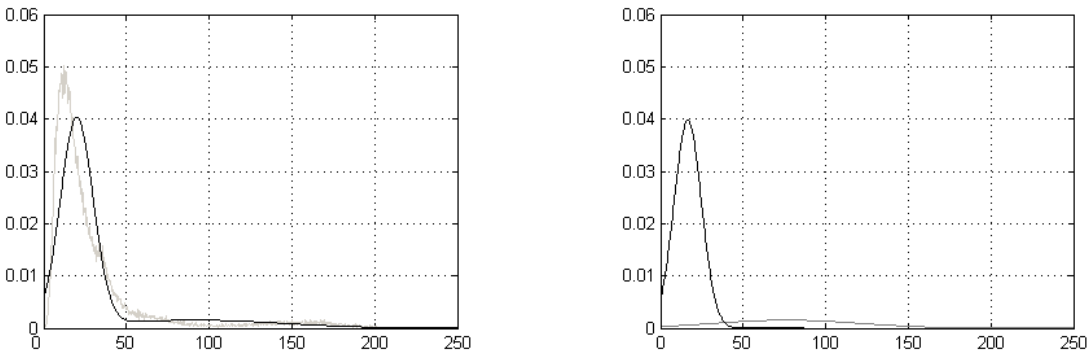

Figure 6.4. (a) $h(\rho)$ (grey line) and $p(\rho)$ (black line) obtained with all spectral channels; and (b) $P(\omega_n)p(\rho|\omega_n)$ (black line) and $P(\Omega_c)p(\rho|\Omega_c)$ (grey line) estimated by the EM algorithm under Gaussian assumption (Landsat 5 dataset).

$\vartheta \in [28°,323°)$, $\rho \geq 31$). A further analysis of all the $\binom{6}{2}$ possible combinations of 2D spectral representations pointed out that it is not possible to identify a pair of spectral channels including information about all mentioned kinds of change (this analysis is not reported for space constraints).

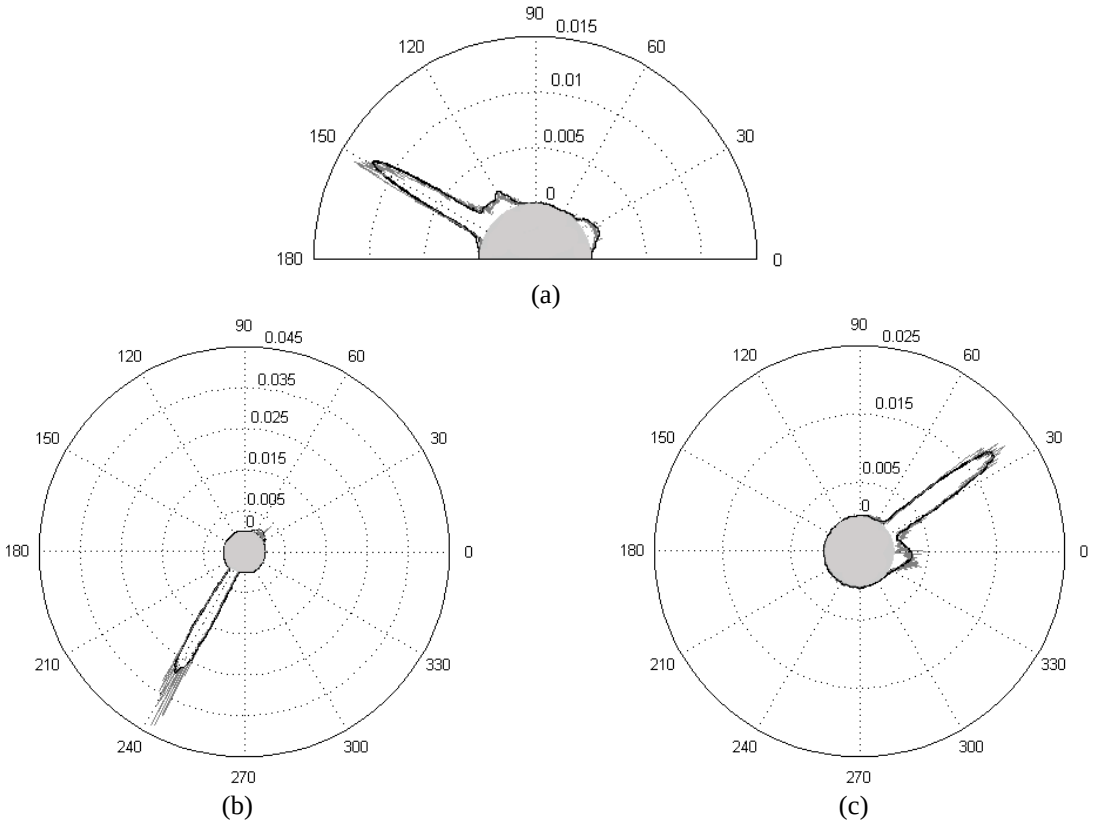

Figure 6.5. (a) $p(\alpha|\rho \geq T)$ (black line) and $h(\alpha|\rho \geq T)$ (grey line) in SA_c; (b) $p(\vartheta|\rho \geq T)$ (black line) and $h(\vartheta|\rho \geq T)$ (grey line) in A_c when using spectral channels 1 and 3; and (c) $p(\vartheta|\rho \geq T)$ (black line) and $h(\vartheta|\rho \geq T)$ (grey line) in A_c when using spectral channels 4 and 7 (Landsat 5 dataset).

Using the derived threshold values (both in magnitude and direction) a change-detection map is computed for each change-detection problem representation. Figure 6.6 (a) shows the change-detection map obtained by isolating the three clusters in SA_c according to (6.19). Each kind of change is clearly identified with a different color (Figure 6.6). Figure 6.6 (b) and (c) show the change-detection maps obtained using the two couples of spectral channels with the CVA. As expected, in these maps only two out of three changes appear (ω_{c_1} and ω_{c_3} considering spectral channels 1 and 3; and ω_{c_2} and ω_{c_3}, considering bands 4 and 7).

A comparison of these maps with the reference map in Figure 6.2 (c) allows us a quantitative evaluation of performance.

Table 6.2, Table 6.3 and Table 6.4 report the confusion matrices for the three considered cases. As one can see, the overall accuracies computed on the three change detection maps are very similar to each other, and always higher than 96%. However the proposed representation allowed us to retain the main information related to changes and to distinguish all different kinds of change. This is because C^2VA preserves the most of the information, although it maps a feature space of dimension 6 into one of dimension 2. It is worth stressing that this result is achieved without the need of any prior information about the kinds of change occurred on the ground. On the contrary, the representations obtained considering only couples of spectral channels [11],[15] resulted in total (or partial) loss of change information depending on the considered pair. One can observe that the CD map obtained considering all the spectral channels suffers of a higher impact of noisy components than the other two. This is because the use of all spectral channels not only preserves change information, but also introduces some

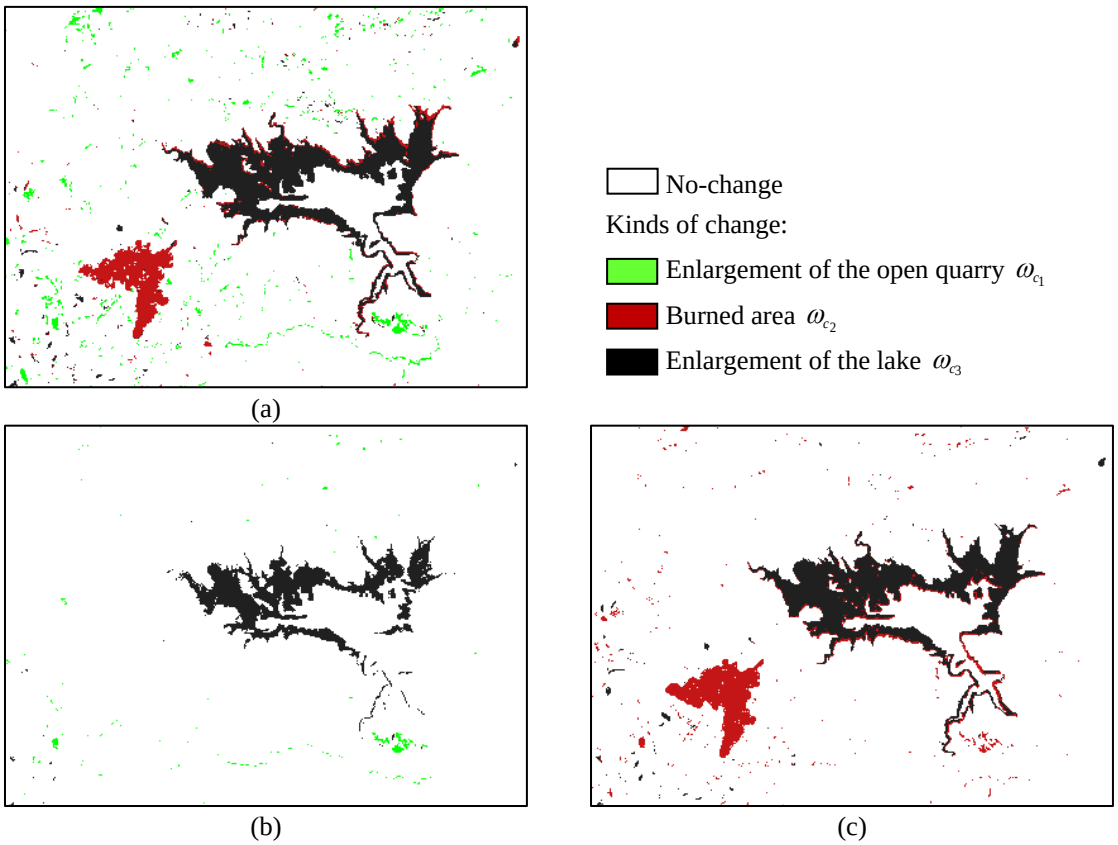

Figure 6.6. Change-detection maps obtained with the proposed change-detection technique applied to: (a) the proposed C^2VA representation; (b) the polar framework (spectral channels 1 and 3); and (c) the polar framework (spectral channels 4 and 7). (Landsat 5 dataset).

noise. However, according to the previous considerations, the slightly higher amount of false alarms that affects the C^2VA change-detection map becomes acceptable from an application point of view, where the possible loss of a kind of change could be more critical.

In order to further assess the effectiveness of the proposed approach a comparison is performed with the results obtained with MTEP. As demonstrated from Table 6.5 the proposed method and MTEP lead to quite similar threshold values and therefore to very close overall accuracies (96.38% versus 96.73%) thus confirming the validity of both the automatic procedure and the selected statistical model for class distribution. Accordingly, the errors of omission and commission among classes have to be ascribed to the overlapping of classes in the considered problem rather than to the proposed method and/or to the selected statistical model[10].

It is worth noting that, in absence of any prior information about relevant spectral bands with respect to the considered problem (*i.e.*, no spectral bands can be neglected) the standard unsupervised procedures simply threshold the magnitude variable obtained from all spectral channels (*i.e.*, only first step of the proposed change-detection procedure is applied). The resulting change-detection map is as the one in Figure 6.6 (a) but different kinds of change are not distinguished. It follows that the proposed technique can significantly improve the change information extracted from the considered dataset by allowing the separation of the contributions from different kinds of change.

[10] Similar observations hold for the results achieved for 2D CVA, as well for the ones obtained on the Quickbird data set.

TABLE 6.2. CHANGE-DETECTION RESULTS OBTAINED BY THE PROPOSED CHANGE-DETECTION METHOD BASED ON THE C^2VA REPRESENTATION APPLIED TO ALL THE SPECTRAL CHANNELS (LANDSAT 5 DATASET).

		True Class				User Accuracy
		ω_{c_1}	ω_{c_2}	ω_{c_3}	ω_n	
Estimated Class	ω_{c_1}	185	0	0	1487	11.06
	ω_{c_2}	5	2160	445	736	64.55
	ω_{c_3}	19	24	7032	1525	81.77
	ω_n	5	230	3	109744	99.78
Producer Accuracy		86.45	89.48	94.01	96.70	
Kappa Accuracy		0.7966				
Overall Accuracy		96.38				

TABLE 6.3. CHANGE-DETECTION RESULTS OBTAINED BY THE PROPOSED CHANGE-DETECTION METHOD APPLIED TO THE POLAR FRAMEWORK (SPECTRAL CHANNELS 1 AND 3) (LANDSAT 5 DATASET).

		True Class				User Accuracy
		ω_{c_1}	ω_{c_2}	ω_{c_3}	ω_n	
Estimated Class	ω_{c_1}	133	0	0	187	41.56
	ω_{c_2}	0	0	0	0	0.00
	ω_{c_3}	10	0	5390	163	96.89
	ω_n	71	2414	2090	113142	96.11
Producer Accuracy		62.15	0.00	72.06	99.69	
Kappa Accuracy		0.6747				
Overall Accuracy		96.01				

TABLE 6.4. CHANGE-DETECTION RESULTS OBTAINED BY THE PROPOSED CHANGE-DETECTION METHOD APPLIED TO THE POLAR FRAMEWORK (SPECTRAL CHANNELS 4 AND 7) (LANDSAT 5 DATASET).

		True Class				User Accuracy
		ω_{c_1}	ω_{c_2}	ω_{c_3}	ω_n	
Estimated Class	ω_{c_1}	0	0	0	0	0.00
	ω_{c_2}	0	2354	109	478	80.04
	ω_{c_3}	105	3	7364	1815	79.29
	ω_n	109	57	7	111199	99.84
Producer Accuracy		0.00	97.51	98.45	97.98	
Kappa Accuracy		0.8705				
Overall Accuracy		97.83				

TABLE 6.5. THRESHOLD VALUES OBTAINED BY THE PROPOSED CHANGE-DETECTION METHOD AND THE MTEP ON THE C^2VA REPRESENTATION APPLIED TO ALL THE SPECTRAL CHANNELS (LANDSAT 5 DATASET).

	T	α_{1_1}	$\alpha_{1_2} \equiv \alpha_{2_1}$	$\alpha_{2_2} \equiv \alpha_{3_1}$	α_{3_2}
C^2VA	45	0°	70°	142°	180°
MTEP	50	0°	60°	140°	180°

As a final remark, it is worth noting that the proposed C^2VA representation made it possible to identify a third kind of minority change in the considered data set that was not observed in previous works neither by photointerpreters, nor by automatic techniques based on the exploitation of spectral channels 4 and 7 in the CVA framework. Moreover, despite the possible loss of change information induced by the 2D representations, numerical results allow one to conclude that the proposed automatic technique for the detection of multiple changes is effective when applied to both C^2VA and 2D CVA representations. In all the cases the proposed technique extracted all information about changes that is available in the considered representation.

6.5.2 Data set 2: Quickbird images

Experiments similar to the ones conducted on the Thematic Mapper data set were carried out on a pair of very high geometrical resolution images acquired by the Quickbird sensor in October 2005 and July 2006 on the city of Trento (Italy) (Figure 6.7). In the pre-processing phase the two images were: i) pan-sharpened; ii) radiometrically corrected; and iii) co-registered. In particular, we considered pan-sharpened images as we expect that the pan-sharpening process can improve the results of the change-detection process, as demonstrated in previous work [99]. To this purpose we applied the minimum mean square error (MMSE) pansharpening method [131] to the panchromatic channel and the four bands of the multispectral images. Concerning radiometric corrections, we simply normalized the images by subtracting from each spectral channel of the two considered images its mean value. The registration process was carried out by using a polynomial function of order 2 according to 12 ground control points (GCPs), and by applying a nearest neighbor interpolation [100]. The final data set is made up of images of 992x992 pixels with spatial resolution on the ground of 0.7m. Between the two acquisition dates some changes related to urban and rural areas occurred on the ground. In particular, three different kinds of change can be observed, *i.e.* K=3 (see circles in Figure 6.7): i) changes in the cover of both buildings (*i.e.*, changes in roofs related to saturation problems of the sensor) and crop fields (*i.e.*, new structures built for covering fields) that have the same spectral signature, ω_{c_1}; ii) seasonal changes in vegetated areas, both in crop fields and wooded zones, ω_{c_2}; and iii) changes along the river bank due to an increase of the water level, ω_{c_3}. In order to perform a quantitative analysis on this data set, we defined a sampled ground truth (based on a spatial random sampling as we do not have a complete knowledge of the changes occurred on the ground) containing: 22652 pixels labeled as ω_{c_1}, 27660 as ω_{c_2}, 6554 as ω_{c_3} and 383396 pixels of no change.

As for the Sardinia data set, we reduced the dimension of the feature space from 4 (the number of the multispectral channels of the Quickbird images) to 2, computing the magnitude of the multispectral difference image according to (6.2) and the angle according to (6.6). In this case u=[$\sqrt{4}/4$, $\sqrt{4}/4$, $\sqrt{4}/4$, $\sqrt{4}/4$].Figure 6.8 (a) shows the considered change-detection problem within the proposed C^2VA domain. We compared this plot with the scatterograms obtained by applying the CVA technique to: channels 2 and 3 (Figure 6.8 (b)), which were randomly selected; and channels 3 and 4 (Figure 6.8 (c)), which were selected according to some prior knowledge about changes occurred on the ground.

The threshold value T for C^2VA which separates the SC_n from the SA_c resulted equal to 350. Four main clusters were identified in SA_c in the scatterogram (see dashed circles in Figure 6.8 (a)) and four

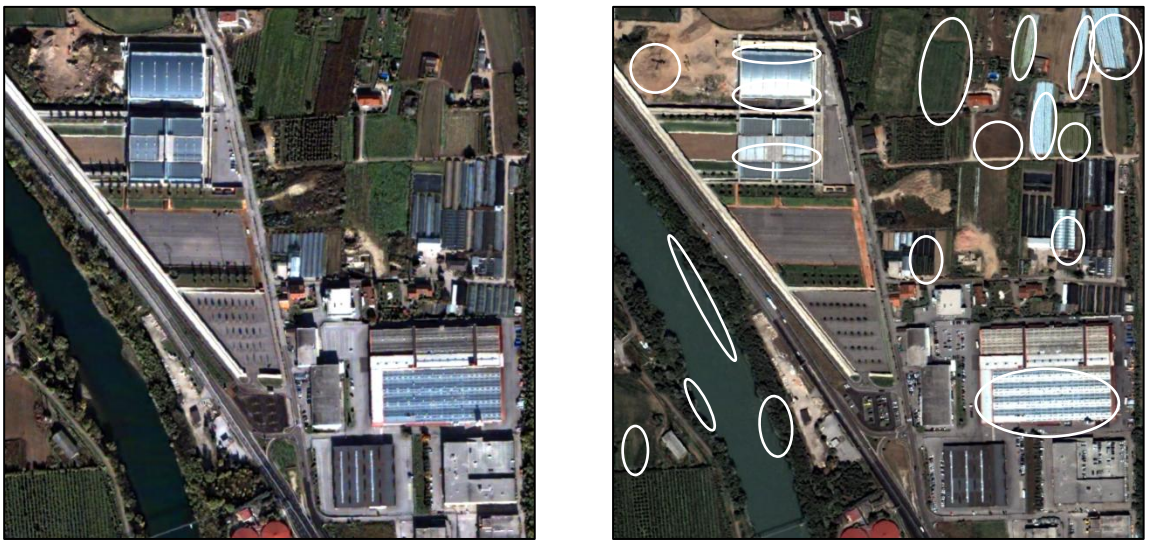

(a) (b)

Figure 6.7. True color composition of an area nearby the city of Trento (Italy) acquired by the Quickbird VHR multispectral sensor in (a) October 2005 and (b) July 2006. White circles identify the main areas affected by changes.

modes are present in $h(\alpha|\rho\geq T)$ (see grey line in Figure 6.9 (a)), therefore K was set equal to 4[11]. The visual analysis of Figure 6.9 (a) points out that estimated distribution $p(\alpha|\rho\geq T)$ (black line) fits quite well the behavior of the real histogram $h(\alpha|\rho\geq T)$ (grey line) confirming the reliability of the Gaussian approximation.

The second step of the thresholding procedure led us to the definition of the following four annular sectors:

$$\begin{aligned} S_1 &= \{\rho,\alpha : \rho \geq 350 \text{ and } 0° \leq \alpha < 27°\} \\ S_2 &= \{\rho,\alpha : \rho \geq 350 \text{ and } 27° \leq \alpha < 110°\} \\ S_3 &= \{\rho,\alpha : \rho \geq 350 \text{ and } 110° \leq \alpha < 156°\} \\ S_4 &= \{\rho,\alpha : \rho \geq 350 \text{ and } 156° \leq \alpha \leq 180°\} \end{aligned} \tag{6.20}$$

Analyzing each sector it is possible to observe that S_1, S_2 and S_3 are associated to: ω_{c_1}, ω_{c_2}, and ω_{c_3}, respectively, whereas S_4 is mainly related to the effects of registration noise. This result was expected as registration noise in VHR images significantly affects the change-detection process introducing clusters with a high magnitude and preferred direction that have properties similar to changed pixels [81]. An analysis of this kind of noise within C^2VA domain is out of the purposes of this work. Therefore in the following SCVs that fall in S_4 and that are identified as being of registration noise will be neglected from further analysis and classified as unchanged patterns.[12]

With regards to the analysis in the polar domain, as for the analysis in the proposed C^2VA domain, we retrieved the threshold value T (T=350 when considering bands 2 and 3 and T=300 for spectral channels 3 and 4). According to the analysis of both the scatterograms (Figure 6.8 (b) e (c)) and the histograms (Figure 6.9 (b) e (c)), the value of K was set to 2 for the case of bands 2 and 3, and to 4 for bands 3and 4.

[11] It is worth noting that also in this case a light grey semi-circle/circle is introduced to slightly shift from the origin of the plot the level corresponding to zero occurrences, thus avoiding a bias in the information visualization.

[12] The reader is referred to [88], [124] for further details on this challenging problem and on techniques for reducing its impacts on the change-detection process.

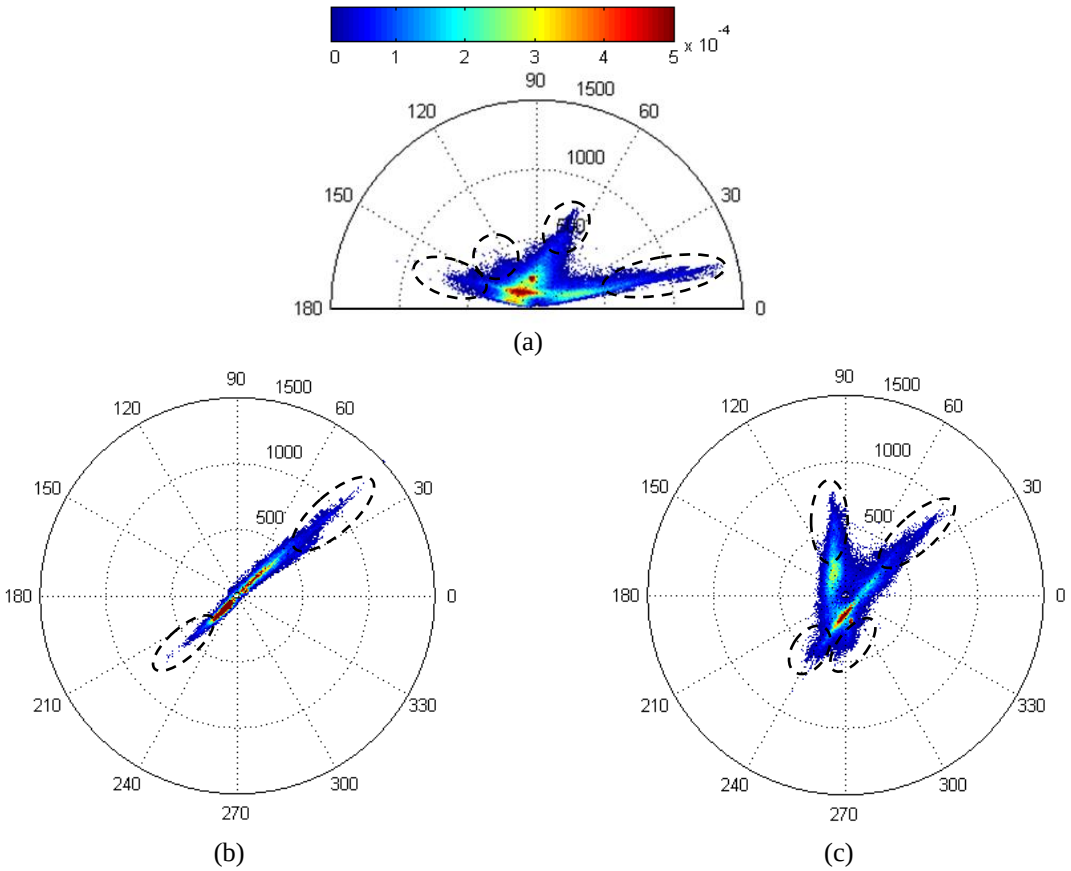

Figure 6.8. Scatterograms obtained by applying: (a) the proposed 2D representation; (b) the polar CVA to spectral channels 2 and 3; and (c) the polar CVA to spectral channels 3 and 4 (Quickbird Dataset).

The second step of the proposed thresholding procedure was applied to distinguish the different contributions to Ω_c. Concerning the first pair of bands (2 and 3) two sectors were identified, S_1 made up of SCVs with $\vartheta \in [0°,103°]$ and S_2 with $\vartheta \in [103°,360°)$. It is possible to show that S_1 is related to changes in building or crop covers spectral channels 2 and 3 it is not possible to extract information about ω_{c_2} and ω_{c_3}. The analysis conducted on the second pair of spectral channels results in the definition of 4 sectors, S_1 made up of SCVs with $\vartheta \in [0°,63°)$, S_2 with $\vartheta \in [63°,168°)$, S_3 with $\vartheta \in [168°,253°)$, and S_4 with $\vartheta \in [253°,360°)$. It can be shown that, as for the proposed method, pixels associated to ω_{c_1} fall in S_1, pixels belonging to ω_{c_2} fall in S_2, pixels belonging to ω_{c_3} fall in S_3, and pixels in S_4 are associated to registration noise. It is worth stressing that the considered spectral channels were selected according to some prior information about changes, whereas the proposed method achieves similar results (*i.e.*, it detects all kinds of change present in the multitemporal data set) without any prior information.

According to the threshold values estimated with the proposed technique for each of the three representations the change-detection map is generated (see Figure 6.10). A quantitative analysis of the results achieved on the three considered representations for the reference data set is reported in Table 6.6, Table 6.7 and Table 6.8. These tables confirm the qualitative evaluation. The proposed technique for multiple change detection applied to both the C^2VA and the CVA (spectral channels 3 and 4) achieved similar results (overall accuracy equal to 95.0% and 95.5% respectively). However, CVA requires prior information about possible kinds of change for selecting spectral channels. Moreover, the proposed multiple-change detection technique permits to identify and separate all different kinds of change, showing good accuracies for all of them (higher than 80 % for user accuracy and higher

than 70% for the producer accuracy). On the contrary, the standard CVA on randomly selected spectral channels (*i.e.*, bands 2 and 3) allows us to identify only the changes in building and crop covers. All other kinds of change are undetected.

It is worth noting that some registration noise effects are still visible in the change-detection maps affecting significantly the user accuracy which is always smaller than 83% for all the kinds of change in the three analyzed cases. Advanced change-detection techniques developed for VHR images (*i.e.* context sensitive or multiscale techniques [13], [132]) could be employed for reducing the effects of the residual registration noise in change-detection maps. These strategies can be easily extended to the proposed C^2VA domain. However this is out of the purpose of this work, for which we just consider the comparison of C^2VA and CVA at pixel level.

As for the Landsat-5 data set a comparison with MTEP results leads to the conclusion that the proposed procedure as well as the assumption of Gaussian distributed classes are effective and reliable. The presence of mislabeled pixels is therefore due to the complexity of the considered problem.

According to the analysis of results it is possible to conclude that the proposed representation allows us to preserve the information about all the possible kinds of change, even by reducing dimensionality from 4 to 2 (and thus introducing ambiguity in the process). On the contrary, the representation obtained considering only couples of channels may result in a total (or partial) loss of information related to specific changes. This depends on the selected spectral bands and thus on the available prior information. Furthermore, the proposed automatic technique for the detection of multiple changes demonstrated to be successful when applied to both C^2VA and 2D CVA representations. In all the cases the proposed technique effectively detected all information about changes available in the considered representation.

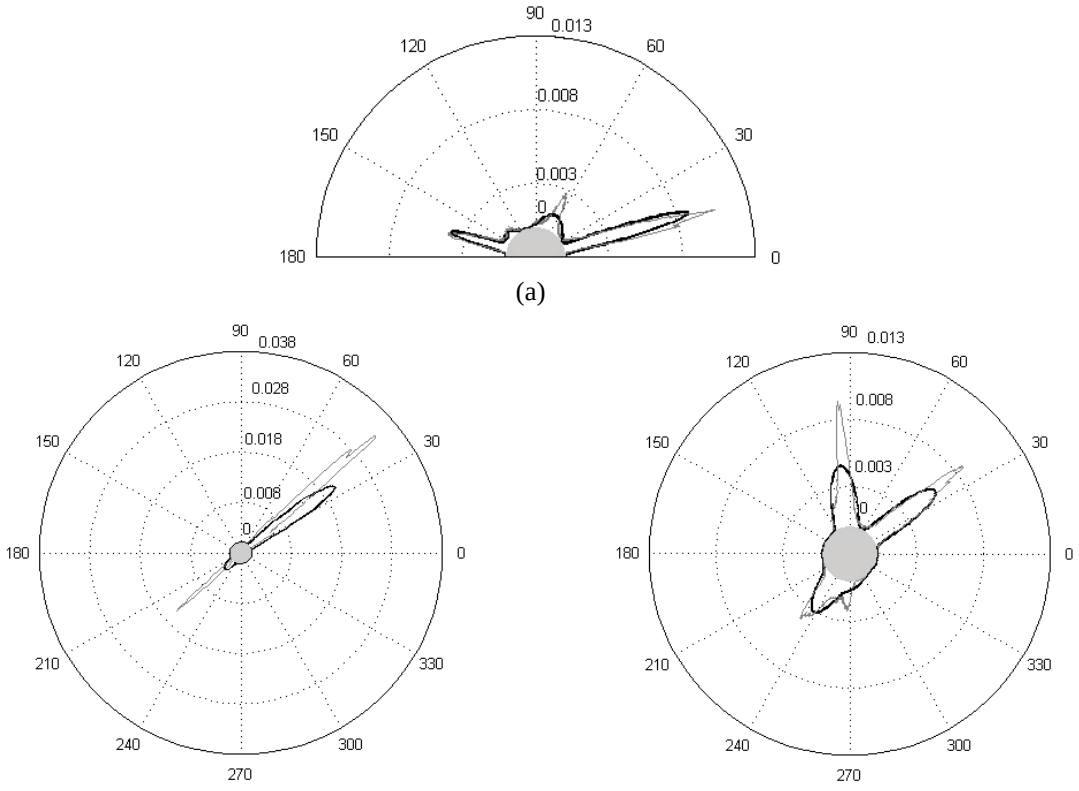

Figure 6.9. (a) Estimated $p(\alpha|\rho \geq T)$ (black line) and $h(\alpha|\rho \geq T)$ (grey line) in SA_c; (b) estimated $p(\vartheta|\rho \geq T)$ (black line) and $h(\vartheta|\rho \geq T)$ (grey line) in A_c when using spectral channels 2 and 3; and (c) estimated $p(\vartheta|\rho \geq T)$ (black line) and $h(\vartheta|\rho \geq T)$ (grey line) in A_c when using spectral channels 3 and 4 (Quickbird Dataset).

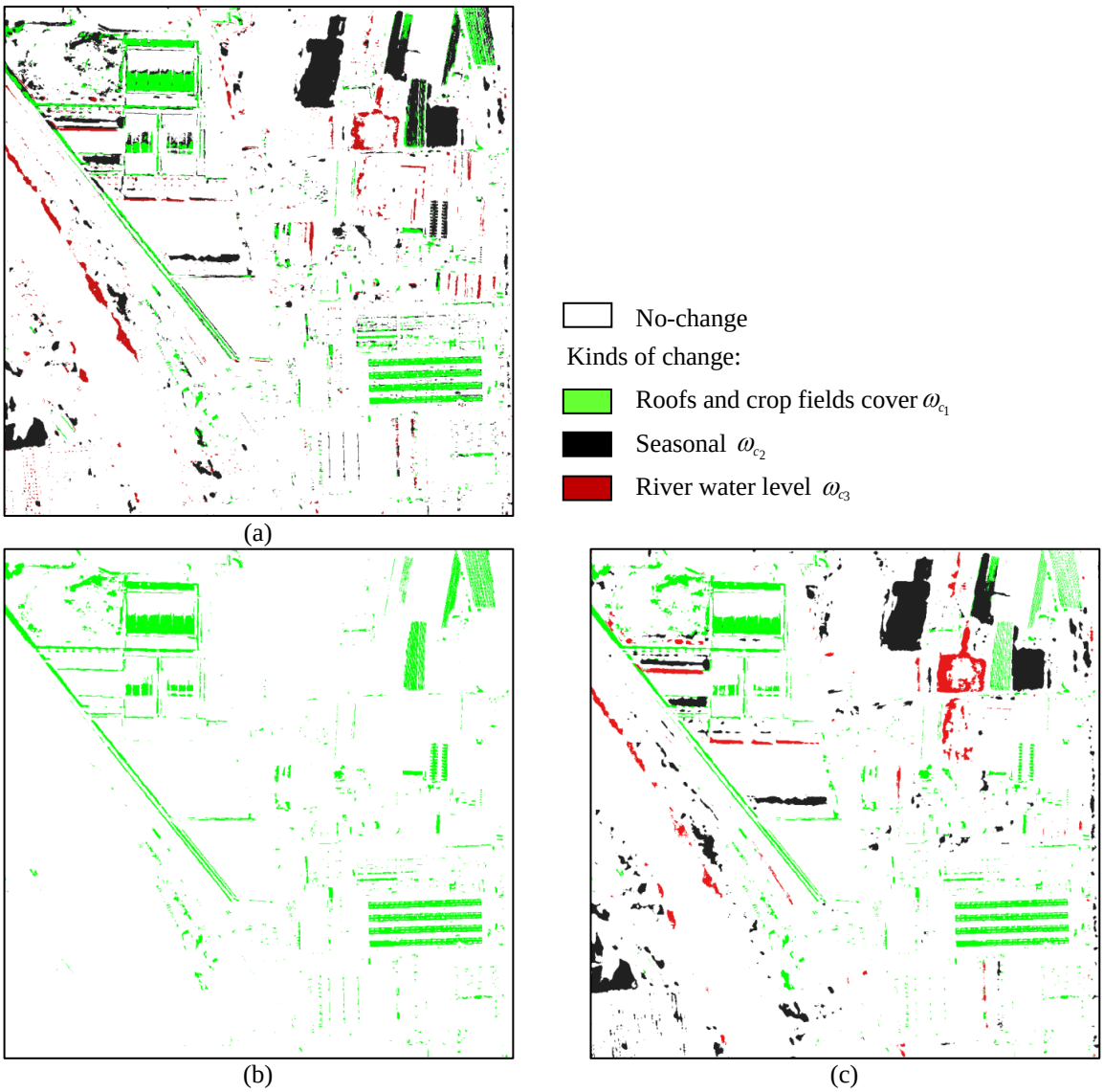

Figure 6.10. Change-detection map obtained with the proposed change-detection technique applied to: (a) the proposed C^2VA domain data representation; (b) the polar framework (spectral channels 2 and 3); and (c) the polar framework (spectral channels 3 and 4). (Quickbird Dataset)

TABLE 6.6. CHANGE-DETECTION RESULTS OBTAINED BY THE PROPOSED CHANGE-DETECTION METHOD BASED ON THE C^2VA REPRESENTATION APPLIED TO ALL THE SPECTRAL CHANNELS (QUICKBIRD DATASET).

		True Class				**User Accuracy**
		ω_{c_1}	ω_{c_2}	ω_{c_3}	ω_n	
Estimated Class	ω_{c_1}	18728	823	0	4896	76.61
	ω_{c_2}	3479	24948	139	6706	70.73
	ω_{c_3}	0	12	5691	2473	69.61
	ω_n	445	1858	722	358671	99.16
Producer Accuracy		82.68	90.26	86.86	96.22	
Kappa Accuracy		0.8077				
Overall Accuracy		94.98				

TABLE 6.7. CHANGE-DETECTION RESULTS OBTAINED BY THE PROPOSED CHANGE-DETECTION METHOD APPLIED TO THE POLAR FRAMEWORK (SPECTRAL CHANNELS 2 AND 3) (QUICKBIRD DATASET).

		True Class				User Accuracy
		ω_{c_1}	ω_{c_2}	ω_{c_3}	ω_n	
Estimated Class	ω_{c_1}	21872	1782	0	6034	73.67
	ω_{c_2}	0	0	0	0	0.00
	ω_{c_3}	0	0	0	0	0.00
	ω_n	780	25874	6547	372700	91.82
Producer Accuracy		96.56	0.00	0.00	98.41	
Kappa Accuracy		0.4944				
Overall Accuracy		90.58				

TABLE 6.8. CHANGE-DETECTION RESULTS OBTAINED BY THE PROPOSED CHANGE-DETECTION METHOD APPLIED TO THE POLAR FRAMEWORK (SPECTRAL CHANNELS 3 AND 4) (QUICKBIRD DATASET).

		True Class				User Accuracy
		ω_{c_1}	ω_{c_2}	ω_{c_3}	ω_n	
Estimated Class	ω_{c_1}	20463	2168	0	5573	72.55
	ω_{c_2}	4	23902	161	4794	82.82
	ω_{c_3}	1	35	4877	2744	63.69
	ω_n	2184	1538	8	360283	98.98
Producer Accuracy		90.34	86.47	96.65	96.49	
Kappa Accuracy		0.8226				
Overall Accuracy		95.52				

6.6. Conclusion

In this chapter an automatic technique for the detection of multiple changes in multitemporal and multispectral remote sensing images has been presented. The proposed method compresses the original *B*D feature space to be explored for the solution of the change-detection problem (*B* is the number of spectral channels acquired by the considered sensor) to a 2D space and applies a 2-step decision strategy for detecting changes. The compression is accomplished by computing the magnitude of spectral change vectors, and the angle (direction) between the spectral difference vector and a reference one. In this way we obtain a 2D representation of the change-detection problem that preserves the relevant information present in all available spectral channels. The change information can be represented according to the two proposed variables in a 2D domain, which is defined as Compressed Change Vector Analysis (C^2VA) domain. The proposed transformation leads to a 2D representation of the change-detection problem without the need of selecting a pair of spectral channels as usually done in standard approaches. This represents a valuable advantage as spectral channel selection would require some prior knowledge about possible changes occurred on the ground which often is not available or incomplete. Accordingly, missed alarms associated to possible unexpected kinds of change only visible in non-selected spectral bands are reduced.

Qualitative and quantitative results obtained on both Lansat-5 and Quickbird images confirmed the effectiveness of the proposed automatic technique for the detection of multiple changes when applied

to both C^2VA and standard 2D CVA. Thus confirming its effectiveness and the reliability of Gaussian approximation for the distribution of the classes (however statistical models different from the Gaussian one could be integrated within the proposed method). Further they point out the better capabilities in representing the change information of the proposed C^2VA representation with respect to the standard 2D CVA. In C^2VA, although the information is projected from a *B*D into a 2D space, it is possible to retrieve the main information related to changes and to distinguish all different kinds of change occurred on the ground. When the C^2VA representation is used the advantage of identifying all kinds of change by using all spectral channels implies an increase of false alarms due to noisy components.

As a final remark, it is worth noting that in complex change-detection problems some ambiguity may rise from the dimension reduction process, mainly due to the simplified representation of the angle variable. This may result in loss of information about the distribution of different kinds of change. Anyway it is preferable to more standard representations based on the use of couple of spectral channels that often implies a significant loss of information about kinds of change.

As future work we plan to exploit the potentialities of the proposed technique in the context of more complex approaches to change detection like those that exploit multiscale/multiresolution information intrinsically present in VHR images and the ones robust to registration noise, like the one described in chapter 5.

PART III:
PRE-PROCESSING TECHNIQUES FOR OPTIMIZING CHANGE DETECTION

Chapter 7

7. Image transformation for change detection in multispectral images[13]

In this chapter different techniques developed in the literature for image transformation and sources separation are studied and compared in the framework of unsupervised change detection in multitemporal remote sensing images. In particular, we consider Principal Component Analysis (PCA), Independent Component Analysis (ICA), and their relative kernelized versions (i.e. Kernel Principal Component Analysis (KPCA) and Kernel Independent Component Analysis (KICA). Different architectures for using the above-mentioned techniques in change detection are investigated, and their capability to discriminate true changes from the different sources of noise analyzed. Experimental results obtained on a pair of very high geometrical resolution Quickbird images point out the main properties of the different methods when applied to change detection.

7.1. Introduction

Change-detection techniques aim at identifying two different classes in multitemporal images: the class of changed areas and that of unchanged ones. Usually change-detection algorithms compare two images acquired at different times on the same geographical area by assuming that they are similar to each other except for the presence of changes on the ground. However, this assumption is seldom completely satisfied due to differences in atmospheric and sunlight conditions of acquired images, as well as in the sensor acquisition geometry (especially with very high resolution (VHR) images). In order to overcome these problems, change-detection techniques generally implement pre-processing steps, which include image co-registration, radiometric and geometric corrections, and noise reduction. Depending on the kind of sensors considered for image acquisition and on the related geometrical resolution, these steps can result in different complexity. Nonetheless, in real problems pre-processing is often not sufficient to guarantee the ideal condition in which radiometric changes in corresponding pixels on the multitemporal images are associated with true changes on the ground. Usually, residual components of noise (e.g. due to residual radiometric differences, residual misregistration,

[13] This chapter is published in *IGARSS, Proceedings of IEEE International Geoscience and Remote Sensing Symposium*, Cape Town, South Africa, July 13-17 2009, pp. II.980-II.983. Title: *"*Ica and Kernel Ica for Change Detection in Multispectral Remote Sensing Images". Authors: S. Marchesi and L. Bruzzone.

etc.) result in false alarms in the change-detection maps, which cannot be easily identified in the phase of post-processing.

In this chapter, we address the aforementioned problem by exploiting data transformation techniques for separating the different sources of noise from real changes in different components to be selectively exploited in the change-detection phase. In particular, we study the effectiveness of PCA and ICA and of theirs kernelized versions, i.e. KPCA and KICA, respectively, as a preliminary step to change detection. These techniques are integrated in standard change-detection methods and their performances are analyzed on different data sets, thus deriving general conclusions on their effectiveness in change-detection applications.

7.2. Image transformation techniques

Let us consider two multispectral images $\mathbf{X}_1$ and $\mathbf{X}_2$ acquired on the same geographical area at different times, t_1 and t_2, respectively. Let $\Omega = \{\omega_n, \Omega_c\}$ be the set of classes to be identified. In particular, ω_n represents the class of no-changed pixels, while $\Omega_c = \{\omega_{c_1}, ..., \omega_{c_K}\}$ the set of the K possible classes of changes occurred in the considered area. The main objective of the present work is to define techniques capable to identify the K different kinds of changes and to separate them from sources of noise (e.g. registration noise). To this purpose we analyze the effectiveness of ICA PCA, KICA and KPCA transformation integrated in simple change-detection architectures, and compare their performances with those of the standard change vector analysis (CVA). In the following some background concepts on PCA, ICA, and their kernelized versions KPCA and KICA, respectively, are reported.

7.2.1 PCA and KPCA

A standard transformation approach to isolate changed areas from unchanged areas is that based on the PCA technique [133]. PCA is a linear transformation which exploits image data second order statistics to extract orthogonal components ordered according to decreasing variances. The transformation can be based on eigenvector analysis of the correlation or of the co-variance matrix. The transformed components are globally uncorrelated under Gaussian hypothesis.

In PCA, the basis vectors are obtained by solving the algebraic eigenvalue problem $\mathbf{R}^{\mathbf{T}}(\mathbf{X}\mathbf{X}^{\mathbf{T}})\mathbf{R} = \mathbf{\Lambda}$ where $\mathbf{X} = \left(\mathbf{x}_1, \mathbf{x}_2, ..., \mathbf{x}_{\mathbf{M}}\right)^{\mathbf{T}}$ is the matrix of samples (samples must be centered), $\mathbf{R}$ is a matrix of eigenvectors, and $\mathbf{\Lambda}$ is the corresponding diagonal matrix of eigenvalues. The projection of data, $\mathbf{C_n} = \mathbf{R_n^T X}$ from the original l dimensional space to a subspace spanne by n principal eigenvectors is optimal in the mean squared error sense. That is, the reprojection of $\mathbf{C_n}$ back into the p dimensional space has minimum reconstruction error.

PCA can be used in change detection either by applying the transformation separately to single date images, or by applying the transformation jointly to the multitemporal images. In many applications, a subset of the resulting transformed components proved to exhibit a more focused representation of the changed areas than the original spectral channels [133]. However PCA is not suitable for separating information sources from sources of noise that are associated with the complexity of many change-detection problems, especially in VHR images [81], acquired by the last generation sensors.

Kernel Principal Component Analysis can be regarded as a generalization of PCA from a linear space to a nonlinear space. In literature, it has been shown to provide a better way of recovering the principal components of the given data. The core idea of KPCA is to project the input space $\mathbf{X} \in R^l$ to a potentially higher dimensional feature space F, through a non-linear mapping

$\Phi : \mathbf{x} \in R^l \rightarrow \Phi(\mathbf{x}) \in F$, so that the nonlinear relation in the input space can be analyzed in a linear way in this feature space and then compute the principal components of the mapped data. Instead of considering the given learning problem in input space R^l, one can deal with $\Phi(\mathbf{x}_1),...,\Phi(\mathbf{x}_M)$ in the feature space *F* and then finds a linear discriminant function in the feature space *F*. The use of this kernel trick avoids the need to compute the feature vector in *F* explicitly. It is sufficient to calculate the inner product of two vectors in *F* with a kernel function $k(\cdot,\cdot)$ so that: $< \Phi(\mathbf{x}_i), \Phi(\mathbf{x}_j) >= k(\mathbf{x}_i, \mathbf{x}_j)$, where $(\cdot,\cdot)$ denotes the inner product. In the literature several kernel functions exist, like Gaussian or polynomial kernels. For a detailed analysis on the algorithm used in this work for retrieving the principal components through the kernel PCA, please refer to [134].

7.2.2 ICA and KICA

A more suitable methodological tool for discriminating sources of noise form true changes (and potentially to distinguish different kinds of change) is the Independent Component Analysis (ICA), which is intrinsically designed for mapping the information sources present in a complex problem in different components. Nonetheless, marginal attention has been devoted to the use of ICA in change detection, without a detailed analysis of its potentialities [135], [136]. The objective of ICA is to extract components with higher-order statistical independence, through a nonlinear transformation function. ICA assumes a statistical model whereby the observed multivariate data are assumed to be linear or nonlinear mixtures of some unknown latent variables. The mixing coefficients are also unknown. The latent variables are non-gaussian and mutually independent and they are called the independent components (sources) of the observed data. In particular, an observed data vector $\mathbf{X} = \left(\mathbf{x}_1, \mathbf{x}_2, ..., \mathbf{x}_M\right)^T$ is modeled by ICA as $\mathbf{X} = A\mathbf{S}$ where $\mathbf{S}$ is a latent vector with independent components and *A* is the $M \times M$ matrix of mixing parameters. Given *N* i.i.d. observations of $\mathbf{X}$, ICA estimates the mixing matrix *A* and recovers the latent vector $\mathbf{S}$ corresponding to any particular $\mathbf{X}$. ICA is usually applied by introducing proper contrast functions and iterative procedures capable to optimize them. A considerable portion of open literature is dedicated to define contrast functions associated with the estimation of the mixing matrix *A* by the Maximum Likelihood principle or by minimizing the mutual information between the components. The obtained components $\mathbf{s}$ are statistically as independent as possible. It is worth noting that the goal of independence is stronger than that of uncorrelatedness which can be obtained on the global data distribution with the PCA technique. It follows that ICA can provide more effective decomposition than PCA, especially for non-Gaussian signals.

As for the Kernel PCA, Kernel ICA is an approach recently introduced in the literature, in which the ICA problem is not solved on the basis of a single nonlinear function, but on an entire reproducing kernel Hilbert space (RKHS) of candidate nonlinear functions [137]. The idea of KICA is to embed the data $\mathbf{X}$ from input space into a feature space *F* using nonlinear mapping and then compute the independent components on the mapped data. In Kernel ICA presented in [137] and used in this work the independent components are derived according to a new kernel measure of independence. Then the *F*-correlation is defined as the maximal correlation between the random variables $f_1(\mathbf{x}_i)$ and $f_2(\mathbf{x}_j)$, where f_1 and f_2 range over *F*:

$$\rho_F = \max_{f_1, f_2 \in F} \operatorname{corr}\left(f_1(\mathbf{x}_i), f_2(\mathbf{x}_j) \right) = \max_{f_1, f_2 \in F} \frac{\operatorname{cov} < f_1(\mathbf{x}_i), f_2(\mathbf{x}_j) >}{\left[\operatorname{var} f_1(\mathbf{x}_i)\right]^{1/2} \left[\operatorname{var} f_2(\mathbf{x}_j)\right]^{1/2}} \tag{7.1}$$

If the variables $\mathbf{x}_i$ and $\mathbf{x}_j$ are independent, then the *F*-correlation is equal to zero. For a detailed description of the algorithm and strategies used for retrieving the independent components through the

kernel ICA, please refer to [137]. Please note that the use of a function space makes it possible to adapt the technique to a variety of sources and thus makes this algorithm more robust to varying source distributions. However, this is obtained at the cost of a significantly increased computational load.

7.3. Change-detection strategies

The proposed architectures exploits a simple change-detection scheme based on multitemporal images comparison and thresholding, after a preliminary phase based on image transformation. The main idea is that through the transformation of the images it is possible to identify and separate changes from other information sources (noise, unchanged areas, etc.). Then, through a simple analysis of the components that contain change information it is possible to identify true changed areas.

Two different transformation strategies were investigated: i) all the spectral channels of the two multitemporal images were jointly transformed; and ii) the multispectral difference image $\mathbf{X_D}$ (obtained by a simple subtraction of corresponding pixels of the same bands at the two dates, i.e. $\mathbf{X_D}=\mathbf{X_2}-\mathbf{X_1}$) was transformed. Concerning the first option, let us denote with $\mathbf{S}_i^t$ the *i*-th component extracted through the transformation method *t* (with $t = (\text{PCA, KPCA, ICA, KICA})$). The number of extracted components corresponds to the total number of the spectral channels of the two multitemporal images. Considering the second strategy, let us denote with $\mathbf{S}_{D,i}^t$ the *i*-th component extracted with the four different methods. In this case the number of transformed components is equal to the number of spectral channels of the difference image. In order to extract changed areas from the components obtained with the transformation methods we applied two different procedures: i) identification of relevant single components and thresholding [15]; and ii) application of the Change Vector Analysis (CVA) technique in the polar domain combining pairs of components [11] (see section 2.4). In the first case the most relevant single component $\mathbf{S}_i^t$ (or $\mathbf{S}_{D,i}^t$) was chosen according to a visual analysis by the user and then the threshold *T* that discriminates ω_n from Ω_c was automatically retrieved by the expectation-maximization algorithms and the Bayes rule for minimum error [15]. Then the change-detection map was generated assigning all the pixels with value higher than the retrieved threshold to the class of change and the others to the class of no-changed.

In the second case, two relevant transformed components were chosen by the user and the spectral change vectors (SCVs) were computed according to a vector difference operator. The magnitude ρ and the direction ϑ variables of the SCVs obtained according to (2.2) were then exploited in the polar framework presented in section 2.4 for defining the change-detection map through the semi-automatic procedure proposed in [11]. In greater detail, the classes of changed and unchanged pixels can be separated by a threshold *T* defined along the magnitude variable. In addition, different kinds of changes can be discriminated as SCVs related to them generate different clusters located in different direction ranges far from the origin. It follows that in order to generate the final change-detection map at first the threshold *T* in the magnitude domain was chosen in an automatic way (as for the previous approach), then the user manually retrieved the couples of thresholds ϑ_{K_1} and ϑ_{K_2} in the direction domain for separating the *K* kinds of change (please refer to [11] for greater details).

7.4. Experimental results

In order to assess the effectiveness of the proposed methods and to understand which transformation technique is the most suitable for change-detection applications, several experiments were carried out on both medium and VHR multispectral and multitemporal images. For space constraints in the

following we report only the results obtained on VHR images. To this purpose, we consider a portion (733×537 pixels) of two images acquired by the Quickbird sensor on the Trentino area (Italy) in October 2005 and July 2006. In the pre-processing phase the two images were: i) pan-sharpened by applying the Gram–Schmidt procedure; ii) radiometrically corrected; and iii) co-registered. The final data set was made up of two pan-sharpened multitemporal and multispectral images that have a residual misregistration of about 1 pixel on ground control points. Figure 7.1(a) and (b) show a real color composition of the pan-sharpened multispectral images $\mathbf{X_1}$ and $\mathbf{X_2}$, respectively. Between the two acquisition dates two kinds of changes occurred: i) new houses were built on rural area (white circles in Figure 7.1(b) - ω_{c_1}); and ii) some roofs in the industrial and urban area were rebuilt (black circles in Figure 7.1(b) - ω_{c_2}). In order to allow one a quantitative evaluation of the effectiveness of the proposed method, a reference map related to the two kinds of changes was defined.

(a) (b)

Figure 7.1: Real color composition of images of the Trento city (Italy) acquired by the Quickbird VHR multispectral sensor in: (a) October 2005; and (b) July 2006 (changes occurred between the two acquisition dates appear in black and white circles).

At first PCA, KPCA, ICA, and KICA were separately applied to: i) the original images originating 8 components (as Quickbird images are made up of four spectral channels –blue, green, red and near infrared), and ii) the difference image generating 4 components. Concerning the Kernel PCA, the computational burden required for running the algorithm on the entire images was too high; for this reason we subsampled the original images (and the difference one) and we applied the algorithm on the subsampled data. Then in the post-processing step, in order to retrieve a complete change-detection map we oversampled of a factor of 5 the obtained map. The algorithm was tested with different parameter values (i.e. different kernels, different values of spread σ for Gaussian kernels, different orders for polynomial kernels). However, on the considered data set, different combinations involved very similar results. In the following we report only the analysis obtained subsampling the image of a factor 5 and using polynomial kernel of third degree. Concerning the Kernel ICA different algorithms (i.e. the Kernel Canonical Correlation Analysis KCCA, and the Kernel Generalized Variance KGV [137]) were tested with different parameter values (i.e. different kernels, different values of spread σ for Gaussian kernels, different orders for polynomial kernels, and different values for regularization parameter) and also in this case different combinations generated very similar results. In the following we report only the analysis conducted using KCCA algorithm with Gaussian kernel having σ=0.5 and regularization parameter set to 0.002.

All the components were visually analyzed in order to choose the most significant ones. Then the two change-detection strategies described in section 7.3 were applied. In details, according to the first

strategy, the selected components were thresholded and the change-detection maps were derived. It is worth noting that this results in a single change-detection map for each kind of change (i.e. each component). Concerning the second strategy the CVA was applied to two significant components of PCA, KPCA, ICA and KICA, and thresholds applied to both magnitude and direction of SCVs in order to generate the final change-detection map. This procedure allowed us to obtain a change-detection map in which the two different kinds of changes are reported and isolated from the noise components (which are contained in other ICA and KICA components).

In Figure 7.2 the most significant components for the change-detection process extracted by both Principal and Independent Component Analysis are reported. As one can observe in Figure 7.2 (b) and (d) the first kind of change is emphasized with respect to the other objects present in the area, while in Figure 7.2 (a) and (c) the second kind of change is extracted. Comparing the images extracted by ICA [Figure 7.2 (a) and (b)] with the ones extracted by PCA [Figure 7.2 (c) and (d)] it is simple to note that the components extracted by the Independent Component Analysis isolate better changes occurred on the ground (this is also confirmed from both the qualitative analysis of the change-detection maps obtained and the quantitative analysis reported in Table 7.1). Figure 7.3 reports an example of the change-detection maps obtained with the ICA transformation. The CD maps obtained on the components extracted by the others transformation techniques and through both the two CD algorithms are visually very similar to the ones reported. A quantitative analysis was performed by comparing the obtained change-detection maps with the reference maps. In addition, a comparison with the results obtained by applying the standard CVA technique to the original spectral channels was carried out.

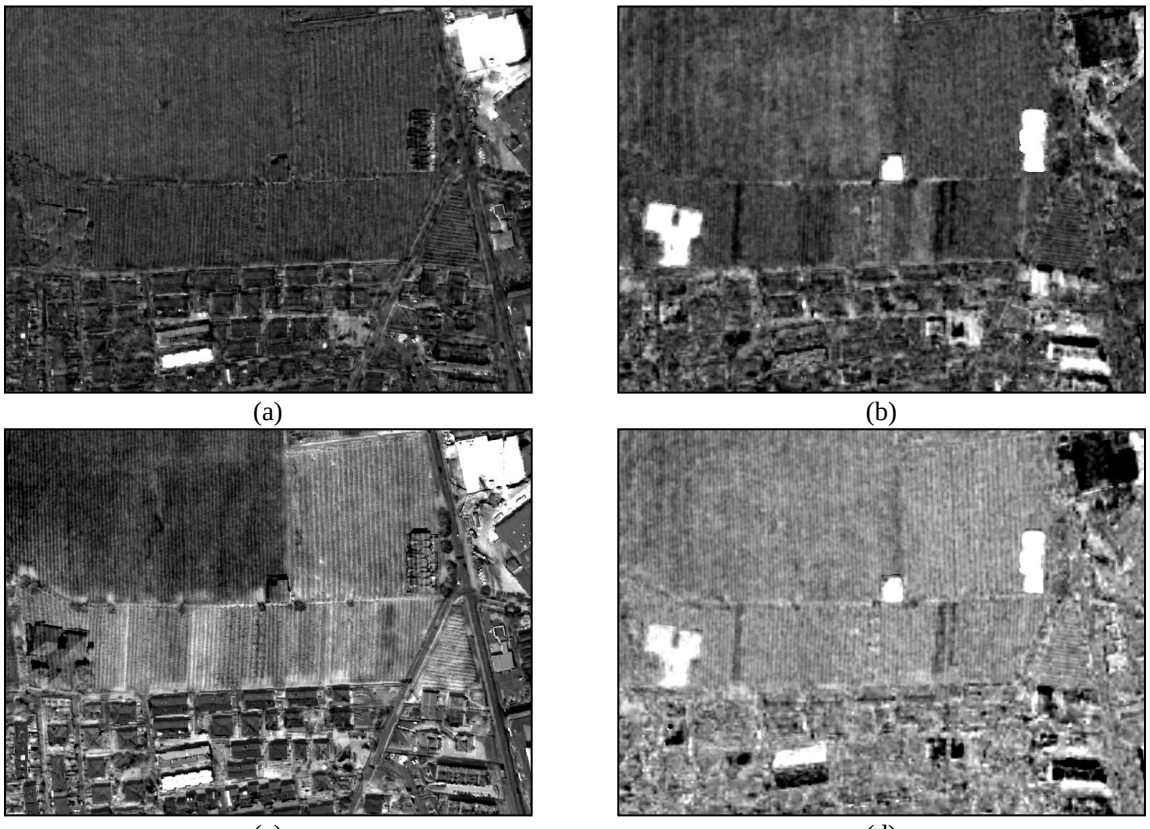

(a) (b) (c) (d)

Figure 7.2. Some of the component extracted by the considered algorithms applied to the eight original spectral channels of the two multitemporal Quickbird images. (a) 4^{th} component extracted through the ICA; (b) 3^{st} component extracted through the ICA; (c) 2^{th} component extracted through the PCA; (d) 6^{st} component extracted through the PCA.

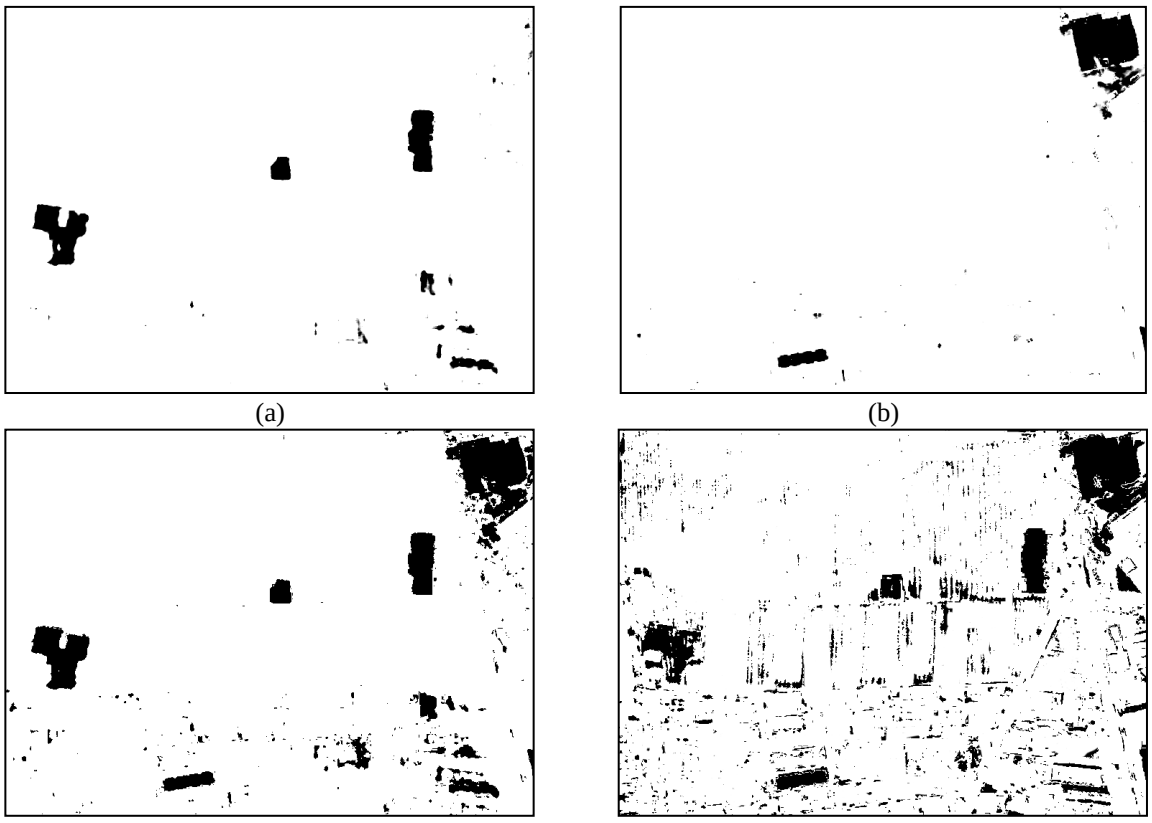

Figure 7.3. Change-detection maps obtained by the ICA components computed on the eight original spectral channels of the Quickbird images. (a) Thresholding of the 6th component; (b) Thresholding of the 1st component; and (c) thresholding of the magnitude of the SCVs obtained from the 1st and the 6th components. And (d) change-detection map obtained through the standard CVA on the original images.

The most significant results are reported in Table 7.1. In particular, the table contains the results (in terms of kappa accuracy) obtained by thresholding the 3th component for ICA and the 6th component for KICA, PCA and KPCA for extracting the change related to new houses (second column), and the 4th component (ICA, PCA and KPCA) and the5th (KICA) for identifying the change related to rebuilt roofs (third column). Furthermore, the accuracies obtained by thresholding the magnitude and direction of the SCVs obtained by both components for detecting both kinds of changes are reported (fourth column).

TABLE 7.1. CHANGE-DETECTION RESULTS OBTAINED BY THE PROPOSED APPROACHES IN TERMS OF KAPPA ACCURACY

Transformation method	ω_{c_1}	ω_{c_2}	ω_{c_1} and ω_{c_2}
ICA	0.774	0.788	0.747
KICA	0.771	0.795	0.808
PCA	0.658	0.549	0.733
KPCA	0.772	0.626	0.738
CVA standard	-	-	0.493

Comparing the numerical results yielded by ICA and KICA with the ones obtained with PCA and standard CVA, one can observe that ICA and KICA, independently from the change-detection strategy applied, involved change-detection maps with higher accuracies. This is mainly due to a consider-

able reduction of false alarms. With respect to the PCA, the first two techniques show better capabilities in separating the sources associated with true changes from sources of noise. The KPCA achieves results slightly better than the ones obtained by PCA, but still lower than the results of both ICA and KICA. In addition the KPCA requires a subsampling of the original images. Concerning the standard CVA algorithm applied to the original spectral channels, one can observe that false alarms due to different kinds of noise (i.e. registration noise, radiometric variations) cannot be eliminated in the generation of the final change-detection map [see Figure 7.3(d)], even if the spectral channels are accurately selected. It is worth nothing that the proposed techniques based on image transformation followed by simple change-detection algorithms allow one to generate different change-detection maps for different kinds of change [see Figure 7.3(a) and (b)] according to the selected transformed components.

7.5. Conclusion

In this chapter different data transformation techniques (PCA, KPCA, ICA and KICA) have been exploited for change-detection purposes. The capability of each technique to separate the information sources associated with true changes (and to differentiate among different changes) from those associated with noise was investigated. Results obtained on different remote sensing images confirmed the effectiveness of the ICA and the KICA techniques in separating the different sources in the change-detection process. In particular, it is possible to conclude that the ICA resulted in the best tradeoff between complexity and change-detection accuracy, while the PCA obtained the poorest change detection results. Kernel PCA resulted to perform better than the standard PCA approach, however its performances were still lower than the ones of ICA and KICA. In addition, the computational burden required by this approach was too high with respect to the other proposed transformation strategies. Finally, Kernel ICA achieved results only slightly better that the ICA, but the computational complexity required from this approach is very high compared to the one required by ICA.

As future developments of this work we aim at studying the capabilities of other image transformation techniques, like the one based on Multivariate Alteration Detection (MAD) and the advanced version of it Iterative Reweighted MAD (IRMAD) proposed in[108]. In addition the performances obtained by all the methods on different data sets should be evaluated.

Chapter 8

8. Analysis of the effects of pansharpening in change detection on VHR images[14]

In this chapter we investigate the effects of pansharpening (PS) applied to multispectral (MS) multitemporal images in change-detection (CD) applications. Although CD maps computed from pansharpened data show an enhanced spatial resolution, they can suffer from errors due to artefacts induced by the fusion process. The rationale of our analysis consists in understanding to which extent such artefacts can affect spatially enhanced CD maps. To this end a quantitative analysis is performed which is based on a novel strategy that exploits similarity measures to rank PS methods according to their impact on CD performance. Many multiresolution fusion algorithms are considered and CD results obtained from original MS and from spatially enhanced data are compared.

8.1. Introduction

The ever increasing availability of multitemporal very high geometrical resolution (VHR) remote sensing images results in new potentially relevant applications related to environmental monitoring and land cover management. Most of these applications are associated with the analysis of dynamic phenomena that result in changes on the Earth surface. The effects of these phenomena can be detected developing CD techniques capable to automatically identify changes occurred between two VHR images acquired at different times on the same geographical area. The last generation of VHR multispectral sensors (e.g., the ones mounted on board of Quickbird, Ikonos, World View-2 satellites) can acquire a panchromatic (PAN) image characterized by very high geometrical resolution (0.7m, 1m, 2.5m, respectively) and low spectral resolution (no spectral diversity and low capacity in distinguishing different kind of changes); and a set of MS images with lower spatial resolution (i.e., 2.8m, 4m, 10m), and higher spectral resolution. In order to take advantage of both high geometrical and spectral resolutions in CD, it is common practice to apply a proper pre-processing, namely pansharpening. PS merges the properties of PAN and MS data for spatial detail injection from PAN to MS, resulting in a set of images with both high spectral resolution and enhanced geometrical resolution.

[14] This chapter is published on *IEEE Geoscience and Remote Sensing letters*, Vol. 7, no. 1, 2010, pp. 53-57. Title: "Analysis of the Effects of Pansharpening in Change Detection on VHR Images". Authors: F. Bovolo, L. Bruzzone, L. Capobianco, A. Garzelli, S. Marchesi and F. Nencini.

However, PS can introduce in the images spatial artifacts and spectral distortions that can affect the accuracy of CD maps. Although several quality indexes have been proposed for evaluating PS methods [10], [138], they are not specifically conceived for CD applications. Only in [139] an analysis that quantifies the impact of PS artifacts on CD in a supervised way is presented.

The aim of this chapter is to analyze the impact of PS on the accuracy of CD investigating whether the improvement in geometrical resolution of CD maps given by PS is significantly affected or not by artifacts introduced by the PS process in an unsupervised way.

To this end five different multiresolution approaches are considered [131], [140], [141], [142] and [143]. A ranking of PS techniques from the most to the less effective for CD is obtained by defining a novel unsupervised objective strategy based on similarity measures for comparing CD maps. In order to avoid the introduction of any bias in the analysis and to better understand the impact of PS on CD, the CD step is performed according to the standard change vector analysis (CVA) technique [11], [15], [17].

The chapter is organized into six sections. Sections 8.2 and 8.3 describe the adopted PS and CD techniques, respectively. The unsupervised approaches based on similarity measures for ranking PS techniques are presented in section8.4. Section 8.5 illustrates the data set used for the experiments and reports experimental results. Finally, section 8.6 draws the conclusion of this work

8.2. Pansharpening techniques

Pansharpening techniques exploit the complementary spatial/spectral resolution properties of PAN and MS images for producing spatially-enhanced (or pansharpened) MS observations. Two main methodological approaches can be considered: i) methods based on spatial details injection from the PAN image into the MS image driven by local filtering operations (which are classified as multiresolution analysis (MRA) fusion methods), and ii) methods that perform fusion after applying a multispectral transformation to the original data without any filtering operation of the PAN image (component substitution (CS) algorithms).

In our analysis we considered five techniques for evaluating the impact of PS on CD, which well represent the two main mentioned categories: the first three can be classified as CS algorithms, whereas the last two are based on MRA.

- The Generalized Intensity Hue Saturation (GIHS) fusion method [140] computes a generalized intensity (GI) image by a weighted linear combination of the MS bands and subtracts it from the PAN image. Such difference image is added to each MS band. Its main critical point, due to GI generation, is that the fusion products may exhibit significant spectral distortions. However, it normally injects more spatial details from PAN to MS than the other four methods considered.
- The Gram-Schmidt (GS) spectral sharpening method [141] considers a simulated PAN image at a lower spatial resolution (obtained, for example, by averaging the original MS bands), and applies to it and to the lower spatial resolution spectral bands the Gram-Schmidt transformation, by adopting the simulated PAN image as the first band in the Gram-Schmidt transformation. The first transformed band is substituted by the higher spatial resolution PAN image after histogram matching. Finally, the inverse Gram-Schmidt transformation is applied to the new set of transformed bands to produce the enhanced spatial resolution MS images.
- The Minimum Mean Square Error (MMSE) pansharpening method [131] applies an optimal Generalized Intensity-Hue-Saturation transformation to the MS bands. The weights of the linear combination which provides the generalized intensity image and the gains that regulate the spatial detail injection are calculated in a minimum mean squared error sense.

- The Context-Based Decision (CBD) method [142] performs selection of spatial details from PAN by thresholding the local correlation coefficient evaluated between the approximation coefficients of PAN and MS obtained from multiresolution analysis (Laplacian pyramid or undecimated wavelet transform). Space-varying sensors equalization by ratio of local root mean squared values of MS and PAN is also applied.
- The Proportional Additive Wavelet to the L component (AWLP) pansharpening method [143] combines a PAN image and an MS image by adding the detail planes of the PAN image to the intensity component of the MS image.

8.3. Adopted change-detection technique

In order to perform the change detection, we considered the Change Vector Analysis (CVA) technique, which is a simple and widely-used unsupervised CD method. CVA has demonstrated its effectiveness in detecting and characterizing different radiometric changes in multitemporal and multispectral images in several application domains[17].The simplicity of CVA allows us to properly evaluate the effects of pansharpening without any significant bias related to the change-detection technique[15]. CVA is usually applied to multispectral images acquired by passive sensors and involves multidimensional spectral vectors in order to exploit all the available information on the investigated change.

This method has been presented in section 2.4, however in order to make the reading easier, we recall in the following the main concepts of this technique.

Let us consider two radiometrically corrected and co-registered pansharpened images, $\mathbf{X_1}$ and $\mathbf{X_2}$ of size $I \times J$, acquired over the same geographical area at different times, t_1 and t_2. Let $\Omega=\{\omega_n, \Omega_c\}$ be the set of classes of no-changed and changed pixels to be identified. In greater detail, ω_n represents the class of no-changed pixels and $\Omega_c=\{\omega_{c1}, \omega_{c2}, \ldots, \omega_{cK}\}$ is a meta-class that gathers all the K possible classes (kinds) of change occurred in the considered area.

Let B be the number of spectral channels of $\mathbf{X_1}$ and $\mathbf{X_2}$. The CVA technique emphasizes change information computing a MS difference image $\mathbf{X}_D$ by subtracting spectral feature vectors in corresponding spatial position of $\mathbf{X_1}$ and $\mathbf{X_2}$. Let $\mathrm{X}_{b,D}$ be the image representing the bth (b=1,…,B) component of $\mathbf{X}_D$. The B-dimensional problem described by $\mathbf{X}_D$ is reduced to a 1-dimensional problem through the magnitude variable, computed as [see also (2.2)]:

$$\rho = \sqrt{\sum_{b=1}^{B} \mathrm{X}_{n,\mathrm{D}}^2} = \sqrt{\sum_{b=1}^{B} \left(\mathrm{X}_{b,2} - \mathrm{X}_{b,1}\right)^2} \tag{8.1}$$

According to this expression, no-changed pixels present small magnitude values, whereas changed pixels show large values [11], [15]. Let $x_\rho(i,j)$ be a generic pixel in spatial position (i,j) in the magnitude image. The CD map Y where changed and no-changed pixels are separated can be computed according to the following decision rule:

$$y(i,j) = \begin{cases} \Omega_c & \text{if } x_\rho(i,j) \geq T \\ \omega_n & \text{if } x_\rho(i,j) < T \end{cases} \tag{8.2}$$

where $y(i,j)$ is the label associated to the pixel at spatial position (i,j) in Y, and T is the decision threshold. T can be defined either manually or automatically [15].

[15] More complex techniques would implicitly reduce the impact of pansharpening artifacts on change-detection maps.}

8.4. Unsupervised Strategy for the Evaluation of the Impact of Pansharpening on Change Detection

As no prior information about the investigated scene is generally available, we propose an unsupervised strategy based on a similarity measure for evaluating the impact of pansharpening techniques on the change detection. In order to properly understand the impact of different pansharpening techniques on change detection, we perform the analysis at different resolution levels: i) the one of the panchromatic image (*e.g.*, 0.7m for Quickbird images); and ii) the one of the multispectral image (*e.g.*, 2.8m for Quickbird images). In the first case the original MS images are fused with the PAN one, while in the latter the original panchromatic and multispectral images are spatially degraded down to a lower resolution before applying pansharpening. This option allows one a comparison between fused products at the resolution of the multispectral images with the original multispectral set.

Let us consider a set of multitemporal pansharpened pairs obtained applying different pansharpening techniques to two multitemporal images acquired over the same geographical area at different times. Pansharpened multitemporal images obtained with the same pansharpening approach are mostly affected by similar PS artifacts, nevertheless differences in artifacts can occur where multitemporal data show radiometric and geometric differences rising from both different acquisition conditions and the presence of changes on the ground. CD performed according to CVA (but also to more advanced techniques) can only partially compensate for such kind of artifacts. Moreover, images obtained with different pansharpening approaches are affected by different artifacts peculiar of the applied pansharpening technique.

As the quality of pansharpened images diminishes (artifacts increases), the change-detection maps quality decreases together with the capability of the adopted CD technique in compensating artifacts effects. If artifacts induced by different pansharpening techniques are independent, low quality change-detection maps obtained from different pansharpened pairs tend to be significantly different to each other and vice versa. According to this observation we propose to use a similarity measure computed among CD maps in order to identify PS techniques that less affect change detection. Such a measure results unbiased and reliable if the effects of artifacts in the CD maps are uncorrelated. It is worth noting that this is true when considering a comprehensive set of pansharpening methods including high-performance (MMSE, CBD, AWLP), and state-of-the-art (GS, GIHS) fusion algorithms which are based on different spatial injection strategies.

The proposed strategy considers N change-detection maps obtained by the CVA on N different pansharpened multitemporal pairs. Let us represent Ω_c and ω_n assigned according to (8.2) with $+1$ and -1, respectively. For each pair of CD maps Y_a and Y_b, with $a,b = 1,...,N$ and $a \neq b$ we compute a measure of similarity H_{ab} of the CD maps on the $I \times J$ pixels of the images as:

$$H_{ab} = \frac{1}{IJ} \sum_{i=1}^{I} \sum_{j=1}^{J} y_a(i,j) \cdot y_b(i,j) \tag{8.3}$$

where $y_a(i,j)$ and $y_b(i,j)$ are the labels of the pixel in position (i,j) in the CD maps Y_a and Y_b, respectively. As $y_a(i,j)$ and $y_b(i,j)$ can assume values in {-1,+1}, their product is equal to 1 if $y_a(i,j) = y_b(i,j)$ and to -1 otherwise. Accordingly, the value of the similarity measure H_{ab} is equal to 1 if Y_a and Y_b are identical, and is lower than 1 otherwise. In general, H_{ab} belongs to the interval [-1,+1]. On the basis of this measure, two different strategies can be implemented: i) comparison of the similarities among CD maps obtained with different PS techniques; ii) comparison of the similarities of change-detection maps with a reference map.

i. *Comparison of the similarities among change-detection maps*: an absolute measure of similarity of each map Y_a to all the others can be defined by computing the average value of H_{ab}, i.e.,

$$H_a = \frac{1}{N-1} \sum_{a=1, b \neq a}^{N} H_a \tag{8.4}$$

According to the value of H_a, the N considered PS techniques can be ranked from the less affecting CD (high average similarity) to the most affecting it (low average similarity). This strategy can be applied either to full-scale pansharpened images as well as to reduced-resolution pansharpened images.

ii. *Comparison of the similarities of CD maps with a reference map*: instead of considering relative reference change-detection maps, an absolute reference Y_{ref} can be defined. Two procedures can be considered for defining Y_{ref}. The first one is based on a supervised method. Thus Y_{ref} can be a map built according to available prior information about changes occurred on the ground, or, in the case of the spatially degraded data set, it can be the CD map computed applying the CVA to the original multitemporal MS images (MSmap) which represents an upperbound of CD performance at this resolution as computed from artifacts-free multitemporal data. The second procedure computes Y_{ref} by applying a majority voting rule to the set of N CD maps Y_a ($a=1,...,N$) as:

$$y_{ref}(i,j) = \begin{cases} \Omega_c & \text{if } \sum_{a=1}^{N} y_a(i,j) > 0 \\ \omega_n & \text{if } \sum_{a=1}^{N} y_a(i,j) \leq 0 \end{cases} \tag{8.5}$$

In this case the similarity can be computed by applying (8.3) with $Y_a = Y_{ref}$. The rationale of this procedure is to assume that the CD map obtained according to majority voting (MVmap) represents a reliable CD result where the main artifacts are filtered out. This assumption holds when considering PS methods that result in uncorrelated artifacts.

It is worth noting that the statistical significance of the proposed measures increases with the number and the diversity of the considered PS methods.

8.5. Experimental results

A multitemporal data set made up of two multispectral and panchromatic Quickbird images acquired on the Trento city (Italy) in October 2005 and July 2006 was considered to evaluate the impact of the different investigated multiresolution fusion techniques on the CD process. In the preprocessing phase images were: i) radiometrically corrected; and ii) co-registered by means of 12 ground control points. Final multispectral images are made up of 380x376 pixels while panchromatic images consist of 1520 x 1504 pixels. Between the acquisition dates some changes related to urban and rural areas occurred on the ground (white circles in Figure 8.1).

In the first experiment we expanded original images according to a simple interpolation by a factor four. As expected, the obtained multitemporal images show a low geometrical details content (see EXP column, Figure 8.2). The corresponding CD map (see Figure 8.2) is unreliable and geometrical details are mostly blurred or lost. According to this observation expanded multitemporal pairs were not further considered.

In the second experiment we applied the five pansharpening methods (N=5) described in section 8.2 to the considered data set and to a degraded version of it in order to obtain two sets of 5 pairs of spatially enhanced multitemporal and multispectral images: i) one at the geometrical resolution of the PAN image (0.7 m), and ii) one at the geometrical resolution of the MS image (2.8 m). Please note that the latter one has been obtained by applying PS to original data spatially degraded by four according to the protocol proposed in [138].

(a) (b)

Figure 8.1. True-color composition of the pansharpened images of the Trento city (Italy) acquired by the Quickbird VHR multispectral sensor in (a) October 2005 and (b) July 2006 (occurred changes appear in white circles).

In order to estimate which pansharpened pair resulted in the CD map with the best trade-off between geometrical details content and differences induced by panshrpening artifacts, we exploited the proposed unsupervised strategy. First we applied the CVA technique to multitemporal pairs of fused images at both resolutions and to the original multispectral images. The eleven magnitude images were thresholded according to (8.2). For the considered data set we found that T=500 was a reasonable value. This value was used for each magnitude image because small spectral differences due to the adopted PS technique do not significantly alter the statistics of the classes of interest. Fixing the value of T avoids possible bias due to the use of automatic thresholding techniques. The value of T, in fact, strictly depends on the considered CD problem and different automatic thresholding techniques can be adopted[15],[17].

In Table 8.1 the similarity measures (8.3) obtained using as reference both the MVmap computed according to (8.5), and the average similarity measure in (8.4) are reported for all pansharpened pairs at both resolutions. For the 2.8m resolution data the similarity measure obtained using as reference the change-detection map computed on the original MS data (MSmap) is also reported (see first column of Table 8.1). If we evaluate the similarity between MVmap and MSmap we retrieve a value equal to 0.965. This value is higher than all the similarities computed by considering the CD maps produced from the different PS pairs, thus confirming the effectiveness of MVmap as reference.

Although CD results are scale dependent, from Table 8.1 one can see that the impact of pansharpening is very similar for the two scales. In particular, the MMSE fusion pansharpening method always attained the best global score, followed by AWLP, whereas GIHS, GS and CBD provided, on average, poorer results. In few cases, PS methods can perform differently at different resolutions, *e.g.*, CBD which provides better results at 2.8m (3rd in ranking) than at 0.7m (5th in ranking). An opposite situation occurs for GIHS: 2nd in ranking at 0.7m, and 4th at 2.8m. Table 8.2 confirms this ranking at 2.8m spatial resolution. Results summarized in Table 8.1 and comments above are confirmed by the qualitative analysis of the change-detection maps at 0.7m resolution (Figure 8.2, 3rd row). As one can observe, the CD map obtained with MMSE pansharpened images shows a better visual quality. In particular, border regions and geometrical details are better modeled. This map, but also the other ones, shows a higher quality than the one obtained from MS images simply interpolated by a factor of four (see EXP column, Figure 8.2), thus confirming that PS improves CD performance.

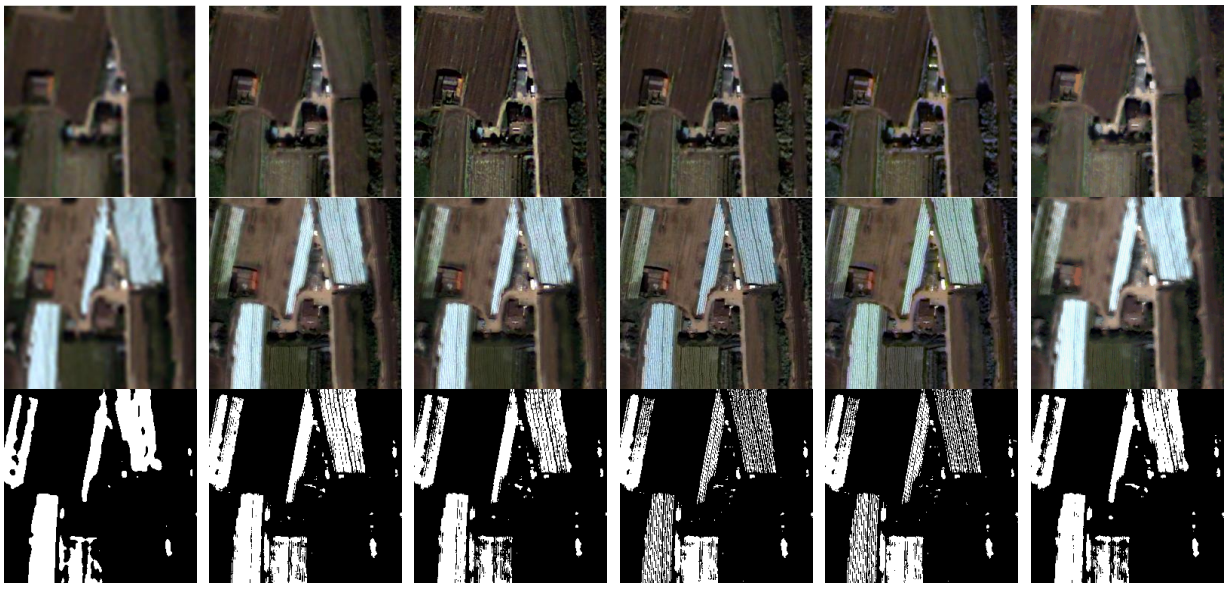

EXP MMSE AWLP GS GIHS CBD

Figure 8.2. True-color composite of 256x256 details of 0.7m Quickbird data acquired on October 2005 (first row) and July 2006 (second row) for the upscaled and five pansharpened images. CD maps obtained for the upscaled and the five pansharpened multitemporal pairs at 0.7 m of resolution (third row).

TABLE 8.1. ESTIMATED SIMILARITY MEASURES WITH RESPECT TO THE MSMAP AT 2.8 m AND TO THE MVMAP AT 2.8 AND 0.7 m; AVERAGE SIMILARITY MEASURE H_a AT 2.8 AND 0.7 m. HIGHEST SCORES APPEAR IN BOLD TYPE.

	Geometrical Resolution 2.8m			**Geometrical Resolution 0.7m**	
PS method	Y_{ref} = MSmap	Y_{ref} = MVmap	H_a	Y_{ref} = MVmap	H_a
MMSE	**0.963**	**0.996**	**0.979**	**0.995**	**0.978**
AWLP	0.961	0.986	0.976	0.982	0.973
GIHS	0.961	0.980	0.975	0.982	0.974
GS	0.960	0.980	0.976	0.981	0.973
CBD	0.960	0.983	0.974	0.979	0.971

In order to better understand the CD results, we compared them with the quality of multitemporal panshaperned images measured according to quality indexes such as ERGAS (relative dimensionless global error in synthesis), Q4, and Spectral Angle Mapper (SAM). ERGAS [144] is given by:

$$\text{ERGAS} = 100 \frac{d_h}{d_l} \sqrt{\frac{1}{B} \sum_{i=0}^{B-1} \left(\frac{\text{RMSE}(i)}{\mu(i)} \right)^2} \tag{8.6}$$

where $\frac{d_h}{d_l}$ is the ratio between the pixel sizes of the PAN and MS images (e.g., $\frac{1}{4}$ for Quickbird and Ikonos data), and $\mu(i)$ is the mean of the i-th band. ERGAS measures a distortion and thus must be as small as possible. Q4 is the unique image quality index based on quaternion theory for MS images having four spectral bands [10]. The highest value of Q4, attained if and only if the test MS image is equal to the reference, is one. SAM denotes the absolute value of the angle between two spectral vectors. SAM equal to zero denotes absence of spectral distortion, but possible radiometric distortion. SAM is averaged over the whole image to yield a global distortion index.

To evaluate all mentioned indexes reference original bands are required. Therefore pansharpening quality assessment was carried out only on data at the geometrical resolution of the multispectral image (i.e., numerical values are calculated considering fused and original data at 2.8m resolution).

TABLE 8.2. QUALITY INDEXES OF PANSHARPENED IMAGES AT 2.8 m; FIRST (SECOND) DATE ON THE LEFT (RIGHT). BEST SCORES APPEAR IN BOLD TYPE.

	ERGAS		Q4		SAM	
MMSE	3.65	**2.80**	0.840	**0.899**	3.85	**3.15**
CBD	**3.52**	2.85	**0.851**	0.896	**3.65**	3.24
AWLP	3.94	2.97	0.843	0.890	4.46	3.47
GS	4.31	3.75	0.773	0.800	4.19	4.04
GIHS	4.46	3.65	0.718	0.787	4.52	3.75

A qualitative analysis of Figure 8.2 points out that the MMSE and AWLP methods effectively preserve spectral properties. Fused images obtained by GS and GIHS clearly show over-enhancement in the vegetated regions, which affects CD. The MMSE method and, to a lesser extent, the AWLP algorithm, guarantee a more accurate texture injection, especially in the green wavelength. Quality index values reported in Table 8.2 are in accordance with these observations. Best spatially-averaged results at 2.8m are provided by the CBD and MMSE methods, followed by AWLP, whereas GIHS and GS show a significantly lower performance. It is worth noting that despite the CBD method is characterized by high quality indexes (high global quality of the fused image), it may locally introduce fusion artifacts, *i.e.* no spatial injection, due to statistical instabilities. When such local inaccuracies appear on image regions where changes occurred, CD performance degrades (see Table 8.1)

Comparing numerical values reported in Table 8.1 and Table 8.2, it appears that pansharpened image pairs characterized by better quality indexes not always result in CD maps with higher similarity measures, as in the case of CBD. Therefore the proposed quality index for CD maps obtained from spatially-enhanced images at 0.7m without any reference data becomes relevant. It is worth noting that the validity of the proposed measure is confirmed by the agreement between similarities computed at full and degraded resolution, where information about original bands can be exploited.

8.6. Conclusion

Although it has been proven that the pansharpened images result in higher quality change-detection maps with respect to images interpolated by a factor four, pansharpening artifacts can significantly impact on the change-detection process. In this chapter a quantitative and qualitative analysis of the effects of different pansharpening methods on change-detection is presented. The impact of PS on CD was analyzed both at degraded and full scale, according to a novel strategy based on similarity measures. At degraded scale, the available reference change-detection maps have been compared to the maps obtained from pairs of pansharpened spatially-degraded multispectral images. At full resolution, which is the most relevant in practical CD applications, spatially-enhanced images have been considered. The two analyses resulted in similar ranking of PS methods from the one that less affect change detection to the one that most affect it, confirming that the proposed technique can be effectively employed for adaptively selecting in an unsupervised way the most reliable pansharpening technique for different data sets and CD problems. Finally, it has been shown that pansharpened image pairs with higher quality indexes not necessarily result in more accurate CD maps, thus proving the usefulness of the proposed approach. Specifically, extreme care should be taken on the choice of the pansharpening algorithm for change detection with a particular attention to PS techniques based on local statistics estimation.

Chapter 9

9. Conclusions

This chapter draws the conclusion of the research activity described in the thesis; in particular, it summarizes and discusses the results obtained and presents an outlook of the possible future developments.

In this thesis we analysed and modelled the main properties of multitemporal VHR remote sensing images in order to derive effective pre-processing techniques and unsupervised change-detection methods. In particular, starting from a deep analysis on the properties of registration noise (RN) in multitemporal VHR images, we derived: (i) a technique for an adaptive estimation of the registration noise distribution; (ii) a technique for the registration of multitemporal images; (iii) a change-detection technique robust to registration noise; (iv) a change-detection strategy for the automatic detection and separation of different kinds of change; and (v) a study on the effects of both image transformation and pansharpening on the results of the change-detection process.

For each considered topic an analysis of the state of the art was conducted, and the limitations of literature techniques were highlighted. Starting from this analysis, novel solutions were theoretically developed, implemented and finally applied to both simulated and real remote sensing data in order to assess their effectiveness.

All these studies and techniques contributed to improve the state of the art on the analysis of multitemporal VHR images, facing and solving relevant problems related to VHR images. In the following a summary of the main conclusion that can be drawn for each of the considered topic is reported.

In chapter 3 the properties of registration noise have been analyzed in the context of a polar framework for CVA. Then, on the basis of the derived properties, a novel method for an adaptive estimation of the statistical distribution of such kind of noise in multitemporal VHR images has been proposed. In this study we have considered images acquired by different sensors and we have analyzed the effects of RN when: i) the misregistration between the two considered images increases and ii) the resolution of the original images decreases. From this analysis, four different properties have been derived, associated both to unchanged and changed pixels. These properties point out that misregistration may significantly affect the accuracy of change detection and show some important effects due to this specific kind of noise on VHR images. It is worth noting that on the basis of the con-

ducted analysis, we can conclude that the properties of RN in VHR multispectral images are significantly different from those on high or medium resolution images. The analysis of the properties of registration noise resulted also in the definition of an adaptive technique for the estimation of the RN distribution in the polar domain. The proposed technique estimates the conditional density of RN providing valuable information for the design of a change-detection procedure. In order to assess the reliability of the proposed estimation technique we have performed an analysis of the results obtained with the estimation method on a couple of test sites made up of two real multitemporal images acquired by the Quickbird sensor. These results confirm the effectiveness of the proposed technique in identifying and modeling RN also in presence of real multitemporal noisy images acquired under different conditions.

As mentioned before, starting from this work we have derived two important developments: 1) an adaptive registration strategy based on the estimated local behavior of the RN; and 2) an effective change-detection method robust to RN for VHR images.

Concerning the registration strategy, in chapter 4, we have proposed a novel method for the registration of VHR remote sensing images, which is especially effective for applications related to change detection. The proposed method automatically extracts control points (CPs) that are associated with areas in the images that result in the most critical effects of the misalignment in image comparison. These points are identified thanks to the estimation of RN distribution derived in chapter 3. CPs are used to derive a disparity map that is then exploited for the warping of one image on the other. The proposed method exhibits the following properties: (i) capability to automatically identify CPs associated with the most critical points of the images where misregistration has a high probability to results in false alarms; (ii) robustness to the presence of changes between the images. Results obtained on both simulated and real data confirm the validity of the proposed method in identifying effective CPs, in estimating the disparity map and in performing the final co-registration between the considered images.

Chapter 5 presents a context-sensitive multiscale technique robust to registration noise for change detection in VHR images. The technique takes advantages from the analysis of the distribution of RN performed in chapter 3. In details, the proposed method performs a quantization-based multiscale analysis of the Spectral Change Vectors (SCVs) computed according to the Polar Change Vector Analysis (CVA) in the magnitude-direction domain in order to identify SCVs associated with registration noise. The retrieved information on registration noise is then exploited in the framework of a parcel-based decision strategy that takes advantage of spatial-context information in defining the final change-detection map. This step is performed at full resolution in order to preserve all the high geometrical detail information characteristic of VHR images. The qualitative and quantitative analysis of the results obtained on two data sets made up of a small and a large pair of Quickbird images point out that the proposed technique involves a low amount of false alarms in change-detection maps and a high accuracy in modeling both geometrical details and homogeneous areas. In greater detail, the achieved results are significantly better than the ones yielded by standard change-detection techniques. It is worth noting that despite the proposed method has been developed for VHR remote sensing images (where the impact of misregistration is more relevant), it can be suitable also for the analysis of optical data at lower resolution and, under given conditions, also for other kinds of images.

Chapter 6 proposes an automatic technique for the detection of multiple changes in multitemporal images. The proposed method compresses the original multidimensional feature space to a 2D space and applies a 2-step decision strategy for detecting changes. The compression is accomplished by computing the magnitude of spectral change vectors, and the angle (direction) between the spectral

difference vector and a reference one. Then the change information is represented in a 2D domain, which is defined as Compressed Change Vector Analysis (C^2VA) domain. The proposed transformation leads to a 2D representation of the change-detection problem without the need of selecting a pair of spectral channels as usually done in standard approaches. This represents a valuable advantage as spectral channel selection would require some prior knowledge about possible changes occurred on the ground (which often is not available or incomplete). After representing the information in the C^2VA domain changes are extracted according to a 2-steps procedure: i) changed pixels are separated from no-changed ones according to a standard unsupervised method; and ii) the pixels labeled as being changed are analyzed in order to separate contributions from different kinds of change. Qualitative and quantitative results obtained on both Landsat-5 and Quickbird images confirmed the effectiveness of the proposed automatic technique for the detection of multiple changes when applied to both C^2VA and standard CVA. In C^2VA, although the information is projected from a multidimensional into a 2D space, it is possible to retrieve the main information related to changes and to distinguish all different kinds of change occurred on the ground. On the contrary, standard representations based on the use of couple of spectral channels often imply loss of information.

Finally in chapters 7 and 8 we have analyzed the effects of some pre-processing techniques on the results of the change-detection process. Chapter 7 presents an analysis of the capability of different data transformation techniques (i.e. ICA, PCA and their kernelized version KICA and KPCA, respectively) to separate the information sources associated with different true changes from those associated with noise. To this purpose, we have applied the different data transformation techniques to the original multitemporal images and have analyzed the transformed component for extracting changes. To this end, we have applied standard change-detection methods (i.e. standard CVA and polar CVA) to the extracted components. Results obtained on different remote sensing images (both VHR and medium resolution images) confirmed the effectiveness of these techniques in separating the different sources in the change-detection process. In particular, it has been possible to conclude that the ICA resulted in the best tradeoff between complexity and change-detection accuracy, while the PCA obtained the poorest change-detection results. The kernelized version (KICA and KPCA) achieved results only slightly better than the ones of their standard version, but the computational complexity required from them is very high compared with the ones required by ICA and PCA.

In chapter 8, a quantitative and qualitative analysis of the effects of different pansharpening (PS) methods on the results of change detection is presented. Although it has been proven that the pansharpened images result in higher quality change-detection maps with respect to images interpolated by a factor of four and although it is necessary to work on PS image in order to obtain change-detection results with higher level of geometrical resolution, the artifacts coming from pansharpening can significantly impact on the change-detection process. For this reason it is important to study the impact of different PS methods to the results of the CD process. The impact of pansharpening on change detection has been analyzed both at degraded and full scale, according to a novel strategy based on similarity measures. At degraded scale, the available reference CD maps have been compared to the maps obtained from pairs of pansharpened spatially-degraded multispectral images. At full resolution, spatially-enhanced images have been considered. The two analyses resulted in similar ranking of PS methods from the one that less affect CD to the one that most affect it, confirming that the proposed strategy based on similarity measures can be effectively employed for adaptively selecting in an unsupervised way the most reliable pansharpening technique for different data sets and change-detection problems. Finally, it has been shown that pansharpened image pairs with higher quality indexes not necessarily result in more accurate CD maps, thus proving the usefulness of the proposed strategy.

As future developments of the research work presented in this dissertation, it would be interesting to: (i) explore other advanced solutions to the registration problem: considering the proposed strategy for the automatic extraction of control points, advanced algorithms for searching the displacement vector (i.e. optimization of the research through genetic algorithms) and for transforming the images should be investigated; (ii) exploit the potentialities of the proposed technique for the identification and separation of different kinds of change in the context of more complex approaches to change detection like those that exploit multiscale/multiresolution information intrinsically present in VHR images and the ones robust to registration noise; (iii) consider techniques being able to extract semantic information associated with changes in order to face the problems of shadows, of seasonal variation of the vegetation phenology, etc (i.e. changes that usually show significant intensity in the magnitude domain, even if, from a semantic point of view, the related area is not changed).

Bibliography

[1] X. Jia J.A. Richards, *Remote Sensing digital image analysis*, 4th ed., Springer-Verlag, Ed. New York, USA, 2004.

[2] Satellite Imaging Corporation Website. [Online]. http://www.satimagingcorp.com/satellite-sensors.html

[3] EROS satellite (Wikipedia Website). [Online]. http://en.wikipedia.org/wiki/EROS_%28satellite%29

[4] GeoEye Website. [Online]. http://www.geoeye.com/

[5] RapidEye Website. [Online]. http://www.rapideye.de/

[6] CNES Website. [Online]. http://smsc.cnes.fr/PLEIADES/

[7] "Proceedings of Multitemp 2009," in *IEEE Fifth International Workshop on the Analysis of Multi-temporal Remote Sensing Images*, Groton, Connecticut, 28-30 July 2009.

[8] X. Dai, S. Khorram, "The effects of image misregistration on the accuracy of remotely sensed change detection," *IEEE Transaction on Geoscience and Remote Sensing*, vol. 36, no. 5, pp. 1566-1577, September 1998.

[9] L. Bruzzone, S. B. Serpico, "An iterative technique for the detection of land-cover transitions in multitemporal remote-sensing images," *IEEE Transaction on Geoscience and Remote Sensing*, vol. 35, no. 4, pp. 858-867, July 1997.

[10] L. Alparone, S. Baronti, A. Garzelli, F. Nencini, "A global quality measurement of pan-sharpened multispectral imagery," *IEEE Geoscience and Remote Sensing Letter*, vol. 1, no. 4, pp. 313-317, October 2004.

[11] F. Bovolo, L. Bruzzone, "A theoretical framework for unsupervised change detection based on change vector analysis in polar domain," *IEEE Transaction on Geoscience and Remote Sensing*, vol. 45, no. 1, pp. 218-236, January 2007.

[12] B. Zitrova, J. Flusser, "Image registration methods: a survey," *Image and Vision Computing*, vol. 21, no. 11, pp. 977-1000, October 2003.

[13] F. Bovolo, "A multilevel parcel-based approach to change detection in very high resolution multitemporal images," *IEEE Geoscience and Remote Sensing Letters*, vol. 6, no. 1, pp. 33-37, January 2009.

[14] H. Wank, E. C. Ellis, "Image misregistration error in change measurements," *Photogrammetric Enginnering and Remote Sensing*, vol. 71, no. 8, pp. 1037-1044, September 2005.

[15] L. Bruzzone, D. F. Prieto, "Automatic analysis of the difference image for unsupervised change detection," *IEEE Transaction on Geoscience and Remote Sensing*, vol. 38, no. 3, pp. 1171-1182, May 2000.

[16] M. J. Canty, *Image analysis, classification, and change detection in remote sensing: with algorithms for ENVI/IDL*, 2nd ed., CRC Press, Ed., 2009.

[17] R.J. Radke, S. Andra, O. Al-Kofahi, B. Roysam, "Image change detection algorithms: a systematic survey," *IEEE Transaction on Image Processing*, vol. 14, no. 3, pp. 294-307, February 2005.

[18] P. R. Coppin, I. Jonckheere, K. Nachaerts, "Digital Change Detection Techniques," *International Journal of Remote Sensing*, vol. 25, no. 9, pp. 1565-1596, 2004.

[19] M. J. Duggin, C. J. Robinove, "Assumptions implicit in remote sensing data acquisition and analysis," *International Journal of Remote Sensing*, vol. 11, no. 10, pp. 1669-1694, October 1990.

[20] D. L. Civico, "Topographic normalization of Landsat Thematic Mapper digital imagery," *Photogrammetric Engineering and Remote Sensing*, vol. 55, no. 9, pp. 1303-1309, 1989.

[21] A. Singh, "Digital change detection techniques using remotely-sensed data," *International Journal of Remote Sensing*, vol. 10, no. 6, pp. 989-1003, 1989.

[22] J. R. C. Townshend, C. O. Justice, "Spatial variability of images and the monitoring of changes in the normalized difference vegetation index," *International Journal of Remote Sensing*, vol. 16, no. 12, pp. 2187-2195, 1995.

[23] T. Fung, "An assessment of TM imagery for land-cover change detection," *IEEE Transaction on Goescience and Remote Sensing*, vol. 28, no. 4, pp. 681-684, July 1990.

[24] J. Li, S. Qian, X. Chen, "Object-oriented method of land cover change detection approach using high spatial resolution remote sensing data," in *IEEE Geoscience and Remote Sensing Symposium*, vol. 5, Toulouse, 2003, pp. 3005-3007 vol. 5.

[25] G. G. Hazel, "Object-level change detection in spectral imagery," *IEEE Transaction on Geoscience and Remote Sensing*, vol. 39, no. 3, pp. 553-561, March 2001.

[26] M. J. Carlotto, "A cluster-based approach for detecting man-made objects and changes in imagery," *IEEE Tranaction on Geoscience and Remote Sensing*, vol. 43, no. 2, pp. 374-387, February 2005.

[27] I. Niemeyer, P. R. Marpu, S. Nussbaum, "Change detection using the object features," in *IEEE International Geoscience and Remote Sensing Symposium*, Barcelona, 2007, pp. 2374-2377.

[28] L. Cannavacciuolo, W. Emery, G. Moser, S.B. Serpico, "A contextual change detection method for high-resolution optical images of urban areas," in *Urban Remote Sensing Joint Event*, Paris, 2007, pp. 1-7.

[29] M. Molinier, J. Laaksonen, "Detecting man-made structures and changes in satellite imagery with a content-based information retrieval system built on self-organizing maps," *IEEE Transaction on Geoscience and Remote Sensing*, vol. 45, no. 4, pp. 861-874, April 2007.

[30] F. Pacifici, F. Del Frate, C. Solimini, W.J. Eremy, "An innovative neural-net method to detect temporal changes in high-resolution optical satellite imagery," *IEEE Transaction on Geoscience and Remote Sensing*, vol. 45, no. 9, pp. 2940-2952, September 2007.

[31] O. Debeir, E. Wolff A. Carleer, "Comparison of very high spatial resolution satellite image segmentation," in *SPIE Image and Signal Processing for Remote Sensing*, 2004, pp. 532-542.

[32] R.M. Harlick, L.S. Shapiro, "Image Segmentation Techniques," *Computer Vision, Graphics and Image Processing*, vol. 29, no. 1, pp. 100-132, 1985.

[33] A. Annoni P. Smits, "Updating land-cover maps by using texture information for very high-resolution space-born imagery," *IEEE Transaction on Geoscience and Remote Sensing*, vol. 37, no. 3, pp. 1244-1254, 1999.

[34] W. Wang, Z. Zhao, H. Zhu, "Object-oriented change detection method based on multi-scale and multi-feature fusion," in *Urban Remote Sensing Joint Event*, Shangai, 2009, pp. 1-5.

[35] T. Celik, K. K. Ma, "Unsupervised change detection for satellite images using dual-tree complex wavelet transform," *IEEE Transaction on Geoscience and Remote Sensing*, vol. 48, no. 3, pp. 1199-1210, March 2010.

[36] Y. Bazi, F. Melgani, H. D. Al-Sharari, "Unsupervised change detection in multispectral remotely sensed imagery with level set methods," *IEEE Transaction on Geoscience and Remote Sensing*, vol. 48, no. 8, pp. 3178-3787, August 2010.

[37] J. A. Benediktsson, F. Bovolo, L. Bruzzone M. Dalla Mura, "An unsupervised technique based on morphological filters for change detection in very high resolution images ," *IEEE Geoscience and Remote Sensing Letters*, vol. 5, no. 3, pp. 433-437, 2008.

[38] A. A. Nielsen, M. J. Canty, "Kernel principal component analysis for change detection," in *SPIE Europe Remote Sensing Conference*, Cardiff, 2008, pp. 71090T.1-71090T.10.

[39] F. Del Frate F. Pacifici, "Automatic change detection in very high resolution images with pulse-coupled neural networks," *IEEE Geoscience and Remote Sensing Letters*, vol. 7, no. 1, pp. 58-62, January 2010.

[40] L. Brown, "A survey of image registration techniques," *ACM Computing Surveys*, vol. 24, no. 4, pp. 325-376, December 1992.

[41] G. Hong, Y. Zhang, "The image registration technique for high resolution remote sensing image

in hilly area," in *International Society of Photogrammetry and Remote Sensing Symposium*, Tempe, 2005.

[42] M. Manfredi, M. Aldrighi, F. Dell'Acqua, "Eigenmethod for feature matching of pre- and postevent images exploiting adjacency," *IEEE Transaction on Geoscience and Remote Sensing*, vol. 48, no. 7, pp. 2890-2898, July 2010.

[43] X. Guo, W. Zhang, G. Ma, "Automatic urban remote sensing images registration based on road networks," in *Urban Remote Sensing Joint Event*, Shangai, 2009, pp. 1-6.

[44] Y. Li, C. H. Davis, "Pixel-based invariant feature extraction and its application to radiometric co-registration for multi-temporal high-resolution satellite imagery," *IEEE Journal of Selected Topics in Applied Earth Observation and Remote Sensing*, p. accepted, 2010.

[45] N. Taleb, K. Kpalma, J. Ronsin Y. Bentoutou, "An automatic image registration for applications in remote sensing," *IEEE Transaction on Geoscience and Remote Sensing*, vol. 43, no. 9, pp. 2127-2137, September 2005.

[46] V. Arevalo, J. Gonzalez, "Improving piecewise linear registration of high-resolution satellite images through mesh optimization," *IEEE Transaction on Geoscience and Remote Sensing*, vol. 46, no. 11, pp. 3792-3802, November 2008.

[47] G. Danchao, T. Xiaotao, L. Shizhong, H. Guojun, "Image registration of high resolution remote sensing based on straight line feature," in *International Society for Photogrammetric and Remote Sensing Symposium*, Beijing, 2008, pp. 1819-1823.

[48] Y. Zhao, S. Liu, P. Du, M. Li, "Feature-based geometric registration of high spatial resolution satellite imagery," in *Urban Remote Sensing Joint Event*, Shangai, 2009, pp. 1-5.

[49] J. Inglada, J. Michel, T. Feuvrier, "A generic framework for disparity map estimation between multi-sensor remote sensing images," in *IEEE Geoscience and Remote Sensing Symposium*, Boston, 2008, pp. III.435-III.438.

[50] M. di Bisceglie, C. Galdi, G. Giangregorio, S. L. Ullo M. Ceccarelli, "Image registration using non-linear diffusion," in *IEEE Geoscience and Remote Sensing Symposium*, Boston, 2008, pp. V.220-V.223.

[51] A. Borzì, M. di Bisceglie, C. Galdi, G. Giangregorio, "Robust registration of satellite images with local distortion," in *IEEE Geoscience and Remote Sensing Symposium*, Capetown, 2009, pp. III.251-III.254.

[52] J. Orchard, R. Mann, "Registering a multisensor ensemble of images," *IEEE Transaction on Image Processing*, vol. 19, no. 5, pp. 1236-1247, May 2010.

[53] W. Wang, Y. Liu, B. Zheng, J. Lu, "A method of shape based multi-sensor image registration," in *Urban Remote Sensing Joint Event*, Shangai, 2009, pp. 1-5.

[54] J. Inglada, A. Giros, "On the possibility of automatic multisensor image registration," *IEEE Transaction on Geoscience and Remote Sensing*, vol. 42, no. 10, pp. 2104-2120, October 2004.

[55] D. Zhang, L. Yu, Z. Cai, "A matching-based automatic registration for remotely sensed imagery," in *IEEE Geoscience and Remote Sensing Symposium*, Denver, 2006, pp. 956-959.

[56] J. Tao, N. Xiliang, F. Lei, L. Guolin, J. Min, S. Lin, "Registration study of great resolution difference remote sensing images based on invariant feature," in *IEEE Geoscience and Remote Sensing Symposium*, Honolulu, 2010, p. accepted.

[57] S. R. Lee, "A coarse-to-fine approach for remote-sensing image registration based on a local method," *International Journal on Smart Sensing and Intelligent Systems*, vol. 3, no. 4, pp. 690-702, December 2010.

[58] E. S. Kasischke R. D. Johnson, "Change vector analysis: a technique for the multispectral monitoring of land cover and condition ," *International Journal of Remote Sensing*, vol. 19, no. 3, pp. 411-426, 1998.

[59] W. A. Malila, "Change vector analysis: an approach for detecting forest changes with Landsat," in *Laboratory for Application of Remote Sensing Symposium*, W. Lafayette, IN, 1980, pp. 326–336.

[60] J. L. Michalek, T. W. Wagner, J. J. Luczkovich, R. W. Stoffle, "Multispectral change vector analysis for monitoring coastal marine environments," *Photogtammetric Enginnering and Remote Sensing*, vol. 59, no. 3, pp. 381-384, 1993.

[61] J. Chen, P. Gong, C. He, R. Pu, P. Shi, "Land-use/land-cover change detection using improved change-vector analysis," *Photogrammetric Engineering and Remote Sensing*, vol. 69, no. 4, pp. 369–379, 2003.

[62] K. Nackarets, K. Vaesen, B. Muys, P. Coppin, "Comparative performance of a modified change vector analysis in forest change detection," *International Journal of Remote Sensing*, vol. 26, no. 5, pp. 839-852, 2005.

[63] T. Warner, "Hyperspherical direction cosine change vector analysis," *International Journal of Remote Sensing*, vol. 26, no. 6, pp. 1201-1215, 2005.

[64] L. Fonseca, B. Manjunath, "Registration techniques for multisensory remotely sensed imagery," *Photogtammetric Engineering and Remote Sensing*, vol. 62, no. 9, pp. 1049-1056, September 1996.

[65] A. Goshtasby, J. Le Mogne, "Special issue on image registration," *Pattern Recognition*, vol. 32, no. 1, pp. 1-150, January 1999.

[66] G. J. Wen, J. J. Lv, W. X. Liu, "A high-performance feature-matching method for image registartion by combining spatial and similarity information," *IEEE Transaction on Geoscience and Remote Sensing*, vol. 46, no. 4, pp. 1266-1277, April 2008.

[67] J. R. G. Townshend, C. O. Justice, C. Gurney, "The impact of misregistartion on change detection," *IEEE Transaction on Geoscience and Remote Sensing*, vol. 30, no. 5, pp. 1054-1060, September 1992.

[68] L. Bruzzone, R. Cossu, "An adaptive approach for reducing registration noise effects in unsupervised change detection," *IEEE Transaction on Geoscience and Remote Sensing*, vol. 41, no. 11, pp. 2455-2465, November 2003.

[69] M. Beauchemin, K. B. Fung, "An adaptve filter for the reduction of artifacts caused by image misregistration," in *International Workshop on the Analysis of Multi-Temporal Remote Sensing Images*, Biloxi, Mississippi USA, 2005, pp. 174-176.

[70] D. A. Stow, "Reducing the effects of misregistration on pixel-level change detection," *International Journal of Remote Sensing*, vol. 20, no. 12, pp. 2477-2483, August 1999.

[71] L. De Carvalho, F. J. Acerbi, J. Scolforo, J. De Mello, A. De Oliveira, "Wavechange: a procedure for change detection based on wavelet product spaces," in *International Workshop on the Analysis of Multi-Temporal Remote Sensing Images*, Leuven, Belgium, 2007, pp. 1-5.

[72] P. Gong, E.F. Ledrew, J.R. Miller, "Registration-noise reduction in difference images for change detection," *International Journal of Remote Sensing*, vol. 13, no. 4, pp. 773-779, March 1992.

[73] S. G. Mallat, "A theory of multiresolution signal decomposition: the wavelet representation," *IEEE Transaction on Pattern Analysis and Machine Intelligence*, vol. 11, no. 7, pp. 674-693, July 1989.

[74] F. Bovolo, L. Bruzzone, "A detail perserving scale-driven approach to change detection in multitemporal SAR images," *IEEE Transaction on Geoscience and Remote Sensing*, vol. 43, no. 12, pp. 2963-2972, December 2005.

[75] A.W. Bowman, A. Azzalini, *Applied smoothing techniques for data analysis: Kernel approach with S-plus illustrations*. Oxford, USA: Oxford University Press Inc., 1997.

[76] E. Parzen, "On estimation of a probability density function and mode," *The Annals of Mathematical Statistics*, vol. 33, no. 3, pp. 1065-1076, September 1962.

[77] E.A. Patrick, F.P. Fischer, "A generalized k-nearest neighbor rule," *Information and Control*, vol. 16, no. 2, pp. 128-152, April 1970.

[78] D.L. Reilly, L.N. Cooper, C. Elbaun, "A neural model for category learning," *Biological Cybernetics*, vol. 45, no. 1, pp. 35-41, August 1982.

[79] L. Bruzzone, D. F. Prieto, "An adaptive parcel-based technique for unsupervised change detection," *International Journal of Remote Sensing*, vol. 21, no. 4, pp. 812-822, 2000.

[80] L. Bruzzone, D. F. Prieto, "An adaptive semiparametric and context-based approach to unsupervised change detection in multitemporal remote-sensing images," *IEEE Transaction on Image Processing*, vol. 11, no. 4, pp. 452-466, April 2002.

[81] F. Bovolo, L. Bruzzone, S. Marchesi, "Analysis and adaptive estimation of registration noise distribution in multitemporal VHR images," *IEEE Transaction on Geoscience and Remote Sensing*, vol. 47, no. 8, pp. 2658-2671, August 2009.

[82] F. L. Bookstein, "Principal warps: thin-plate splines and the decomposition of deformations," *IEEE Transaction on Pattern Analysis and Machine Intelligence*, vol. 11, no. 6, pp. 567 - 585 , June 1989.

[83] H. Chui, A. Rangarajan, "A new point matching algorithm for non-rigid registration," *Computer Vision and Image Understanding*, vol. 89, no. 2-3, pp. 114-141, February 2003.

[84] J. Yang, Y. Wang, S. Tang, S. Zhou, Y. Liu, W. Chen, "Multiresolution elastic registration of X-ray angiography images using thin-plate spline," *IEEE Transaction on Nuclear Science*, vol. 54, no. 1, pp. 152-166, February 2007.

[85] L. H. Chen, S. Chang, "A video tracking system with adaptive predictors," *Pattern Recognition*, vol. 25, no. 10, pp. 1171-1180, October 1992.

[86] W. Y. Kan, J. V. Krogmeier, P.C. Doerschuk, "Model-based vehicle tracking from image sequences with an application to road surveillance," *Optical Engineering*, vol. 35, no. 6, pp. 1723-1729, June 1996.

[87] L. Li, W. Huang, I. Yu-Hua Gu, and Q Tian, "Statistical Modeling of Complex Backgrounds for Foreground Object Detection," *IEEE Transaction on Image Processing*, vol. 13, no. 11, pp. 1459-1472, November 2004.

[88] S. C. Liu, C. W. Fu, and S. Chang, "Statistical change detection with moments under time-varying illumination," *IEEE Transaction on Image Processing*, vol. 7, no. 9, pp. 1258-1268, September 1998.

[89] C. Dumontier, F. Luthon, J.-P. Charras, "Real-Time DSP Implementation for MRF-Based Video Motion Detection," *IEEE Transaction on Image Processing*, vol. 8, no. 10, pp. 1341-1347, October 1999.

[90] L. Li, M.K.H. Leung, "Integrating Intensity and Texture Differences for Robust Change Detection," *IEEE Transaction on Image Processing*, vol. 11, no. 2, pp. 105-112, August 2002.

[91] L. Bruzzone, S. B. Serpico, "Detection of changes in remotely sensed images by the selective use of multi-spectral information," *International Journal of Remote Sensing*, vol. 18, no. 18, pp. 3883-3888, December 1997.

[92] M. Bosc, F. Heitz, J. P. Armspach, I. Namer, D. Gounot, L. Rumbach, "Automatic change detection in multimodal serial MRI: Application to multiple sclerosis lesion evolution," *Neuroimage*, vol. 20, no. 2, pp. 643–656, October 2003.

[93] M. J. Dumskyj, S. J. Aldington, C. J. Dore, E. M. Kohner, "The accurate assessment of changes in retinal vessel diameter using multiple frame electrocardiograph synchronised fundus photography," *Current Eye Research*, vol. 15, no. 6, pp. 625-632, June 1996.

[94] D. Lu, P. Mausel, E. Brondízio, E. Moran, "Change detection techniques," *International Journal of Remote Sensing*, vol. 25, no. 12, pp. 2365–2407, 2004.

[95] M. J. Carlotto, "Detection and analysis of change in remotely sensed imagery with application to wide area surveillance," *IEEE Transaction on Image Processing*, vol. 6, no. 1, pp. 189-202, January 1997.

[96] F. Bovolo, L. Bruzzone, S. Marchesi, "A multiscale change-detection technique robust to registration noise," in *Pattern Recognition and Machine Intelligence*, Kolkata, 2007, pp. 77-86.

[97] M. Baatz, U. Benz, S. Dehghani, M. Heynen, A. Höltje, P. Hofmann, I.Lingenfelder, M. Mimler, M. Sohlbach, M. Weber, G. Willhauck, *eCognition User Guide 4*.: Definiens Imaging,

2004.

[98] L. Bruzzone, L. Carlin, "A multilevel context-based system for classification of very high spatial resolution images," *IEEE Transaction on Geoscience and Remote Sensing*, vol. 44, no. 9, pp. 2587-2600, September 2006.

[99] F. Bovolo, L. Bruzzone, L.Capobianco, A. Garzelli, S. Marchesi, F. Nencini, "Analysis of the effects of pansharpening in change detection on VHR images," *IEEE Geoscience and Remote Sensing Letters*, vol. 7, no. 1, pp. 53-57, January 2010.

[100] RSI. (2003) ENVI User Manual. [Online]. http://www.RSInc.com/envi

[101] G. Camps-Valls, L. Gomez-Chova, J. Munoz-Mari, J.L. Rojo-Alvarez, M. Martinez-Ramon, "Kernel-based framework for multitemporal and multisource remote sensing data classification and change detection," *IEEE Transaction on Geoscience and Remote Sensing*, vol. 46, no. 6, pp. 1822-1835, June 2008.

[102] N. Ghoggali, F. Melgani, "Genetic SVM approach to semisupervised multitemporal classification," *IEEE Geoscience and Remote Sensing Letters*, vol. 5, no. 2, pp. 212-216, April 2008.

[103] L. Bruzzone and M. Marconcini, "Domain Adaptation Problems: a DASVM Classification Technique and a Circular Validation Strategy," *IEEE Transactions on Pattern Analysis and Machine Intelligence*, vol. 32, no. 5, pp. 770-787, 2010.

[104] L. Bruzzone, R. Cossu, and G. Vernazza, "Detection of land-cover transitions by combining multidate classifiers," *Pattern Recogniton Letters*, vol. 25, no. 13, pp. 1491-1500, 2004.

[105] L. Gueguen,M. Datcu, "Mixed Information Measure: Application to Change Detection in Earth Observation," in *Fifth International Wotkshop on the Analysis of Multi-Temporal Remote Sensing Images*, Mystic, Connecticut, USA, 2009.

[106] G. Mercier, G. Moser,S. B. Serpico, "Conditional copulas for change detection in heterogeneous remote sensing images," *IEEE Transactions on Geoscience and Remote Sensing*, vol. 46, no. 5, pp. 1428 - 1441, May 2008.

[107] D. Faur, C. Vaduva, I. Gavat, M. Datcu, "An information theory based image processing chain for change detection in earth observation," in *15th International Conference on Systems, Signals and Image Processing*, Bratislava, 2008, pp. 129 - 132.

[108] A. A. Nielsen, "The regularized iteratively reweighted MAD method for change detection in multi- and hyperspectral data," *IEEE Transaction on Image Processing*, vol. 16, no. 2, pp. 463-478, February 2007.

[109] J. M. Canty, A. A. Nielsen, "Visualization and unsupervised classification of changes in multispectral satellite imagery," *International Journal of Remote Sensing*, vol. 27, no. 18, pp. 3961 - 3975, September 2006.

[110] L. Bruzzone, D. F. Prieto, "A minimum-cost thresholding technique for unsupervised change detection," *International Journal of Remote Sensing*, vol. 21, no. 18, pp. 3539-3544, 2000.

[111] L. Bruzzone and D. Fernández-Prieto, "A Minimum-Cost Thresholding Technique for Unsupervised Change Detection," *Int. J. Remote Sens.*, vol. 21, no. 18, pp. 3539-3544, 2000.

[112] T. Celik, "Unsupervised Change Detection in Satellite Images Using Principal Component Analysis and k-Means Clustering," *IEEE Geoscience and Remote Sensing Letters*, vol. 6, no. 4, pp. 772-776, October 2009.

[113] F.A. Kruse, A.B. Lefkoff, J.W. Boardman, and K.B. Heidebrecht, "The Spectral Image Processing System (SIPS)—Interactive Visualization and Analysis of Imaging Spectrometer Data," *Remote Sens. Environ.*, vol. 44, no. 2/3, pp. 145-163, 1993.

[114] G. Girouard, A. Bannari, A. Harti, A. Desrochers, A., "Validated spectral angle mapper algorithm for geological mapping: comparative study between Quickbird and Landsat-TM," in *Proc. of 20th International Society for Photogrammetry and Remote Sensing Congress*, Istanbul, Turkey, 2004, pp. 599-605.

[115] C. Hecker, M. van der Meijde, H. van der Werff, F. D. van der Meer, "Assessing the influence

of reference spectra on synthetic SAM classification results," *IEEE Transaction on Geoscience and Remote Sensing*, vol. 46, no. 12, pp. 4162-4172, December 2008.

[116] Y. Amano, N. Takagi, A. Getz, "A study on the classification of urban region using Hyper-spectrum data at AVIRIS," in *IEEE International Geoscience and Remote Sensing Symposium*, Boston, USA, 2008, pp. IV - 687 - IV - 690.

[117] Y. Sohn, N. S. Rebello, "Supervised and unsupervised spectral angle classifiers," *Photogrametric Engineering and Remote Sensing*, vol. 68, no. 12, pp. 1271-1280, 2002.

[118] N. Keshava, "Distance metrics and band selection in hyperspectral processing with application to material identification and spectral libraries," *IEEE Transaction on Geoscience and Remote Sensing*, vol. 42, no. 7, pp. 1552-1565, July 2004.

[119] D. Bash, P. Muela, Y. M. Villegas, "Assessing land cover changes using standardized principal component and spectral angle mapping techniques," in *Proc. of Pecora 15/Land Satellite Information IV/ISPRS Commission I/FIEOS*, 2002.

[120] F. Van Der Meer, "Spectral unmixing of Landsat Thematic Mapper data," *International Journal of Remote Sensing*, vol. 16, no. 16, pp. 3189-3194, 1995.

[121] P. E. Dennisona, K. Q. Halliganb, D.A.Robertsc, "A comparison of error metrics and constraints for multiple endmember spectral mixture analysis and spectral angle mapper," *Remote Sensing for Environment*, vol. 93, no. 3, pp. 359–367, November 2004.

[122] D. Gillis, J. Bowles, "Target detection in hyperspectral imagery using demixed spectral angles," in *Image and Signal Processing for Remote Sensing, SPIE*, Barcelona, 2004, pp. 244-254.

[123] R. A. Schowengerdt, *Remote Sensing: Models and Methods for Image Processing*, 2nd ed. San Diego: CA: Academic, 1997.

[124] T. K. Moon, "The expectation-maximization algorithm," *Signal Processing Magazine*, vol. 13, no. 6, pp. 47–60, November 1996.

[125] A. P. Dempster, N. M. Laird, D. B. Rubin, "Maximum likelihood from incomplete data via the EM algorithm," *Journal of the Royal Statistical Society*, vol. 39, no. 1, pp. 1-38, 1977.

[126] J. MacQueen, "Some methods for classification and analysis of multivariate observations," in *5-th Berkley Symposium on Mathematical Statistics and Probability*, Berkley, University of California, 1967, pp. 281-297.

[127] D. Pelleg, A. W. Moore, "X-means: extending k-means with efficient estimation of the number of clusters," in *17th International Conference on Machine Learning*, Stanford, CA, USA, 2000, pp. 727-734.

[128] R. Tibshirani, G. Walther, T. Hastie, "Estimating the number of clusters in a data set via the gap statistic," *Journal of the Royal Statistical Society: Series B (Statistical Methodology)*, vol. 63, no. 2, pp. 411 - 423, 2001.

[129] M. Halkidi, M. Vazirgiannis, "Clustering validity assessment: finding the optimal partitioning of a data set," in *IEEE International Conference on Data Mining*, San Josè, California, 2001, p. 187.

[130] A. K. Jain, "Cluster analysis," in *Handbook of Pattern Recognition and Image Processing*, T. Y. Young and K. S. Fu, Eds.: New York: Academic, 1986.

[131] A. Garzelli, F. Nencini, L. Capobianco, "Optimal MMSE pansharpening of very high resolution multispectral images," *IEEE Transaction on Geoscience and Remote Sensing*, vol. 46, no. 1, pp. 228-236, January 2008.

[132] S. Marchesi, F. Bovolo, L. Bruzzone, "A context-sensitive technique robust to registration noise for change detection in VHR multispectral images," *IEEE Transaction on Image Processing*, vol. 19, no. 7, pp. 1877-1889, July 2010.

[133] T. Fung, E. LeDrew, "Application of principal component analysis to change detection," *Photogrammetric Engineering and Remote Sensing*, vol. 53, no. 12, pp. 1649-1658, December 1987.

[134] B. Schölkopf, A. Smola, K.R. Müllerr, "Kernel Principal Component Analysis," in *Advances in*

Kernel Methods--Support Vector Learning, C. J. C. Burges, and A. J. Smola B. Schölkopf, Ed. Cambridge, MA, 1999, pp. 327-352.

[135] J. Zhong, R. Wang, "Multi-temporal remote sensing change detection based on independent component analysis," *International Journal of Remote Sensing*, vol. 27, no. 10, pp. 2055-2061, May 2006.

[136] M. Ceccarelli, A. Petrosino, "Unsupervised change detection in multispectral images based on independent component analysis," in *IEEE International Workshop on Imagining Systems and Techniques*, Piscattaway, NJ, 2006, pp. 54-59.

[137] M.I. Jordan F.R. Bach, "Kernel independent component analysis," *The Journal of Machine Learning Research*, vol. 3, pp. 1-48, March 2003.

[138] L. Wald, T. Ranchin, M. Mangolini, "Fusion of satellite images of different spatial resolutions: assessing the quality of resulting images," *Journal of Photogrammetric Engineering and Remote Sensing*, vol. 63, no. 6, pp. 691-699, June 1997.

[139] C. A. Shah, L. J. Quackenbush, "Analyzing multi-sensor data fusion techniques: a multi-temporal change detection approach," in *ASPRS Annual Convention*, Tampa, Florida, 2007.

[140] T. M. Tu, S. C. Su, H. C. Shyu, P. S. Huang, "A new look at IHS-like image fusion methods," *Information Fusion*, vol. 2, no. 3, pp. 177-186, September 2001.

[141] C.A. Laben, B. V. Brower, "Process for enhancing the spatial resolution of multispectral imagery using pan-sharpening," Eastman Kodak Co, US Patent 6011875, 2000.

[142] B. Aiazzi, L. Alparone, S. Baronti, A. Garzelli, "Context-riven fusion of high spatial and spectral resolution data based on oversampled multiresolution images," *IEEE Transaction on Geoscience and Remote Sensing*, vol. 40, no. 10, pp. 2300-2312, October 2002.

[143] X. Otazu, M. Gonzales-Audicana, O. Fors, J. Nnez, "Introduction of sensor spectral response into image fusion methods. Application to wavelet-based methods," *IEEE Transaction on Geoscience and Remote Sensing*, vol. 43, no. 10, pp. 2376-2385, October 2005.

[144] T. Ranchin, B. Aiazzi, L. Alparone, S. Baronti, L. Wald, "Image fusion - The ARSIS concept and some successful implementation schemes," *Journal of Photogrammetric and Remote Sensing*, vol. 58, no. 1/2, pp. 4-18, June 2003.

[145] J. S. Denga, K. Wanga, Y. H. Dengb, G. J. Qic, "PCA-based land-use change detection and analysis using multitemporal and multisensor satellite data," *International Journal of Remote Sensing*, vol. 29, no. 16, pp. 4823-4838, 2008.